U.S. GEOLOGICAL SURVEY

VERTICAL MASS TRANSFER IN OPEN CHANNEL FLOW

By

Harvey E. Jobson

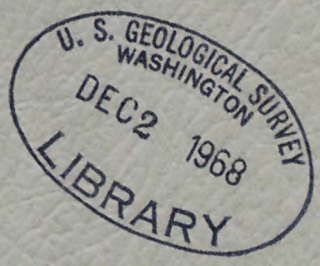

Open-file Report

September 1968

U.S. GEOLOGICAL SURVEY

VERTICAL MASS TRANSFER IN OPEN CHANNEL FLOW

By

Harvey E. Jobson

[Fort Collins, Colo.?] 68-146

Open-file Report

September 1968

68-146

TABLE OF CONTENTS

TABLE OF CONTENTS - Continued

TABLE OF CONTENTS - Continued

TABLE OF CONTENTS - Continued

LIST OF TABLES

LIST OF FIGURES

ABSTRACT OF DISSERTATION

VERTICAL MASS TRANSFER IN OPEN CHANNEL FLOW

The vertical mass transfer coefficient and particle fall velocity were determined in an open channel shear flow. Three dispersants, dye, fine sand and medium sand, were used with each of three flow conditions. The dispersant was injected as a continuous line source across the channel and downstream concentration profiles were measured. From these profiles along with the measured velocity distribution both the vertical mass transfer coefficient and the local particle fall velocity were determined.

The effects of secondary currents on the vertical mixing process were discussed. Data was taken and analyzed in such a way as to largely eliminate the effects of these currents on the measured values.

A procedure was developed by which the local value of the fall velocity of sand sized particles could be determined in an open channel flow. The fall velocity of the particles in the turbulent flow was always greater than their fall velocity in quiescent water.

Reynolds analogy between the transfer of momentum and marked fluid particles was further substantiated. The turbulent Schmidt number was shown to be approximately 1.03 for an open channel flow with a rough boundary. Eulerian turbulence measurements were not sufficient to predict the vertical transfer coefficient.

Vertical mixing of sediment is due to three semi-independent processes. These processes are: secondary currents, diffusion due to tangential velocity fluctuations and diffusion due to the curvature of

the fluid particle path lines. The diffusion coefficient due to tangential velocity fluctuations is approximately proportional to the transfer coefficient of marked fluid particles. The proportionality constant is less than or equal to 1.0 and decreases with increasing particle size. The diffusion coefficient due to the curvature of the fluid particle path lines is not related to the diffusion coefficient for marked fluid particles and increases with particle size, at least for sediment particles in the sand size range. The total sediment transfer coefficient is equal to the sum of the coefficient due to tangential velocity fluctuations and the coefficient due to the curvature of the fluid particle path lines.

A numerical solution to the conservation of mass equation is given. The effects of the transfer coefficient, fall velocity and bed conditions on the predicted concentration profiles are illustrated.

Harvey E. Jobson
Civil Engineering Department
Colorado State University
Fort Collins, Colorado

ACKNOWLEDGMENTS

The writer expresses his appreciation for the counsel and encouragement of his major professor, Dr. D. B. Simons and of his committee members, Dr. E. V. Richardson, Dr. W. W. Sayre, Dr. J. Gessler and Dr. F. M. Stein.

The entire study was made possible by the financial support of the U.S. Geological Survey for which the writer wishes to express his gratitude.

Special appreciation is expressed to Dr. W. W. Sayre, the writer's Geological Survey advisor, for the idea which originated the study. Sincere thanks is expressed to Dr. Sayre for his constant encouragement, his many helpful suggestions and for the many hours spent in reviewing the manuscript.

Special thanks is extended to R. S. McQuivey whose help in taking and analyzing the turbulence data was indispensable.

The many hours that Baum Koo Lee spent in plotting graphs and making numerical calculations are gratefully acknowledged.

Appreciation is also expressed for those fellow students and Geological staff members who helped in the collection of the data. The staff members include C. F. Nordin, R. S. McQuivey, R. E. Rathbun, E. V. Richardson, W. W. Sayre, and W. Gaskill. Some of the students include: J. P. Bennett, N. Grigg, T. Keefer, C. Neuhauser, C. Ramirez, V. R. Schneider and T. Yang.

LIST OF SELECTED SYMBOLS

Symbol	Definition	Dimensions	Units
A	Probability of deposit	--	--
a	Arbitrary reference distance above the bed	L	--
c	Concentration of dispersant	--	--
$\overline{\overline{C}}$	Concentration averaged across the flow	--	--
C_a	Concentration at a distance above the bed	--	--
C_b	Concentration averaged in the vertical	--	--
C_D	Drag coefficient	--	--
c_m	Measured concentration	--	--
D	Diameter of a sphere	L	--
DX	Longitudinal step Y_N/M	L	ft
DY	Vertical step Y_N/N	L	ft
E	Dimensionless transfer coefficient $\frac{\varepsilon_\Gamma}{Y_N u_*}$	--	--
E_r	Remainder of equation 48	--	--
F	External driving force	T^{-1}	--
F(n)	Eulerian spectral distribution of turbulence	T^{-1}	--
FI	Injected dispersant flux per unit width	M/T^3	lb/ft sec
g	Acceleration of gravity	L/T^2	ft/sec^2
M	Increments in the horizontal per unit length	--	--
N	Increments in the vertical	--	--
n	Frequency	T^{-1}	--
Pr	Prandtl number	--	--
R_L	Lagrangian correlation coefficient	--	--

LIST OF SELECTED SYMBOLS - Continued

Symbol	Definition	Dimensions	Units
R_p	Particle Reynolds number	--	--
RR	Recovery ratio	--	--
RRM	Measured recovery ratio	--	--
S	Slope of energy line	--	--
Sc	Schmidt number	--	--
T	Time	T	--
t	Time	T	--
U	Average stream velocity	L/T	ft/sec
UI	Reciprocal of the dimensionless velocity u_*/u	--	--
u_i	Velocity in the $i^{\underline{th}}$ coordinate direction	L/T	--
u'_i	Fluctuating component of u_i	L/T	--
$\overline{u}_i$	Time average component of u_i	L/T	--
u_{max}	Velocity at the surface of the channel	L/T	--
u_p	Dispersant particle velocity in x direction	L/T	--
u_s	Instantaneous velocity of a sediment particle	L/T	--
u'_{sf}	Particle velocity relative to the turbulent fall velocity and the instantaneous fluid velocity	L/T	--
u''_{sf}	Particle velocity relative to the quiescent fall velocity and the instantaneous fluid velocity	L/T	--
u_*	Shear velocity	L/T	ft/sec
v_L	Lagrangian particle velocity	L/T	--
v_p	Dispersant particle velocity in y direction	L/T	--

LIST OF SELECTED SYMBOLS - Continued

Symbol	Definition	Dimensions	Units
VS	Dimensionless fall velocity V_{ST}/u_*	--	--
V_{sq}	Particle fall velocity in a quiescent fluid	L/T	cm/sec
V_{ST}	Particle fall velocity in a turbulent fluid	L/T	cm/sec
W	Channel width	L	--
w_p	Dispersant particle velocity in z direction	L/T	--
X	Relative distance from the source $\frac{x}{Y_N}$	--	--
x	Coordinate distance along the channel	L	--
X_o	Position of first measured concentration profile in depths	--	--
Y	Distance traveled by a particle in time t	L	--
y	Vertical coordinate distance	L	--
Y_N	Depth of flow	L	ft
Z	Rouse number $V_{sq}/\kappa u_*$	--	--
z	Transverse coordinate distance	L	--
α	Ratio of sediment to momentum transfer coefficient	--	--
α_1	Proportionality constant between ε_T and ε_m	--	--
α_2	Maximum value of ε_c	L^2/T	--
Γ	Any transferable scalar quantity	--	--
Γ'	Fluctuating component of Γ	--	--
$\overline{\Gamma}$	Time averaged component of Γ	--	--
γ	Specific weight of a water particle	M/T^2L^2	--

LIST OF SELECTED SYMBOLS - Continued

Symbol	Definition	Dimensions	Units
γ_s	Specific weight of a sediment particle	M/T^2L^2	--
ε	Molecular diffusion coefficient	L^2/T	--
ε_c	Coefficient describing the turbulent transfer of sediment due to the curvature of fluid particle pathlines	L^2/T	--
ε_d	Turbulent mass transfer coefficient for marked fluid particles	L^2/T	--
ε_m	Turbulent momentum transfer coefficient	L^2/T	--
ε_s	Secondary current "diffusion" coefficient	L^2/T	--
ε_{se}	Total turbulent transfer coefficient for sediment	L^2/T	--
ε_T	Coefficient describing the turbulent transfer of sediment due to rectilinear velocity fluctuations	L^2/T	--
ε_Γ	Turbulent transfer coefficient of any quanity	L^2/T	--
$\overline{\overline{\varepsilon}}_\Gamma$	Transfer coefficient averaged across the flow as indicated in equation 8	L^2/T	--
η	Relative depth y/Y_N	--	--
$\eta_,$	Arbitrary relative depth	--	--
θ	Strength of secondary currents	--	--
κ	Von Karman's coefficient	--	--
Λ_L	Lagrangian integral time scale	T	--
Λ_t	Eulerian integral time scale	T	--
ν	Kinematic viscosity of water	L^2/T	--
ξ	x component of vorticity	$1/T$	--
ρ	Density of water	M/L^3	--

LIST OF SELECTED SYMBOLS - Continued

Symbol	Definition	Dimensions	Units
ρ_s	Density of a sediment particle	M/L^3	--
Σ	Concentration gradient $\frac{\partial c}{\partial \eta}\Big\vert_{\eta_1}$	--	--
ψ	Local concentration $C\vert_{\eta_1}$	--	--
Ω	Vertical sediment flux $\frac{\partial}{\partial X}\int_{\eta_1}^{1.0} \frac{u}{u_*} c \, d\eta$	--	--
τ_{ij}	Shear stress	M/LT^2	--
τ_o	Shear stress at the flume floor	M/LT^2	--

Chapter I

INTRODUCTION

The exact nature of transport and mixing processes in turbulent flow has long intrigued fluid dynamicists and mathematicians. Few areas of fluid mechanics theory and research appear to have received more attention in recent years. Yet it is clear that much remains to be learned before these processes are completely understood. Problems in waste dispersion have stimulated interest in investigation of turbulent diffusion. With increasing demands being placed on the worlds water and air resources, it becomes increasingly imperative that the turbulent mixing of dispersants be better understood.

Many theories have been advanced and experiments performed describing the dispersion of fluid or dissolved dispersants. Unfortunately, attempts to extend these results to describe the dispersion of discrete particles such as sediment have met with very limited success. The differential equations describing the transport of any scalar quantity are identical. It is generally assumed that the transfer of discrete particles is similar to the transfer of momentum. Predictions based on this analogy have led to contradictions between experiment and theory.

Because sediment particles tend to settle through the fluid, determination of their fall velocity in the fluid also presents a problem. It is often assumed that this fall velocity is unaffected by the turbulent fluctuations of the fluid, but no convincing criteria have been presented indicating under what conditions this assumption is true.

Various federal agencies and university research groups have been investigating the turbulent transfer of various quantities for a number of years. This study is part of a continuing effort made by the Water Resources Division of the U. S. Geological Survey to better understand the various mechanisms involved in the transport of suspended sediment.

A. M. Al-Saffar (1964) used a new procedure to experimentally determine the vertical mass transfer coefficient in an open channel flow. This procedure can be extended to determine the vertical sediment transfer coefficient as well as the particle fall velocity. The basic procedure is to inject a continuous line source of dispersant across the width of a channel and to measure the rates of change of the concentration of the dispersants with increasing distance from the source. From an integrated form of the general conservation of mass equation the evaluation of both the transfer coefficient and the turbulent fall velocity, as functions of depth, is theoretically possible.

Briefly stated the goals of this investigation were to investigate certain turbulent transfer processes in an open channel shear flow. More specifically, the goals were to:

a. Evaluate the turbulent mass transfer coefficient for a dispersant having the same properties as the ambient fluid.

b. Compare this with the measured momentum transfer coefficient (that is, check Reynolds analogy for the equivalence of momentum and mass transfer).

c. Evaluate the turbulent mass transfer coefficient for sediment particles and compare this with the mass transfer coefficient for a dye.

d. Evaluate the fall velocity of the sediment particles in a turbulent shear flow.

e. Use the measured values of the transfer coefficient and fall velocity in conjunction with a numerical solution of the conservation equation in order to check the mathematical model of the mixing process.

This investigation was concerned mainly with the vertical components of the turbulent transfer coefficient and fall velocity, however, secondary currents, since they can affect the measured values of both of these quantities,also had to be given some attention.

Chapter II

THEORETICAL DEVELOPMENT AND REVIEW OF LITERATURE

A. The Conservation Equation

The basic conservation equation can be derived from applying the conservation of mass to an incremental volume of the flow. This equation stated for the conservation of a scaler quantity (Γ) per unit mass of fluid is

$$\frac{\partial \Gamma}{\partial t} + \frac{\partial (u_i \Gamma)}{\partial x_i} = \frac{\partial}{\partial x_i}\left[\varepsilon \frac{\partial \Gamma}{\partial x_i}\right] + F \qquad (1)$$

where Γ is the transferable scalar quantity, u_i is the velocity of the transferable scalar quantity in the i^{th} direction (u_i is generally assumed to be the velocity of the fluid, however, in some cases it may not be), ε is the molecular diffusion coefficient. The molecular diffusion coefficient will be zero when the transferable quantity is unaffected by the molecular activity of the fluid. The symbol F is a "driving force" or source, for instance, if heat is the transferable quantity, then F is the heat generation by dissipation of the kinetic energy in the fluid. The x's are the coordinate distances and t is time. In this discussion only cases where the "driving force" is zero and where the molecular diffusion is negligible (in comparison with the other terms) will be considered. It has been shown (Elder, 1959, p. 548) (Mickelsen, 1960) that the molecular diffusion is small in comparison to the turbulent transfer, at least in most cases.

For turbulent flow conditions, both the velocity and the transferable quantity have values which fluctuate randomly with time, however, here the primary interest is in the time averaged values of the fluctuating quantities. Thus, the quantities will be divided into the usual time averaged and fluctuating component as

$$\Gamma = \overline{\Gamma} + \Gamma'$$

$$u_i = \overline{u}_i + u_i'$$

where

$$\overline{\Gamma} = \frac{1}{T}\int_o^T \Gamma \, dt$$

$$\overline{u}_i = \frac{1}{T}\int_o^T u_i dt \ .$$

The value of T used in this averaging procedure is chosen as to permit masking of the turbulent fluctuations but not so long as to sufficiently damp the other variations of the quantities with time. Carrying out the usual averaging procedure (Hinze, 1959, p. 6) and letting $F = \varepsilon = 0$, one obtains

$$\frac{\partial \overline{\Gamma}}{\partial t} + \frac{\partial \overline{u}_i \, \overline{\Gamma}}{\partial x_i} = - \frac{\partial}{\partial x_i} \left[\overline{u_i' \, \Gamma'} \right] \ . \qquad (2)$$

At this point a turbulent transport coefficient is defined,

$$\varepsilon_{\Gamma ij} \equiv - \frac{\overline{u_i' \, \Gamma'}}{\partial \overline{\Gamma} / \partial x_j} \ , \qquad (3)$$

that is analagous to Boussinesq's (Hinze, 1959, p. 25) momentum transfer coefficient. The quantity $\varepsilon_{\Gamma ij}$ is commonly called the turbulent diffusion tensor and the quantity

$$\varepsilon_{\Gamma ij} \frac{\partial \overline{\Gamma}}{\partial x_j}$$

is the net flux of the scalar quantity through a differential area. Because

$$\overline{u_i' \Gamma'} \quad \text{and} \quad \frac{\partial \overline{\Gamma}}{\partial x_j}$$

are vector quantities, $\varepsilon_{\Gamma ij}$, must be either a scalar or at least a second order tensor (Hinze, 1959, p. 25). Except for isotropic turbulence, a scalar value of $\varepsilon_{\Gamma ij}$ would not seem very reasonable. With the above definition the conservation equation becomes

$$\frac{\partial \overline{\Gamma}}{\partial t} + \frac{\partial \overline{u_i}\ \overline{\Gamma}}{\partial x_i} = \frac{\partial}{\partial x_i}\left[\varepsilon_{\Gamma ij}\ \frac{\partial \overline{\Gamma}}{\partial x_j}\right] \tag{4}$$

which is often referred to as the turbulent diffusion equation with convection. The second term is also usually written as $\overline{u}_i \frac{\partial \overline{\Gamma}}{\partial x_i}$ since $\frac{\partial \overline{u}_i}{\partial x_i}$ is zero for an incompressible flow. The reason that the equation has been left in the form of Equation 4 will become apparent later. Equation 4 is valid for any scalar quantity including the concentration of discrete particles. For discrete particles the terms in Equation 4 must be defined such that u_i represents the particle velocity in the i^{th} direction, the percentage of the volume actually occupied by the particles must be negligible and $\varepsilon_{\Gamma ij}$ must be the particle transfer coefficient.

Equation 4 will now be applied to an open channel flow. The origin of the coordinate system will be at the floor of the channel with the coordinate x in the direction of the primary flow, the coordinate y normal to the channel bed, positive upwards, and the coordinate z the horizontal normal to the primary flow. When tensor notation is used the directions 1, 2 and 3 will correspond to the directions x, y and z.

The velocities will be represented by u, v, and w in the x, y, and z directions respectively. It will be assumed that the off-diagonal terms of the diffusion tensor are zero when the coordinate system is set up in this manner (Pai, 1957, p. 179). With the indicated coordinate system the conservation equation for a transferable scalar quantity becomes

$$\frac{\partial \Gamma}{\partial t} + \frac{\partial \overline{u}_i \overline{\Gamma}}{\partial x_i} = \frac{\partial}{\partial x_i} \left[\varepsilon_{\Gamma i} \frac{\partial \Gamma}{\partial x_i} \right] \tag{5}$$

where the coefficient $\varepsilon_{\Gamma ij}$ can be represented by a single index because all off-diagonal terms have been assumed to be zero.

In the discussion to follow, only cases where the following restrictions apply will be considered. These restrictions are: A. steady uniform flow, B. transverse and longitudinal concentration gradients are small in comparison to the vertical gradients, C. the transferred quantity is some dispersant which can be described by a concentration, D. concentrations are independent of time. With these restrictions, the conservation equation reduces to

$$u_p \frac{\partial c}{\partial x} = \frac{\partial}{\partial y} \left[\varepsilon_\Gamma \frac{\partial c}{\partial y} \right] - \frac{\partial}{\partial y} \left[v_p c \right] - \frac{\partial}{\partial z} \left[w_p c \right] \tag{6}$$

where u_p, v_p, and w_p are the time averaged values of the dispersant velocities, c is the time averaged concentration and ε_Γ is the turbulent transfer coefficient in the direction corresponding to the direction of the derivative. The term on the left hand of Equation 6 is the convective transport term for convection in the longitudinal direction, the first term on the right of Equation 6 describes the turbulent transfer, the second term on the right describes combined convection due both to the particle fall velocity and to the vertical components

of the secondary current terms, and the last term on the right of Equation 6 describes the horizontal convection due to secondary currents. For a substance which tags the fluid particles such as dye, or very small dispersant particles, it will be assumed that the particle or dispersant velocities are equal to the fluid velocity. For a dispersant consisting of larger particles such as silt or sand it is usually assumed that at least the longitudinal and transverse particle velocities are equal to the mean fluid velocities. However, it is often assumed that the vertical component of the particle velocity is not equal to the vertical component of the fluid velocity.

The remaining portion of this chapter will be devoted to discussion of the three terms on the right side of Equation 6. These terms describe the mixing due to turbulent diffusion, secondary currents, and particle fall velocity. The secondary currents will be discussed first, because an understanding of their significance is important in understanding the significance of the other two terms. Then the particle fall velocity will be discussed, and finally, but probably most importantly, the turbulent transfer term will be discussed.

B. Secondary Currents

1. Definition

Because secondary currents have an important effect on many hydraulic measurements, some understanding of these currents is required in order to properly interpret these hydraulic measurements. "When the hydraulic engineer speaks of a flow channel he visualizes boundaries confining a flow which is predominately one-directional. Such flows have been observed to possess a rotation or circulation around an axis

parallel to the main flow velocity, transforming it into a helical or multihelical flow" (Einstein and Li, 1958, p. 1085). In this discussion these superimposed rotations will be called secondary currents. Secondary currents can be classified mainly into two catagories, one occurring in straight non-circular conduits, and the other in curved conduits (Rao and Seetharamiah, 1967), (Chiu and McSparran, 1966), (Liggett, et.al., 1965). Only the first type will be discussed here, although both are important to the mixing process in open channels.

2. Causes and Descriptions

Observations and considerations of secondary currents were first advanced during the latter half of the nineteenth century in order to explain why the maximum water velocity occurs below the surface. D. C. Wood (Chiu, 1967), F. P. Stearns and Max Moeller (Nemenyi, 1946) were among the earliest investigators of the subject. A convincing description of the phenomena was first given by Prandtl (Tracy, 1965). Prandtl reasoned by a momentum analysis that the paths of the secondary currents moved along the bisectors of the corner angles toward the corner and then along the adjoining sides away from the corner. He hypothesized that the isovels are the key to describing the secondary currents.

H. A. Einstein and H. J. Tracy were among the first to investigate the relationship of turbulence to the secondary currents. Einstein and Li (1958) analytically studied the time rate of change of the x component of vorticity and concluded that the secondary currents will not develop spontaneously in a straight laminar uniform flow, but that one would expect secondary currents to develop spontaneously in turbulent flows where the lines of constant velocity are not parallel. Tracy (1965)

interpreted the results of Einstein and performed experiments which support this interpretation. Tracy presented Einstein's results as

$$\frac{D\xi}{Dt} = \frac{\partial^2 \overline{v' w'}}{\partial z^2} - \frac{\partial^2 \overline{v' w'}}{\partial y^2} + \frac{\partial^2 (\overline{v'^2} - \overline{w'^2})}{\partial z \partial y} \qquad (7)$$

where ξ is a measure of the rotation of a fluid particle about an axis normal to the y-z plane, and v' and w' are turbulent fluctuations in velocity in the y and z directions respectively. Tracy reasoned that the left side of this equation is a description of the secondary current pattern and says nothing about its cause. He also reasoned that the first two terms on the right side are "apparent" shear stresses and exist as a result of the secondary currents, thus again cannot be its cause. These terms would tend to damp or reduce secondary currents by offering resistance to their movement. He reasoned that the last term is the only term that is independent of the currents, thus must be the driving force that causes the currents to form. For this reason a sufficient condition for the existence of the secondary currents is the existence of the last term of the above equation. However, a zero value of the last term in a region does not rule out the existence of secondary currents there. Secondary currents may be generated only near the walls or corners, however, because the secondary stream lines must close on themselves, the currents are convected from the regions in which they are formed and decay in other areas.

It has been shown that the secondary currents are directly related to the mean velocity distribution as predicted by Prandtl. Liggett, Chiu, and Miao (1965) transformed the equations of motion and continuity into an orthogonal curvilinear coordinate system which has the isovels of the main flow as one of the set of coordinate lines, the velocity gradient lines as another and the third coordinate is along the channel. The resulting system of equations is determinate if the variation of the primary velocity in the cross section is known and if the variation of the momentum transport (shear) across the isovels is known. They found the general stream line patterns to be almost independent of the assumptions used for determining the shear distribution. Chao-Lin Chiu (1967) put further interpretation on Liggett's results. He found that the effective shear driving the secondary currents is directly related to the curvature of the isovels. He also found that where the isovels are concave relative to the wall (i.e. on or near the bisector of a corner angle) the effective shear tends to maintain the secondary flow toward the wall or into the corner. If the isovels are convex relative to the wall the effective shear supports fluid particles moving away from the wall.

3. Secondary Current Patterns

Many and sometimes conflicting proposed secondary current patterns have been suggested by various investigators at various times. Some of these patterns are presented in the sequel.

Figure 1-a gives the secondary current pattern proposed by Prandtl (1952) for flow in a triangular closed conduit. Liggett and others (1965) have measured the secondary current pattern in a triangular open

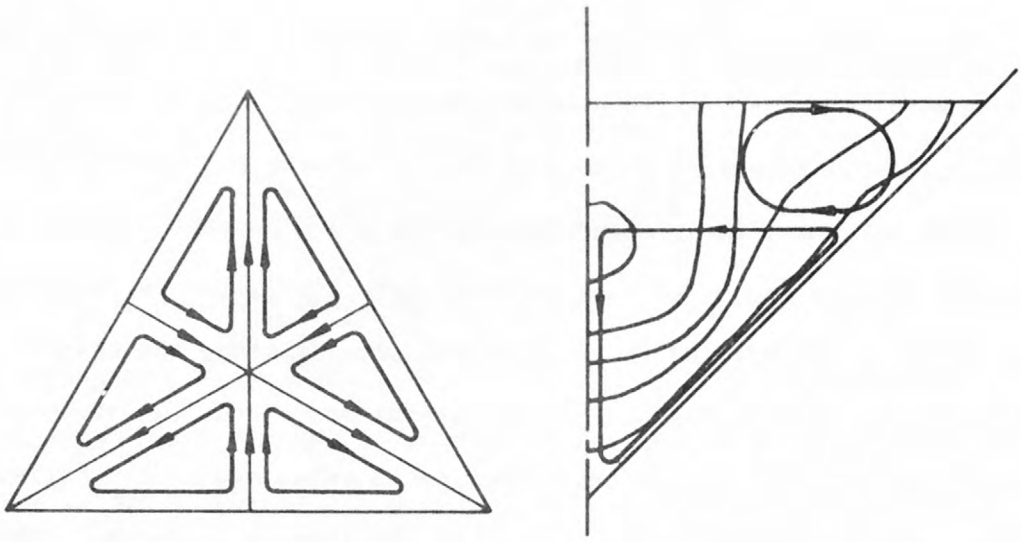

(a) Flow in a triangular closed conduit

(b) Flow in a triangular open channel

Figure 1.--Secondary current patterns in triangular conduits.

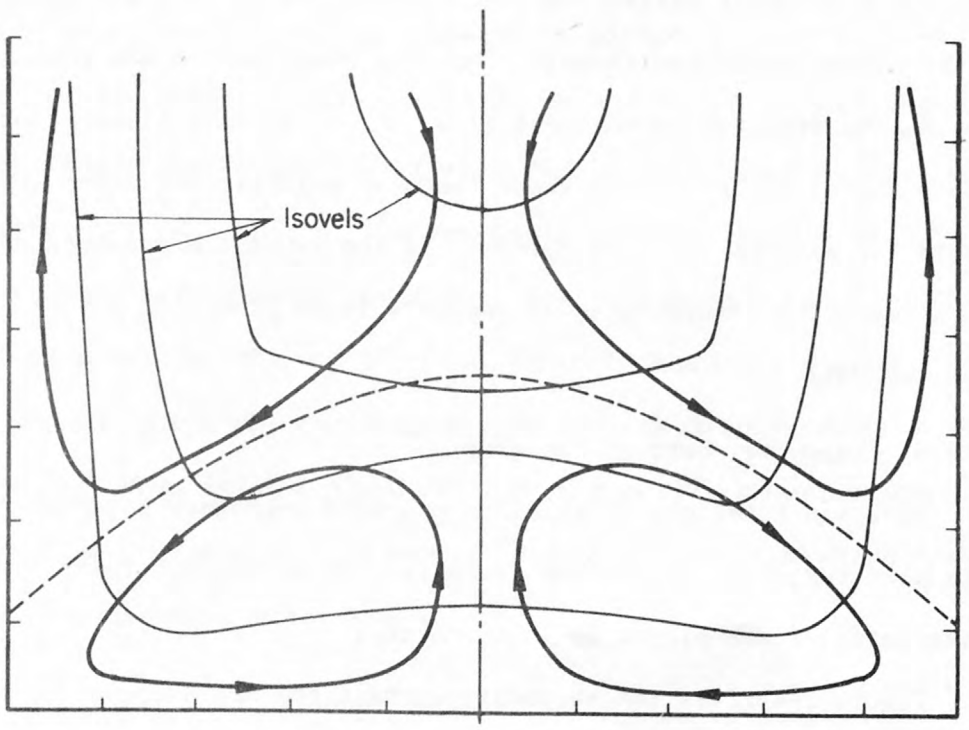

Figure 2.--Secondary current patterns in rectangular conduits.

channel. His measured secondary currents and isovels are shown in Figure 1-b.

Measurements have also been made in closed rectangular conduits. Figure 2 shows the secondary currents and isovels that were measured by Tracy (1965) in the corners of a wide rectangular closed channel.

According to the measurements of Elder (Hinze, 1967, p. S123) a rough boundary tends to enlarge the secondary spiral next to that boundary relative to the one next to an adjoining smooth boundary.

Many proposed secondary current patterns have been advanced for flow in a straight rectangular open channel, some of the early descriptions include those of Max Moeller, F. P. Stearns, and A. H. Gibson, (Nemenyi, 1946) who independently observed secondary currents in straight open channels. All three agreed that the patterns of secondary currents were as shown in Figure 3-a. R. W. Powell (1946) reasoned after considering Prandtl's work that the secondary currents should be as are shown in Figure 3-b. Lossievsky (Nemenyi, 1946) made the following observations concerning secondary flow patterns:

a. For a broad rectangular cross section the pattern should be as that shown in Figure 3-a.

b. For rectangular channels with large ratios of depth to width the pattern should be the same as that shown in Figure 3-a except the direction of rotation should be reversed.

c. For intermediate depth to width ratio a more complicated and rather unstable pattern of secondary currents exist.

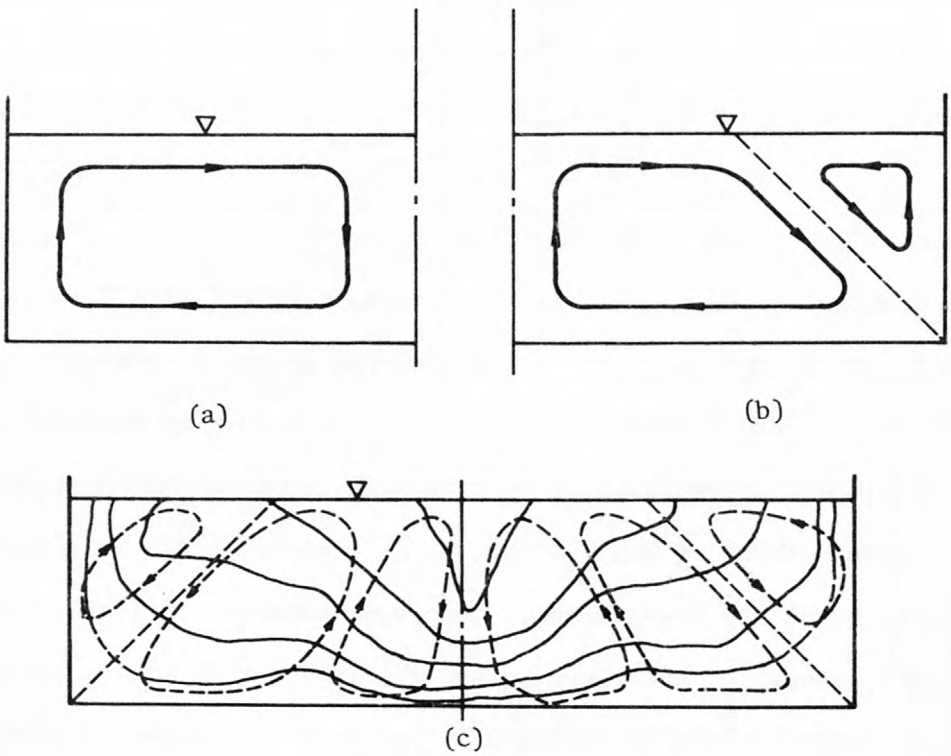

Figure 3.--Some proposed secondary current patterns in open channels.

d. For a strongly unsymmetrical cross section, one single stable secondary spiral exists.

Vito A. Vanoni (1946) when working with sediment transport in a flume noted that the sand seemed to be transported in streaks along the bottom. He noted three symmetrically spaced streaks occurring in the center portion of the flume and minor streaks occurring along the corners. He concluded that these streaks were the result of secondary currents but he also believed that the secondary currents were caused by the unequal sediment distribution across the flume. Vanoni's width to depth ratio was approximately 6 and the walls were slightly smoother than the floor. J. W. Delleur and D. S. McManus (1959) suggested that Vanoni's channel had four major spirals with alternating directions of rotation and with a downdraft area at the centerline of the channel. The writer agrees with their pattern qualitatively except that it should be modified by the addition of minor spirals along the walls as shown in Figure 3-c. Delleur and McManus made mean cross sectional velocity distribution measurements in a small rectangular flume. Their flume had hydraulically smooth walls and floor and their width depth ratio was approximately 6.9. Some of their measured isovels are shown in Figure 3-c, also shown in Figure 3-c are secondary current lines as proposed by the writer based on the analysis proposed by Chiu.

4. Mixing Due to Secondary Currents

Secondary currents have long been considered a factor in the vertical mixing process. However estimates of the importance of secondary currents on the measured concentration profiles vary. Some consider it

as possibly the main cause of sediment suspension such as Rao and Seetharamiah (1967, p. 473) and Leliavsky (Chiu and McSparran, 1966, p. 58). Some consider it as a primary factor in explaining the difference between measured equilibrium concentration profiles and those predicted from two dimensional flow assumptions (Nemenyi, 1946, p. 123). Finally some (Vanoni, 1946, p. 127) consider it only of minor importance. Chao-Lin Chiu and J. E. McSparran (1966) have analyzed the effects of secondary currents on the concentration in the corner regions of a rectangular channel. The results of this analytical and experimental study indicates that secondary currents have a remarkable effect on the pattern of the isopleths of suspended sediment in a corner.

It is the purpose of the next few pages to shed some additional light on the effect of secondary currents on the vertical concentration distribution. The general three dimensional conservation of mass equation (Equation 6) together with reasonable assumptions will be used to infer the effect of secondary currents on the vertical transfer process. The vertical particle velocity, v_p, is equal to the vertical stream velocity minus the particle fall velocity in a turbulent fluid (V_{ST}). It has been found experimentally that the x and z components of the particle velocity are nearly equal to the x and z components of the fluid velocity (Elder, 1959, p. 557) at least for reasonably small particles.

Unfortunately, too little is known about the secondary circulation in open channels to solve Equation 6 in the general case. In order to reduce Equation 6 to a more tractable form the following restrictions are imposed:

a. Quantities will be averaged over the entire width of the channel.

b. Uniform flow and steady-state equilibrium diffusion so that the concentration is independent of x.

c. The turbulent fall velocity is constant.

To accomplish simplification by space averaging the following quantities are defined:

$$\left.\begin{aligned} \overline{\overline{C}} &\equiv \frac{1}{W}\int_W c\, dz \\ \frac{\partial \overline{\overline{c}}}{\partial y} &\equiv \frac{1}{W}\int_W \frac{\partial c}{\partial y}\, dz \\ \overline{\overline{\varepsilon}}_\Gamma &\equiv \frac{1}{W\,\frac{\partial \overline{\overline{c}}}{\partial y}}\int_W \varepsilon_\Gamma \frac{\partial c}{\partial y}\, dz \end{aligned}\right\} \qquad (8)$$

where W is the width of the channel. With the above restrictions Equation 6 can be averaged over the width of the channel to obtain

$$0 = \frac{1}{W}\int_W \frac{\partial}{\partial y}\left(\varepsilon_\Gamma \frac{\partial c}{\partial y} + V_{ST}\, c\right) dz - \frac{1}{W}\int_W \frac{\partial}{\partial y}(cv)\, dz + \frac{1}{W}\int_W \frac{\partial}{\partial z}\left(\varepsilon_\Gamma \frac{\partial c}{\partial z} - wc\right) dz \qquad (9)$$

The last term is zero because w and $\varepsilon_\Gamma \frac{\partial c}{\partial z}$ are identically zero at both boundaries. The derivative of the first two terms can be taken out of the integrals by use of Leibnitz's Rule. Integrating and using the space averaged definitions in Equation 8 one obtains

$$0 = \frac{\partial}{\partial y}\left[\overline{\overline{\varepsilon}}_\Gamma \frac{\partial \overline{\overline{c}}}{\partial y} + V_{ST}\,\overline{\overline{C}} - \frac{1}{W}\int_W cv\, dz\right]. \qquad (10)$$

Now integrating Equation 10 from some arbitrary depth to the surface one obtains

$$0 = \bar{\bar{\varepsilon}}_{\Gamma} \frac{\partial \bar{\bar{c}}}{\partial y} + V_{ST} \bar{\bar{C}} - \frac{1}{W} \int_{W} cv \, dz \tag{11}$$

where all terms are evaluated at this arbitrary depth because the total transport across the surface must be zero.

The last term in Equation 11 is an expression for the vertical flux of sediment per unit length of channel due to the vertical component of the secondary circulation. When one recalls that

a. The vertical mixing due to secondary currents is directly dependent on the vertical concentration gradient (Dobbins, 1944, p. 630),

b. The definition of a turbulent diffusion coefficient depends on the time averaged flux of dispersant due to turbulent velocity fluctuations

$$\varepsilon_{\Gamma} \frac{\partial c}{\partial y} \equiv \overline{-v'c'} = \frac{-1}{T} \int_{o}^{T} v'c' \, dt, \tag{3}$$

c. The values in the last term of Equation 11 could be divided into their space averaged values and their deviations from these values so that this term could be written as

$$\frac{1}{W} \int_{W} cv \, dz = \frac{1}{W} \int_{W} v'c' \, dz + \frac{1}{W} \int_{W} \bar{v} \, \bar{c} \, dz$$

where here the primed values denote deviations from the space averaged mean and the barred values denote the space averaged values. The last term in this expression must be zero from

continuity considerations. Keeping these considerations in mind it seems reasonable to define a secondary current "diffusion" coefficient as

$$\varepsilon_s \frac{\partial \overline{\overline{c}}}{\partial y} \equiv - \frac{1}{W} \int_W vc \, dz \quad . \tag{12}$$

The following observations are to be noted about this "diffusion" coefficient.

a. The coefficient has meaning only when all quantities have been averaged over the entire width of the channel,

b. Like the Boussinesq mass transfer coefficient, it has a constant value only after a relatively long diffusion time (Hinze, 1959, p. 303),

c. Its value is a function of the relative depth as well as the intensity and patterns of the secondary currents.

The above analysis indicates that the equilibrium sediment distribution is affected by secondary circulation and that the equilibrium diffusion equation could be written as

$$[\varepsilon_s + \overline{\overline{\varepsilon}}_{se}] \frac{\partial \overline{\overline{c}}}{\partial y} + V_{ST} \overline{\overline{C}} = 0 \tag{13}$$

where ε_{se} is used to denote the vertical turbulent transfer coefficient for sediment particles. It is again pointed out that Equation 13 applies only when all quantities have been averaged across the entire width of the channel as indicated by Equation 8. It is also pointed out that in general Equation 6 cannot be reduced to the two dimensional equation even for the equilibrium case unless one assumes that the effects of the secondary currents are negligible.

Turbulent transfer is basically a convective process. However by averaging over an interval of time (large compared to the integral time scale of the turbulence) then the turbulent transfer process can be analyzed as a diffusive process through an analogy with molecular diffusion. This section has merely extended this analogy so that one is averaging over an area large compared to the scale of the secondary cells as well as averaging over a time which is long compared to the integral time scale of the turbulence.

A crude estimate of the relative importance of secondary currents on the sediment suspension process can be obtained by making the following assumptions:

a. An equilibrium steady state flow condition.

b. The turbulent fall velocity, the sediment transfer coefficient (ε_{se}) and the absolute value of the vertical component of the fluid velocity are independent of z.

c. The two dimensional steady state diffusion equation applies to the local concentration profiles.

d. The channel can be divided into two regions, one where the secondary currents are up, that is the updraft regions, and the other where the secondary currents are down.

With these assumptions the expression

$$\varepsilon_s = \frac{\varepsilon_{se} \left| v \right|^2}{V_{ST}^2 - \left| v \right|^2} \tag{14}$$

can be derived. This expression can only be valid for values of V_{ST} which are much larger than the vertical components of the secondary currents.

The strength of secondary currents are often expressed as the angle that the fluid particle paths make with the direction of the primary flow. This angle is usually small, thus the ratio of the secondary velocity divided by the primary velocity can be expressed as being equal to tan θ or simply θ since the angles are always small. Typical values of θ have been estimated to be between 0.5 and 3 degrees (Nemenyi, 1946, p. 117), (Liggett, et. al., 1965, p. 109), (Tracy, 1965, p. 20), (Ciray, 1967, p. 410) with an average of about 1.5 degrees. The absolute value of the secondary current velocity used in the Equation 14 should probably be less than U tan 1.5° because it should represent some sort of space averaged value. Figure 4 shows the variation of the ratio of the secondary current "diffusion" coefficient to the sediment transfer coefficient as computed from Equation 14. In order to solve Equation 14, values of $\frac{U}{u_*} = 7.0$ or a Chezy coefficient of about 40 and a value of $\kappa = 0.4$ were assumed. The terms U, u_*, and k represent the mean velocity, shear velocity, and Von Karman coefficient respectively. It can be seen from Figure 4 that any value of the vertical transfer coefficient computed from the equilibrium sediment profiles would be larger than ε_{se} if the space averaged concentration profile were used. If point concentration profiles were used the value of ε_{se} would depend on the position of the profile relative to the secondary cell. The writer believes that this is the effect noted by Vanoni (1946, p. 97) when he found about a 30% disagreement between the vertical sediment transfer coefficient computed from profiles measured in different positions across the flume.

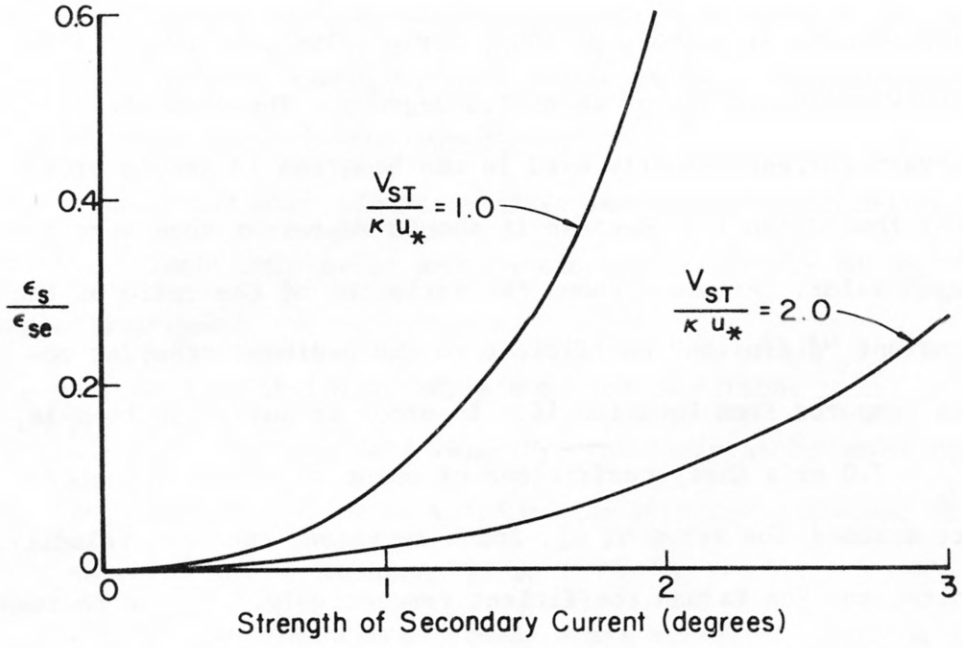

Figure 4.--Secondary current "diffusion" coefficient estimated from equation 14.

C. Particle Fall Velocity

1. The Sediment Particle

The entrainment, transportation and subsequent deposition of a sediment particle depends not only on the characteristics of the flow involved, but also on the properties of the sediment itself. In the following few pages an attempt will be made to cover some of the most important properties that are related to turbulent transfer.

Because the size and shape of the grains making up a sediment vary over wide ranges, it is meaningless to consider in detail the properties of an individual particle. It is natural to resort to statistical methods to describe these properties. The statistical methods used in this investigation were presented by G. H. Otto (Task Committee, 1963, p. 98).

The most important property of the sediment particle or grain is its size. The settling velocity of the particle directly characterizes its reaction to flow and ranks next to size in importance. It has been found convenient to group sediments into size classes or grades according to a scale. The scale chosen in this investigation is the one proposed by the sub-committee on Sediment Terminology of the American Geophysical Union (Task Committee, 1962, p. 80), which is an extension of the Wentworth scale.

Natural sediment particles are irregular in shape, therefore, any length or diameter that is to be used to characterize their size should be defined. The definitions used here are the same as those presented by the sub-committee on Sedimentation of the Inter-Agency Committee, Water Resources, (Inter-Agency No. 12, 1957, p. 11).

2. Fall Velocity in a Quiescent Fluid

The simplest shape for which information on fall velocity is available is the sphere. Because natural sediment particles are not spherical, their fall velocity cannot be calculated directly from sphere data. Nevertheless, the relationships developed for the fall velocity of a sphere are found to be quite useful.

For a sphere of diameter D, fall velocity V_{sq}, and for values of the particle Reynolds number $R_p = \frac{V_{sq}\, D}{\nu}$ less than approximately 0.1, the fall velocity is given by Stokes law,

$$V_{sq} = \frac{g\, D^2}{18\, \nu} \left[\frac{\gamma_s - \gamma}{\gamma}\right] \tag{15}$$

where ν and γ are respectively the kinematic viscosity and specific weight of the fluid, g is the acceleration of gravity and γ_s is the specific weight of the sphere. The fall velocity over the entire range of Reynold's numbers, in terms of the drag coefficient C_D is given by

$$V_{sq}^2 = \frac{4}{3} \frac{gD}{C_D} \left[\frac{\gamma_s - \gamma}{\gamma}\right] . \tag{16}$$

The drag coefficient in the Stokes range, i.e., $R_p < 0.1$ is given by $C_D = \frac{24}{R_p}$. For larger Reynold's numbers, C_D is still a function of R_p but it cannot be expressed analytically. However, C_D has been determined experimentally by observing fall velocities in still fluids or by measuring the drag of spheres in wind and water tunnels. A graphical relationship between C_D and R_p can be found in almost any basic fluid mechanics textbook.

Sediment grains are never truly spherical and their shape varies over wide ranges. The Subcommittee on Sedimentation of the Inter-Agency Committee on Water Resources (Inter-Agency, No. 12, 1957, p. 24) gives

graphs showing the relationship between the fall velocity, nominal diameter and the Corey shape factor for naturally worn quartz particles. It can be seen from these graphs that the effect of the particle shape becomes progressively less as the particle velocity decreases towards the Stokes range.

Stringham (1965) has experimentally studied the fall velocities of disks, cylinders, oblate and prolate spheroids and spheres falling in quiescent fluids for a range of R_p between 10 and 100,000. He found that the stability of the motion depended on particle shape. The spheres were the most stable and the disks were the least stable. The onset of instability causes an increase in the drag on the particle.

Fall velocities are usually measured by observing individual grains settling in a column of still fluid. In making such measurements, care must be exercised to use containers that are large enough so that the confining effect of the walls on the fluid around the grain is negligible. The Task Committee on Preparation of Sedimentation Manual (Task Committee, 1962, p. 96) has given curves which allow the effect of using a fall column which is too small on the measured fall velocity to be evaluated. These curves and the results of Francis and Monroe (Camp, 1946, p. 899) show that if the particle diameter is less than 1% of the fall column diameter, then the resulting error should be insignificant.

The fall velocity considered above is for a single particle falling in an infinite fluid. The descent of each particle creates a velocity field throughout the fluid. From continuity the downward motion of the particle and the nearby fluid must be compensated for by an upward motion in the other regions of the fluid. If a suspension is not

distributed uniformly throughout the field the resultant fall velocity of a group of particles can greatly exceed that of a single particle, because the compensatory upward flow can occur in regions where there are few particles. The phenomena of particles falling as a group will be called the group settling effect. On the other hand, if the particles are uniformly distributed throughout the fluid each should be retarded in much the same way as a single particle in a cylindrical container (McNown and Lin, 1952). This effect is usually called hindered settling.

There have been many experimental studies of hindered settling (Camp, 1946, p. 899). All experimental studies have shown that the fall velocity of the particles decrease with increasing concentration, but the decrease is small for concentrations less than about 1%. J. S. McNown and Pin-Nam Lin (1952) have studied the phenomena of hindered settling both theoretically and experimentally. They found that theoretically for $R_p > 1.3$ and concentrations greater than 20 ppm that the hindered settling velocity should be greater than the individual particle fall velocity and the effect should increase with increasing R_p. The explanation that they give for this effect was that a falling particle tends to retard those particles below it and increase the fall velocity of those above it. As R_p increases the particle influence extends considerably further behind it than in front of it. They also found that for larger concentrations the hindered settling velocities were less than the single particle settling velocities and the magnitude of the effect varied as a first approximation with the cubed root of the concentration. Most experiments on hindered settling have been on particles within or near the Stokes range.

W. H. Bradley (Loyacano, 1967, p. 25) investigating small particles in the Stokes range, found that vertical density currents were formed which carried groups of particles downward much more rapidly than individual particles would fall. J. N. Loyacano, (1967) found that sediment (fine to medium sand) fell out of suspension in an open channel flow much faster than would be predicted from the use of quiescent fall velocity. He attributed this in part to the way the sediment was injected which was to simulate an instanteous line source at the water surface. Loyacano conducted tests in quiescent fluid which indicated that the group fall velocities could be as much as 300% larger than the single particle fall velocities, at least initially, and that the group fall velocity decreased toward the quiescent fall velocity of a single particle as the particles dispersed. It was also noted that the group fall velocity increased with concentration.

3. Fall Velocity in a Turbulent Fluid

Very little theoretical or experimental work has been performed on the effects of turbulence on the fall velocity of a particle. Some predictions may be made from studies in quiescent fluids. Recall that Stringham (1965) found that the onset of instability caused an increase in drag. From this one may predict, as is often done, that the turbulent fall velocity should be less than the quiescent fall velocity because the particle should be less stable in a turbulent flow than in a quiescent fluid. However, other seemingly equally convincing arguments can be constructed which show that V_{ST} should be greater than V_{sq}.

Although the results of Loyacano are masked to a large extent by the grouping effect, his data seemed to indicate that $V_{ST} > V_{sq}$.

A. S. Kandala, (1966) made fall velocity measurements on large (1/4 to 3/8 inch) spheres in a turbulent flow and found $V_{ST} < V_{sq}$ for small values of the ratio of the mean stream velocity to the quiescent fall velocity. However, as the mean stream velocity increases to above about seven times the quiescent fall velocity the effect of the turbulence was questionable but data appeared to indicate that V_{ST} exceeds V_{sq} in this region. He also found that increasing the bed roughness increased V_{ST}.

H. W. Ho (1964) found that the fall velocity in an oscillating fluid was significantly lower than in a still fluid. Bouvard, (Zimbelman, 1966, p. 19) by considering the velocity to be made up of a mean and fluctuating component and assuming that the drag coefficient was constant, concluded that $V_{ST} < V_{sq}$. D. D. Zimbelman (1966) found that at least for large particles (3/4 - 1/2 inch) the effect of turbulence was insignificant.

Probably the most general conclusion one can make from the previous work in this field is that more research is needed to determine the effect of turbulence on the fall velocity of sand-sized particles.

D. The Diffusion Process

1. The Transfer Coefficient

The concept of a turbulent transfer coefficient was first used to describe the transfer of momentum in a turbulent flow. O. Reynolds (Hinze, 1959, p. 19) was the first to extend the equation of motion for

a fluid to turbulent flow by averaging. He pointed out the existence of turbulent stresses $\rho \overline{u_i' u_j'}$ which are now often called Reynold's stresses. Upon comparing the role of the turbulent stress terms in the equations of motion with the role of the corresponding stress terms caused by viscosity it is tempting to assume that the turbulent stresses are, like the viscous stresses, proportional to the velocity gradient. This assumption was made by Boussinesq (Hinze, 1959, p. 20) who introduced the concept of "apparent", "turbulence" or "eddy" viscosity such that $-\overline{u_i' u_j'} = \varepsilon_m \left[\frac{\partial u_i}{\partial x_j} + \frac{\partial u_j}{\partial x_i} \right]$. The quantity ε_m is often called the eddy viscosity. Boussinesq assumed that the eddy viscosity was a scalar. However, unless the turbulence is isotropic, the eddy viscosity should have different values in different directions. It has been suggested at various times (Hinze, 1959, p. 21) that the eddy viscosity be taken as a vector quantity. However, this precludes a relationship between the turbulent stresses and the deformation tensor. Newer theories on atmospheric turbulence, such as the theory developed by Ertel (Hinze, 1959, p. 22) suggests that the eddy viscosity is more correctly described as a second order tensor.

For application to open channel flow, it has generally been assumed that the off-diagonal terms of the eddy viscosity tensor are zero. In most open channels the flow is very turbulent so that the viscous stresses can be ignored except very near the boundaries. In this case the shear stress can be represented as

$$\frac{\tau_{ij}}{\rho} = -\overline{u_i' u_j'} = \delta_{kj} \varepsilon_{mkj} \left[\frac{\partial u_i}{\partial x_j} + \frac{\partial u_j}{\partial x_i} \right] \qquad (17)$$

where τ_{ij} is the stress in the i^{th} direction acting on an elementary area which is perpendicular to the j^{th} coordinate direction and ρ is the fluid density.

With the simplifications indicated in Equation 17, Equation 4 is valid for the transfer of momentum as well as any scalar quantity. It is reasonable to ask whether the transport process for different quantities such as momentum, heat, matter, discrete particles or turbulent energy can be analogous. It will be understood that the processes are analogous if the transfer coefficients described by Equation 3 are proportional and that the same proportionality applies throughout the entire flow field.

2. Turbulent Transfer Analogies

Many phenomenological theories have been advanced in attempts to relate the turbulent transfer coefficients (momentum, heat, mass, etc) to the flow field or to turbulence. J. O. Hinze (1959, p. 277) gives an excellent description of most of these theories and the implications of them on the validity of an analogy between the transport of the various quantities.

The most common group among the phenomenological theories are the mixing length theories. All mixing length theories are based mainly on two hypotheses (Hinze, 1959, p. 285), first the analogy with the kinetic theory of gases assuming either momentum or vorticity to be the transferable properties of the fluid particles and second the hypothesis according to which the mixing length depends on the flow pattern. Different theories give different results relative to the validity of

the analogy. However, one may be led to conclude that the analogy between mass and momentum transfer is true at least as a first approximation. This conclusion does not extend, however, to large discrete particles.

The turbulent transfer coefficients defined by Equations 3 and 17 are often called Boussinesq transfer coefficients. The ratios of various Boussinesq transfer coefficients have also been given names. For example, the ratio of the momentum to energy transfer coefficients is often called the turbulence Prandtl number (Pr) and the ratio of momentum to mass transfer coefficients is often called the turbulence Schmidt number (Sc). Hinze (1959, p. 298) states that the ratio of momentum to heat transfer is far from constant. W. M. Rohsenow and H. Y. Choi (1961, p. 186) state that the measured values of the Prandtl number range from 0.6 to 1.1. Hinze (1959, p. 298) states that the Schmidt number should be approximately constant.

For the condition where the transfer coefficient is a scalar quantity and constant throughout space, as well as the mean velocity being constant throughout space, and from an analogy with molecular diffusion (Kalinske and Pien, 1943, p. 531) (Frenkiel, 1953, p. 100) the transfer coefficient can be described by

$$\varepsilon_{\Gamma} = 1/2 \frac{d\overline{Y}^2}{dt} \tag{18}$$

where Γ is some property which adheres to each fluid particle during its motion, Y is the distance traveled by any one particle in time t, and $\overline{Y}^2$ is the mean square value of the observed values of Y for a large number of particles. One could imagine this situation would be true in a homogeneous turbulence.

The theory of diffusion by continuous movements of masses of fluid in a homogenous turbulence has been developed by G. I. Taylor (1921) in terms of the Lagrangian correlation coefficient (R_L) of the velocities in a specified direction of a tagged fluid particle. Taylor's result was

$$\frac{d\overline{Y^2}}{dt} = 2\,\overline{v_L'^2}\int_o^t R_L(\xi)d\xi \tag{19}$$

where v_L is the particle velocity. For very short times it is known that the Lagrangian correlation coefficient (R_L) is nearly unity. Therefore, for very short times

$$\frac{d\overline{Y^2}}{dt} = 2\,\overline{v_L'^2}\;\; t\;. \tag{20}$$

For very long times the Lagrangian correlation coefficient approaches zero and $\int_o^t R_L(\xi)d\xi = \Lambda_L$, where Λ_L is the Lagrangian integral time scale. For long times then

$$\frac{d\overline{Y^2}}{dt} = 2\,\overline{v_L'^2}\,\Lambda_L\;. \tag{21}$$

If one accepts the validity of Equation 18, then it can immediately be seen that a constant transfer coefficient exists only after a diffusion time which is long compared to the Lagrangian integral time scale of turbulence. It must be remembered, however, that the analogy of turbulence diffusion to molecular diffusion would be very questionable if the turbulence were not homogeneous in the direction of transfer.

It is quite probable that there is a basic relationship between the Lagrangian turbulence characteristics and the transfer coefficients, even for non-homogenous flow fields. Thus it is not surprising that C. L. Pien (1941) and others have found that Taylor's theory describes the

diffusion in a shear flow at least qualitatively. Another conclusion which can be derived from Taylor's theory is that the gradient assumption for Equation 3 is invalid for short diffusion times which may be analogous to extremely sharp concentration gradients.

3. The Mass Transfer Coefficient

The turbulent mass transfer coefficient (ε_d) as used in this discussion will refer to the transfer of infinitely small particles which have no hydrodynamic effect on the flow conditions and only serve to tag individual fluid particles. The transfer of discrete particles must affect the flow field, at least in the microscopic sense. For this reason transfer of discrete particles will beconsidered as a separate mass transfer process. The Schmidt number as used in this paper will be defined as the ratio of the momentum to mass transfer coefficients. It will be assumed that the analogy between momentum, and mass transfer is complete enough that a single Schmidt number averaged over the entire flow field will have some significance.

There have been relatively few actual measurements of the vertical component of the mass transfer coefficient in open channel flow.

E. R. Holley and J. C. Schuster (1967) report measured values of the radial component of the mass transfer coefficient for flow of water in a pipe. The average of 41 measurements indicates a Schmidt number of 1.28 with extreme values ranging from 0.87 to 2.4.

Pien (1941) has measured the rate of spread of a solution from a point source in an open channel flow. By assuming Equation 18 to be valid in an open channel flow, he was able to compute the mass transfer coefficient. He found the vertical mass transfer coefficient

to be a maximum at about mid-depth and to decrease towards zero at the floor. The coefficient did not seem to approach zero at the surface. Because of his small width-to-depth ratio (approximately 1.5 and 4.5) he did not compute the momentum transfer coefficient. Assuming a logarmithic velocity distribution and a linear shear stress distribution, it can be shown (Sayre, 1968 , p. 12) that

$$\varepsilon_{my} = \kappa Y_N u_* (1-\eta) \eta \qquad (22)$$

where η is the relative depth and Y_N is the depth. Then the maximum value of the momentum transfer coefficient in Pien's channel would have been $\varepsilon_{my} = 0.25 \kappa Y_N u_*$. Using this expression with $\kappa = 0.4$, Pien's measurements indicate Schmidt numbers of 1.1 and 1.5 (based on mid-depth values) for the wide and narrow channels respectively.

Al-Saffar (1964) has made measurements of the vertical component of the mass transfer coefficient in an open channel flow. His basic approach is considerably more sound than any approach tried so far. He established an approximately two dimensional uniform flow, injected a continuous line source of sodium chloride on the surface of the flow, then measured vertical concentration profiles on the centerline at several distances downstream of the source. Neglecting secondary currents, and for a dispersant which has zero fall velocity, Equation 6 reduces to

$$u \frac{\partial c}{\partial x} = \frac{\partial}{\partial y} \left[\varepsilon_d \frac{\partial c}{\partial y} \right].$$

Integrating this equation from some particular depth to the surface it becomes

$$\int_y^{Y_N} u \frac{\partial c}{\partial x} \, dy = \int_y^{Y_N} \frac{\partial}{\partial y} \left[\varepsilon_d \frac{\partial c}{\partial y} \right] dy \quad \text{or}$$

$$\frac{\partial}{\partial x}\int_{y}^{Y_N} u\ c\ dy = \varepsilon_d \frac{\partial c}{\partial y}\bigg|_{Y_N} - \varepsilon_d \frac{\partial c}{\partial y}\bigg|_{y} \quad . \qquad (23)$$

The quantity $\varepsilon_d \frac{\partial c}{\partial y}$ is the net flux of the dispersant across any level; at the surface this must be zero.

Al-Saffar evaluated the left side of the Equation 23 from the measured concentration profiles by assuming that the velocity was constant in the vertical. He then defined the distance between the measured concentration profiles as Δx and assumed that he could approximate the left hand side of Equation 23 as

$$\frac{\partial}{\partial x}\int_{y}^{Y_N} u\ c\ dy \approx \frac{U}{\Delta x}\left[\int_{y}^{Y_N} c\ dy\bigg|_{x+\Delta x} - \int_{y}^{Y_N} c\ dy\bigg|_{x}\right]$$

where Δx was approximately 2-3 normal depths and U is the mean stream velocity. For fully developed uniform open channel flow the transfer coefficient is not a function of x. He evaluated the concentration gradient at various depths y by assuming it was the average of the gradients from the two measured concentration profiles. He then solved for the transfer coefficient from Equation 23. Al-Saffar did not measure the velocity distribution in the vertical but assumed that the Von Karman universal constant was 0.4 and that a logarmithic velocity distribution existed. From this he could compute the theoretical momentum transfer coefficient from Equation 22. In his experiment the mean value of the measured transfer coefficient agreed very nearly with his assumed momentum transfer coefficient. The measured distribution of the mass transfer coefficient also agreed fairly well with the theoretical distribution of the momentum transfer coefficient, although he did find that ε_d was quite a bit less than ε_m at mid depth. The basic

approach used by Al-Saffar is sound. However, many of the details of his experiment and analysis seem to have been very questionable.

4. The Mass Transfer of Discrete Particles

Since the turbulent transfer of discrete particles is considerably different from the turbulent transfer of other quantities, such as fluid mass or momentum one should first justify to some extent at least the existence of a transfer coefficient, that is, the validity of Equation 3. H. E. Hurst and Hunter Rouse (Task Committee, 1963, p.55) have shown that a transfer coefficient does describe the turbulent transfer process for a steady state homogenous suspension of sand in a turbulence tank. W. E. Dobbins (1944) has shown that Equation 5 describes an unsteady sediment diffusion process in the turbulence tank similar to the one used by Rouse. The equation has had little verification in open channel flow except for the equilibrium transport case, other than that given by Loyacano (1967) and Sayre (1968).

Determination of the variations of the sediment transfer coefficient in the vertical has been very difficult and the few measured distributions that have been presented are open to some question. Equation 6 applied to a steady state equilibrium transport of sediment in a two-dimensional open channel takes the form $\varepsilon_{se} \frac{\partial c}{\partial y} - v_p c = 0$. It is often assumed that the vertical particle velocity is equal to the quiescent fall velocity of the particle. If this is assumed then Equation 6 becomes

$$V_{sq}\, c + \varepsilon_{se} \frac{\partial c}{\partial y} = 0. \qquad (24)$$

Equation 24 was first derived by Wilhelm Schmidt (Dobbins, 1944, p. 632).

The vertical distribution of sediment concentration can be computed from Equation 24 if the variation of ε_{se} is known in the vertical. The assumption is often made that

$$\varepsilon_{se} = \alpha \varepsilon_m \tag{25}$$

where α is a constant. The variation of the momentum transfer coefficient can be computed once a velocity and shear distribution in the vertical have been assumed or determined (See Equation 17).

The Von Kármán universal velocity defect law (Vanoni, 1946, p. 70) has been given as

$$\frac{u - u_{max}}{u_*} = \frac{1}{\kappa} \ln \eta \tag{26}$$

where u is the local velocity, u_{max} is the maximum (surface) velocity. For a linear shear stress distribution, Equation 17 and 26 give a parabolic distribution of ε_m as indicated in Equation 22.

If a parabolic velocity distribution of the form (Sayre, 1968, p. 8)

$$\frac{u - U}{u_*} = \frac{1}{\kappa} [-3\eta^2 + 6\eta - 2] \tag{27}$$

is assumed then Equation 17 and a linear shear stress distribution give a uniform distribution of the momentum transfer coefficient. The difference between the assumed velocity distributions above may be very slight, however, the difference in the corresponding distributions of momentum transfer coefficients is very large.

Since a logarathimic velocity distribution is usually assumed for open channels, the parabolic distribution of sediment transfer coefficient

is also usually accepted. Inherent in the use of a parabolic distribution of sediment transfer coefficient are the assumptions:

a. That the momentum transfer coefficient is proportional to the fluid mass transfer coefficient.

b. That the fluid mass transfer coefficient is proportional to the sediment transfer coefficient.

c. That the velocity profile is logarithmic.

d. That the shear stress distribution is linear.

For a parabolic distribution of the momentum transfer coefficient Equation 24 gives a concentration distribution of

$$c/C_a = \left[\frac{1-\eta}{\eta} \quad \frac{a}{Y_N-a}\right]^Z \tag{28}$$

where $Z = \frac{V_{sq}}{\kappa u_*}$ which is often called the Rouse Number, a is an arbitrary reference distance above the bed and C_a is the concentration at y = a. Equation 28 plots as a straight line on log paper as shown in Figure 5. For a uniform distribution of the sediment transfer coefficient Equation 24 gives

$$c/C_a = \exp\left[-\frac{V_{sq}}{\varepsilon_{se}}(y-a)\right] . \tag{29}$$

Most field and flume data plot a reasonably straight line on a graph such as that shown in Figure 5 (Task Committee, 1963). However, the value of Z frequently must be adjusted to fit the data, particularly for values of Z less than 0.7 to 1 (Hubbell and Matejka, 1959). The fact that field and laboratory data plot as a straight line on a graph such as that shown in Figure 5 is sometimes (Task Committee, 1963, p. 62) given as additional justification of the validity of both Equations 25 and 28. However, it is interesting to note that Equation 29 also plots

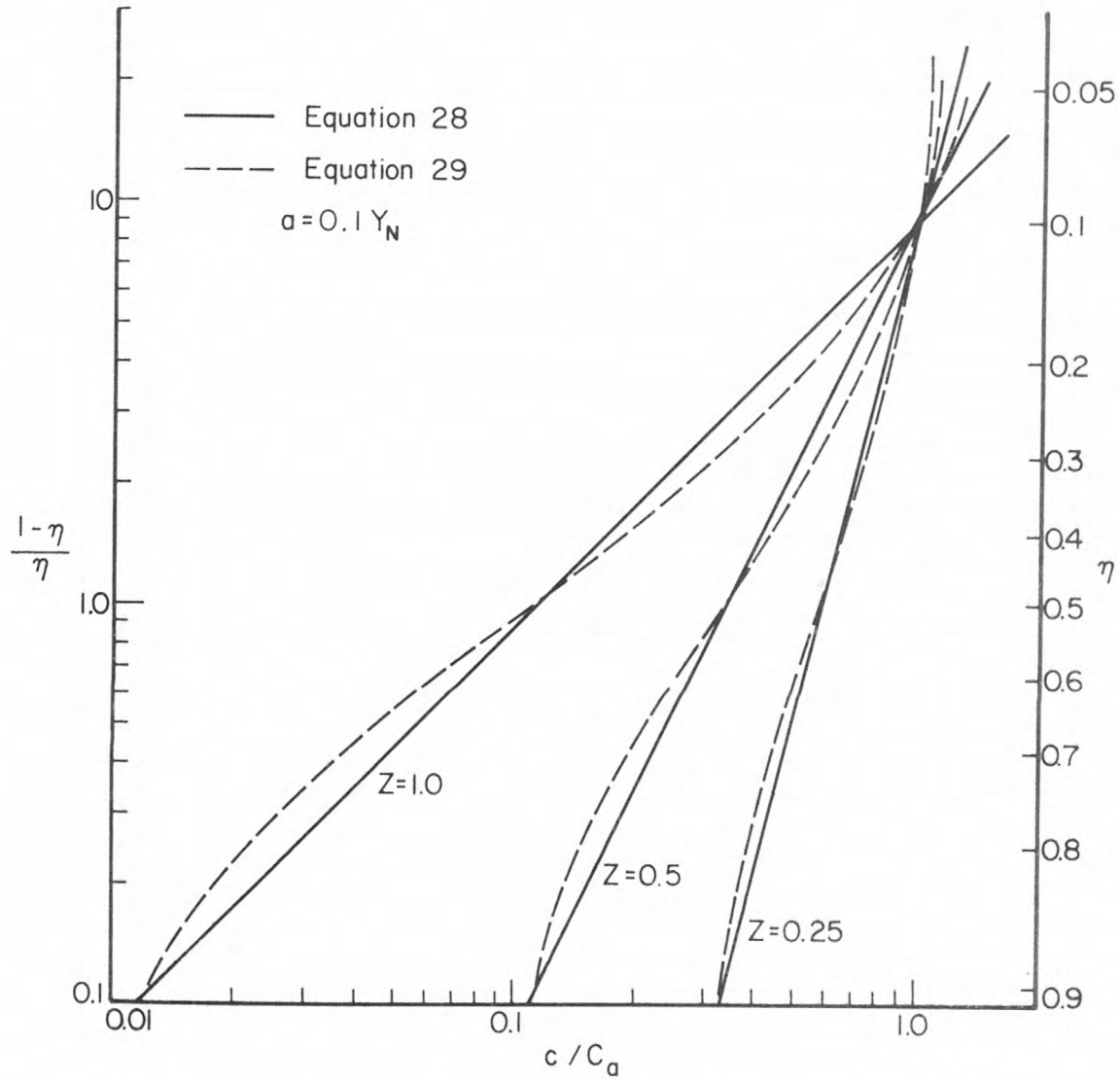

Figure 5.--Equilibrium sediment concentration distributions.

as nearly a straight line on Figure 5, even though the assumed distribution of the transfer coefficient used in Equation 29 is drastically different from that used in Equation 28. Both Equations 28 and 29 have been plotted on Figure 5 for various values of Z.

Considering the above remarks and neglecting the effects of secondary currents, it would still appear that very little can be said about the distribution of the sediment transfer coefficient from equilibrium concentration profiles except possibly for very large values of Z.

Vanoni (1946) has made measurements directly on the concentration profiles in the equilibrium case and found that ε_{se} appeared to be distributed approximately parabolically.

It will be assumed in this paper that if ε_{se} is proportional to ε_m it is only because ε_d is proportional to ε_m. It has been shown previously that this is approximately true. From this point on ε_{se} will be related to ε_d, but indirectly this is also relating it to ε_m.

M. R. Carstens (1952) has advanced one of the most convincing arguments for describing the relationship between ε_d and ε_{se}. Carstens has shown that the sediment particles will lag rectilinear velocity oscillations and that the length of the sediment particle excursion will be less than that of the fluid particles if ρ_s is greater than ρ. Carstens then reasoned from the mixing length theories that ε_{se} should be less than ε_d if $\rho_s > \rho$. He has also shown that the reduction in ε_{se} should increase with the mass of the particle and with the frequency of the turbulent fluctuations.

G. T. Csanady (1963) has studied the dispersion of heavy particles in air. He reasoned that ε_{se} should be less than ε_d because the heavy particles tend to fall through the turbulent eddies, thus the Lagrangian particle correlation should drop to zero faster than the fluid particle correlation. As a direct result of the smaller sediment particle correlation, Carsten's (1952) analysis, and Taylor's theory, it is seen that $\varepsilon_{se} < \varepsilon_d$.

All of the above theories conclude that $\varepsilon_{se} < \varepsilon_d$. S. R. Singamsetti (1966) is one of the very few who have advanced a theory explaining why ε_{se} should be greater than ε_d. He reasoned that in a turbulence composed of eddies that the sediment would be thrown to the outside of the eddy which would increase the effective particle mixing length and the particles rate of diffusion. This theory seems logical if the sediment particles are small in comparison to the size of the eddies and if the rotation of the eddies is strong enough to cause the particle's centrifugal force to be significantly greater than that of a fluid particle.

Vanoni (1946) has made measurements of the turbulent transfer coefficient in open channel flow. The channel that he used had the bottom roughened by gluing sand grains to the floor, thus no significant separation occurred at the boundaries. He found that $\varepsilon_{se} \approx \varepsilon_m$ for .160 mm sand and that $\varepsilon_{se} > \varepsilon_m$ by about 20% for the .100 mm sand. His results are somewhat questionable because of the rather strong secondary currents which he noted during the runs and because he used the quiescent fall velocity in determining the sediment transfer coefficient. Since secondary currents would cause a more uniform concentration in the vertical and

therefore a larger apparent value of ε_{se} it is possible that if this effect were compensated for, then Vanoni's results would indicate that $\varepsilon_{se} \leq \varepsilon_m$ and that ε_{se} decreases with increasing particle size as predicted by Carstens.

V. I. Matyukhin and O. N. Prokof'yev (1966) have shown that the vertical component of ε_{se} tends to decrease with increasing particle size for a wind induced turbulence in water.

Singamsetti (1966) found that the radial diffusion of sediment from a submerged sediment laden water jet was much faster (20-50%) than that of momentum. He found that coarse particles diffused more rapidly than fine particles. As previously stated, he reasoned that this increase in the rate of diffusion of sediment particles over that of momentum was due to the sediment particles being thrown to the outside of the eddies.

Measurements in natural channels usually indicate that $\frac{V_{ST}}{\varepsilon_{se}} Y_N > \frac{V_{sq}}{\varepsilon_m} Y_N$ when Equation 28 is fitted to the data. It is rather doubtful that variation in ε_{se} alone will explain this divergence (Einstein and Chien, 1954, p. 3). For example, secondary currents may be quite strong in natural rivers and V_{ST} may not be the same as V_{sq}. Some measurements indicate that the divergence in $\frac{V_{ST}}{\varepsilon_m} Y_N$ is greater for fine material (Hubbell and Matejka, 1959, p. 71) and some indicate that the divergence is greater for coarse material (Einstein and Chien, 1954, p. 3).

It is proposed here that the previously stated theories, even though they contradict one another, all possess some elements of truth, which can be fitted together into a single consistent hypothesis as follows. All particles will be grouped into three basic sizes. The first size group encompasses the Stokes range. These particles very nearly follow

the turbulent velocity fluctuations and will therefore be considered here to have a transfer coefficient nearly equal to that of dye. W. W. Sayre (1968, p. 32) concluded on the basis of available empirical information that this is approximately true for particles less than 0.1 mm in diameter. The second size group includes particles that are so large that they fall without being affected much by the turbulent fluctuations; therefore, they would diffuse very slowly if at all. This is an extreme example of the type of behavior to which Csanady was referring. The third, or intermediate, size group generally coincides more or less with the sand size range. It is this group that is usually of primary concern in suspended sediment transport theories.

It is proposed that in the intermediate size range the type of turbulence is all important in determining the relationship of the sediment transfer coefficient to that of the mass transfer coefficient for marked fluid particles.

All turbulence is probably a result of production, diffusion or decay of vortices within the flow. The analysis of Singamsetti appears logical as long as the fluid particle paths are curved and the density of the sediment particles is greater than the density of the fluid particles. But the effect of the curvature of the fluid particle paths on diffusion should be greatly affected by the size, intensity, and the regularity of orientation of the vortices. Intense, regularly oriented vortices are usually associated with the turbulence generated by a discontinuity in the mean velocity such as occurs with wakes or jets or in any flow with separation.

In flows where the formation of intense regularly oriented vortices is rare, it is believed that the analysis presented by Carstens is reasonably valid. However, in a flow where these kinds of vortices are numerous, such as in a separation zone or in a jet or wake flow, then it is believed that a major part of the transfer can be due to the effect discussed by Singamsetti. In most open channel flows, it is expected that the total sediment transfer is due to a combined action of the processes discussed by Carstens and Singamsetti.

It is believed that the above hypothesis along with the recognition of the existence of secondary currents can explain the apparently divergent results of previous measurements. Two conclusions which follow directly from the above hypothesis are: first, if the bed roughness is not great enough to cause significant separation, then $\varepsilon_{se} < \varepsilon_{d}$ when the effects of secondary currents are accounted for, and second when the bed forms are such that significant separation occurs, such as in dunes in an open channel, then a large value of ε_{se} may be expected.

The previous discussion stated that the transfer of sediment may occur as the result of two possibly different types of processes depending upon the nature of the turbulent field. In the next few paragraphs a kinematic description of the movement of a sediment particle will be proposed which should clarify these two processes and give some insight into the mechanics of the transfer process.

The following terms are defined:

u_s = instantaneous velocity of a sediment particle

$\vec{u}'_{sf} + \vec{V}_{sq}$ = instantaneous velocity of a sediment particle relative to that of the fluid particles surrounding it.

Then it follows that

$$\vec{u}_s = \vec{u} + \vec{u}''_{sf} + \vec{V}_{sq}$$

or

$$\vec{u}_s = \vec{V}_{sq} = \vec{u} + \vec{u}''_{sf}$$

where u is the instantaneous fluid particle velocity. Now u''_{sf} can be divided into two components, the first component (u''_{sft}) is the component of u''_{sf} parallel to the velocity of the fluid particles surrounding the sediment particle, and the second component (u''_{sfr}) is the component of u''_{sf} perpendicular to the velocity of the fluid particles surrounding the sediment particle. Figure 6 illustrates each of these terms. The velocity u''_{sft} is the result of the greater tangential force required to accelerate a sediment particle and u''_{sfr} is the result of the greater centrifugal force required to make a sediment particle follow a curved path.

One has no assurance that u''_{sf} has a zero mean value. In fact, if the fall velocity in a turbulent fluid is different than it is in a quiescent fluid then u''_{sf} does not have zero mean. In order that Reynold's averaging can be performed later, we will define a turbulent fall velocity as

$$\vec{V}_{ST} \equiv \vec{V}_{sq} + \lim_{T\to\infty} \frac{1}{T} \int_0^T \vec{u}''_{sf} dt \qquad (30)$$

and a relative velocity with zero mean as

$$\vec{u}'_{sf} \equiv \vec{u}''_{sf} - \lim_{T\to\infty} \frac{1}{T} \int_0^T \vec{u}''_{sf}\, dt \ . \qquad (31)$$

Now V_{ST} is not necessarily parallel to the acceleration of gravity but some experiments (Elder, 1959, p. 557) have shown that at least for

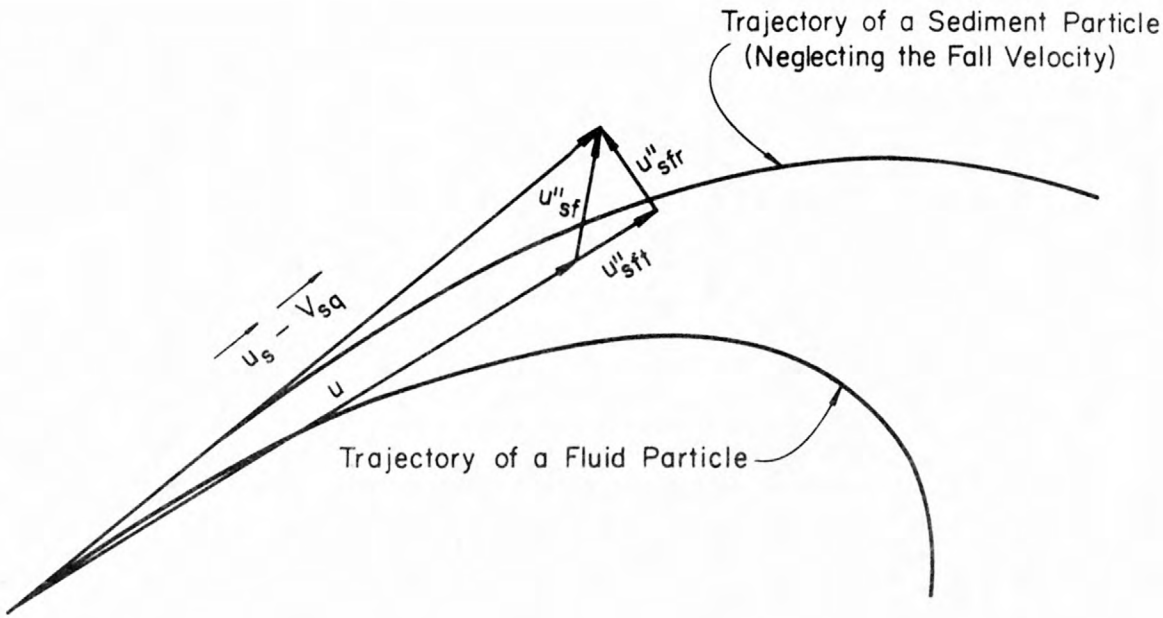

Figure 6.--Relative motions of sediment and fluid particles in turbulent flow.

reasonably small particles, V_{ST} is nearly parallel to g. It will be assumed throughout the rest of this dissertation that V_{ST} is parallel to g. With the above definitions the particle velocity can be expressed, $\vec{u}_s = \vec{u} + \vec{u}'_{sf} + \vec{V}_{ST}$.

It will now be shown how each of these terms is related to the sediment transfer coefficient. Placing the expression for the particle velocity into Equation 2 one obtains

$$\frac{\partial c}{\partial t} + \frac{\partial}{\partial x_i}(u_i\ c) + \frac{\partial(V_{STi}\ c)}{\partial x_i} = -\frac{\partial}{\partial x_i}\left[\overline{u'_{sfti}c'} + \overline{u'_{sfri}c'} + \overline{u'_i\ c'}\right] \quad (32)$$

where u has been divided into the usual mean and fluctuating parts and it is understood here that after averaging u_i and c are the mean fluid velocity and concentration whereas before averaging they represented the instantaneous values. It seems logical to combine the two terms $\overline{u'_{sfti}c'}$ and $\overline{u'_i c'}$ since both u'_{sfti} and u'_i are in the same direction and are interrelated. However $\overline{u'_{sfri}c'}$ derives wholly from the curvature of the fluid particle path lines and is therefore only indirectly related to the other two terms. To preserve the kinematic description the following terms are defined:

$$\varepsilon_{Tj}\frac{\partial c}{\partial x_j} \equiv -\overline{u'_{sftj}c'} - \overline{u'_j\ c'} \quad (33)$$

and

$$\varepsilon_{cj}\frac{\partial c}{\partial x_j} \equiv -\overline{u'_{sfrj}c'} \quad (34)$$

where u'_{sftj} is the component of u'_{sft} in the $j^{\underline{th}}$ direction, u'_{sfrj} is the component of u'_{sfr} in the $j^{\underline{th}}$ direction, ε_{Tj} is the $j^{\underline{th}}$ component of the diffusion tensor which describes the diffusion of sediment due to tangential components of turbulent velocity fluctuations, and ε_{cj}

is the $j^{\underline{th}}$ component of the diffusion tensor which describes the diffusion of sediment due to the curvature of the fluid particle path lines. From Equations 32, 33, and 34, it can be seen that

$$\varepsilon_{se} = \varepsilon_c + \varepsilon_T. \tag{35}$$

Some practical considerations of the variations of the two turbulent sediment transfer coefficients just defined will now be discussed. It is believed that the work of Carstens has some significance in evaluating the value of ε_T. It is further believed that ε_T should be similar to ε_d that is, Equation 25 is valid when $\varepsilon_T >> \varepsilon_c$ and when the frequency spectrum of the turbulence is fairly uniform over the entire flow field. Therefore, ε_{se} should always be less than or equal to ε_d if $\varepsilon_c \simeq 0$. Possibly Eulerian turbulence measurements would be helpful in estimating the value of ε_T. Insofar as Lagrangian turbulent characteristics are related to Eulerian turbulence characteristics, then by Taylor's theory, ε_T should also be related to the Eulerian turbulence measurements.

It is realized that probably all turbulence is the superposition of millions of eddies, however, only when the size of the eddies become large compared to the size of a sediment particle and when their radial accelerations become large is there any significant increase in the scattering of sediment particles due to these eddies. It is suggested that flow separation may be a good index to the existence and significance of the value of ε_c, thus it is believed that the value of ε_c is nearly zero in flows with negligible separation. It is hard to see how Equation 25 has any relevance whatsoever in determining the

distribution of ε_c since ε_c is identically zero for a fluid particle. It seems reasonable that ε_c should be approximately proportional to the radial acceleration of a fluid particle which can be expressed as the eddy peripheral velocity squared divided by the eddy diameter. The eddy diameters should be a minimum and the peripheral velocities a maximum, in the zone of vortex generation. It seems logical, therefore, that ε_c should be a maximum in the zone of vortex generation and decrease very rapidly as the vorticity diffuses into the main body of the flow. Recall that Singamsetti's experiment was conducted entirely in a jet mixing zone where fairly stable ring vortices should be present. Since ε_c can be associated with separation, the size and form of the bed roughness may be very important in determining its value. C. F. Nordin (1968) has made statistical measurements of bed forms in open channels; unfortunately he has not correlated his results with sediment transport.

Chapter III

DESCRIPTION OF THE EXPERIMENT

A. Method of Approach

1. Introduction and Goals

The purpose of this experiment was to measure the turbulent mass transfer coefficient for dye, and to measure the turbulent mass transfer coefficient as well as the particle fall velocity for fine and medium sand in a two dimensional open channel flow. Subsidiary objectives were to compare the value of the various mass transfer coefficients with the momentum transfer coefficient and to compare these transfer coefficients with Eulerian turbulence data and to note any effect of turbulence on the fall velocity of sand.

The general procedure was similar to that used by Al-Saffar (1964), but with certain improvements and modifications. The general procedure was to

a. Inject a continuous line source of dispersant across the channel.

b. Measure the vertical concentration profiles at various points downstream of the injection point.

c. To solve Equation 6 for ε_T and V_{ST}.

2. Simplification of Equations

The conservation equation for a steady uniform open channel flow has been given in Equation 6. It has been pointed out that

a. $u_p = u$

b. $v_p = v - V_{ST}$ where V_{ST} is positive downward

c. $w_p = w$

d. ε_Γ is equal to ε_d for diffusion of dye and

$\varepsilon_T + \varepsilon_c$ for the diffusion of sediment.

With these modifications Equation 6 becomes

$$u \frac{\partial c}{\partial x} = \frac{\partial}{\partial y} \left[\varepsilon_\Gamma \frac{\partial c}{\partial y} + V_{ST} c \right] - \frac{\partial}{\partial y} [cv] - \frac{\partial}{\partial z} [cw]. \tag{36}$$

These experiments involved the steady diffusion from a two-dimensional line source across a steady uniform flow in a flume. The injection of the dispersant was adjusted with respect to z to match the flux of water in the particular vertical, thus insuring that $\frac{\partial c}{\partial z} = 0$. It was at first only assumed that the longitudinal diffusion would have a negligible effect on the vertical concentration profiles. However, later measurements (see Chapter IV - D) proved this assumption to be valid. Measurements were made close to the source and in such transverse positions as to insure that the terms $\frac{\partial}{\partial y} [cv]$ and $\frac{\partial}{\partial z} [cw]$ would have minimal effects on the measured concentration profiles. These terms were ignored in the computations for ε_Γ and V_{ST}. (See the discussion of results for the sampling positions relative to the assumed secondary current patterns.)

Data were normalized by dividing all velocities by the shear velocity and all the distances by the normal depth. Using these scaling parameters, Equation 36 can be written

$$\frac{u}{u_*} \frac{\partial c}{\partial X} = \frac{\partial}{\partial \eta} \left[\frac{\varepsilon_\Gamma}{Y_N u_*} \frac{\partial c}{\partial \eta} + \frac{V_{ST}}{u_*} c \right] \tag{37}$$

where $X = \frac{x}{Y_N}$.

Solution of Equation 37 for ε_Γ and V_{ST} requires that the vertical distribution of the velocity and concentration be known. Since the flow was uniform the velocity distribution in the vertical was of principal

importance; the transverse variation of velocity was also required in order to verify that the flow was approximately two dimensional. Concentration profiles were measured at not less than five different distances downstream of the source.

B. Equipment and Procedure

1. Summary of Procedure

A very brief description of the overall procedure is first given and then a detailed description of the procedure will be presented. The equipment will be described as it is encountered in the detailed description of the run procedure.

The first step in the test procedure was to set up the desired uniform flow conditions in the flume. This was done only once for each of the three flow conditions. All diffusion runs were made before the condition of the flume were changed to the next flow condition. By not adjusting the flume between runs, flow conditions could be reproduced day after day by merely setting the discharge to the desired predetermined value.

After the flume had been adjusted to give the desired uniform flow condition, the details of the flow field were measured. Some of the details of the flow conditions which were measured were:

a. The vertical velocity and turbulence profiles as well as the transverse and longitudinal velocity distributions.

b. The time required for a dispersant to recirculate once through the flume system.

c. The time required from the start of dispersant injection to reach a steady state condition at the sampling locations.

d. The siphon heads required to make the sediment samplers sample the flow at the local mean stream velocity.

After all the necessary background information for a given flow condition had been collected, individual runs were made starting with the diffusion of dye. The typical procedure for conducting a run was as follows:

a. Create uniform flow conditions in the flume.

b. Prepare the dispersant and sampling system.

c. Check the slope, discharge, depth and temperature.

d. Start the injection of the dispersant.

e. Waste the flow through the samplers for a time long enough to insure a steady flow of dispersant.

f. Collect all samples simultaneously except at the last station which was 90' from the source. This sample was collected at a later time, the lag time being computed from the mean stream velocity and the distance of the sample probe from the injection point.

g. Stop injection of the dispersant after all samples had been collected (the length of time between the start of dispersant injection and the time when the last sample was collected was always less than the time required for a dispersant to recirculate through the system).

h. Remeasure the slope, discharge, depth and water temperature.

i. After a sufficient time for the dispersant previously injected to become uniformly distributed throughout the system, but never less than two hours, the procedure from b to h was repeated giving two runs at identical flow conditions. Within a day or two after the run was made the samples were analyzed for concentrations and the results partially analyzed before proceding to the next run.

2. The Flow Conditions

The following are some of the considerations used in designing the experiment.

Since the y component of the transfer coefficient was to be measured, it was desirable to create as nearly a two-dimensional flow condition as possible. The sediment concentration profiles and their rate of change with distance would be required so it was also desirable to keep the depth as large as possible. For this reason the largest flume available (8 ft. wide) was chosen. A width-depth ratio of six was used and the floor of the flume was made very rough in comparison with the smooth walls. It was thought that with these conditions, an approximately two-dimensional flow could be obtained.

Equation 22 shows that the momentum transfer coefficient for a logarithmic velocity profile is proportional to $Y_N u_*$. Since the momentum transfer coefficient is related to the mass transfer coefficient and to some extent to the sediment transfer coefficient, the experiments were performed over as wide a range of $Y_N u_*$ as possible. Considerations of the sampling equipment dictated a constant sixteen inch depth. This left only the shear velocity to vary; three values of the shear velocity were selected. It was also impractical to vary the roughness of the flume.

The minimum slope which could be accurately measured was about .0005. A Froude number of greater than approximately 0.5 was considered undesirable because of the water surface roughness. Therefore, the maximum slope was chosen as about .005. The third flow condition was chosen with a slope which would represent an intermediate flow condition.

The experiments were conducted in an eight foot wide by four foot deep by 200 foot long tilting, recirculating flume. The flume has been described in detail by Loyacano (1967). Longitudinal positions are referred to the flume's stationing which begins with 0 at the head box of the flume and ends with station 200 at the tailgate. The bottom of the flume was roughened with wooden cleats. These cleats were 1 1/16" high and 6" long. The roughness cleats were arranged as shown in Figures 7 and 8. The roughness density and spacing were chosen so as to give the desired flow conditions with the aid of charts and graphs presented by Sayre and Albertson (1963). The cleats were held to the floor with a fiberglass bond.

From the head box the flow entered the flume through several screens. Figure 9 shows these screens in operations for the maximum discharge, i. e. flow condition C. The first twenty-five feet of the flume did not have roughness elements on the floor. At station 30 there was a honeycomb grid made up of twelve inch pieces of 1½" plastic pipe. Figure 10 shows the grid operating with a maximum discharge. For flow condition A, the minimum discharge, an eighteen inch weir was installed at station 25 to serve as a sediment trap. It was found that the weir was inefficient as a sediment trap and that for larger discharges a vortex formed behind the weir which disturbed the downstream flow conditions. After all runs had been completed for flow condition A, the weir was removed.

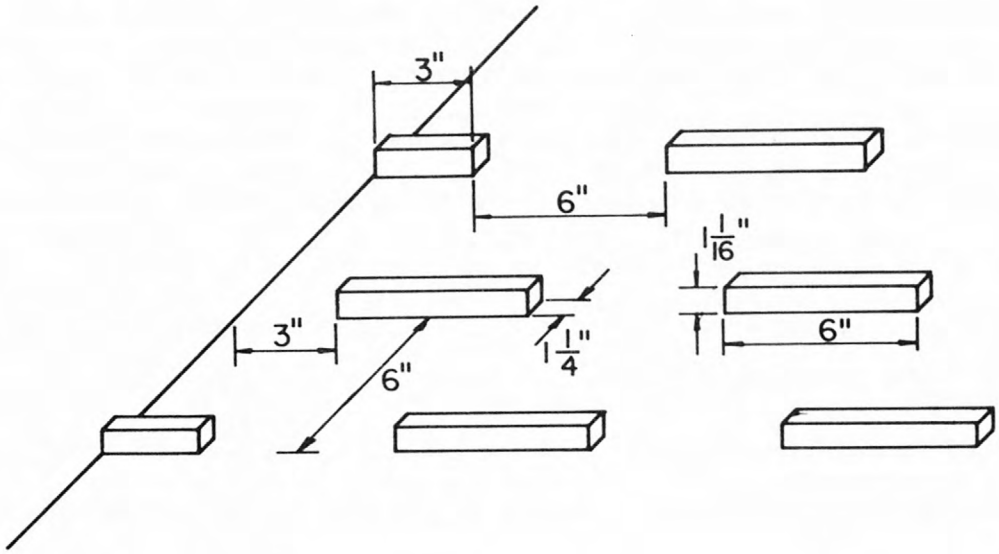

Figure 7.--Arrangement of roughness cleats.

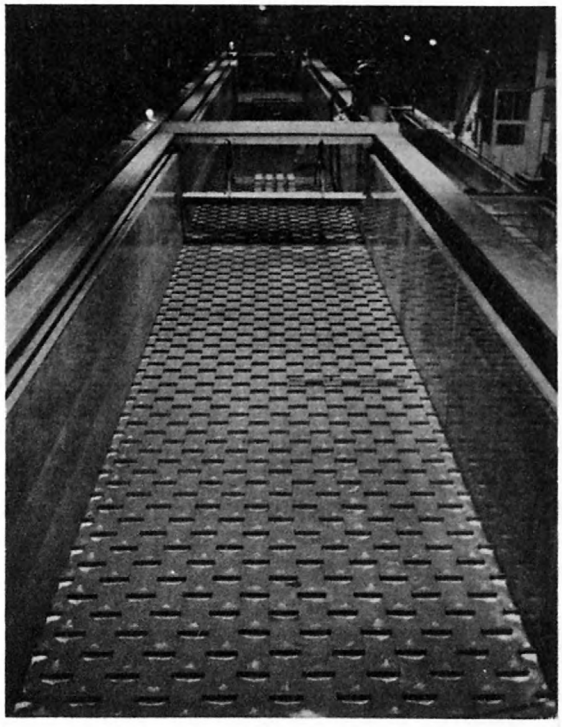

Figure 8.--Flume and roughness cleats.

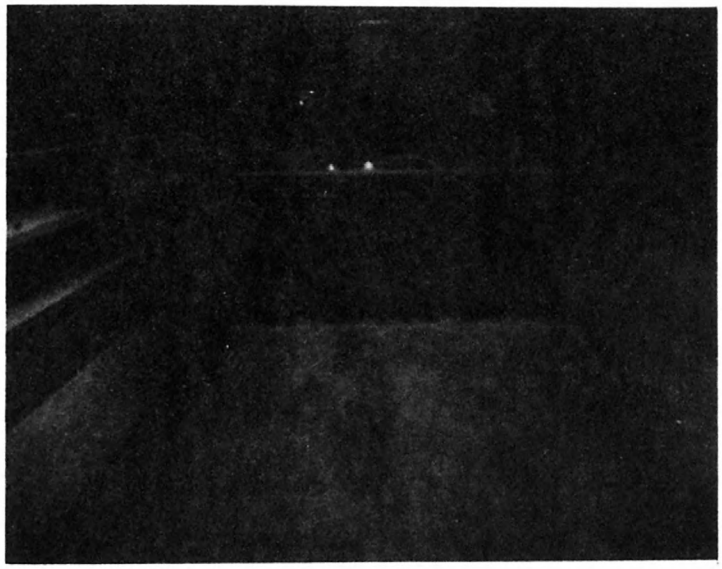

Figure 9.--Entrance screen in operation.

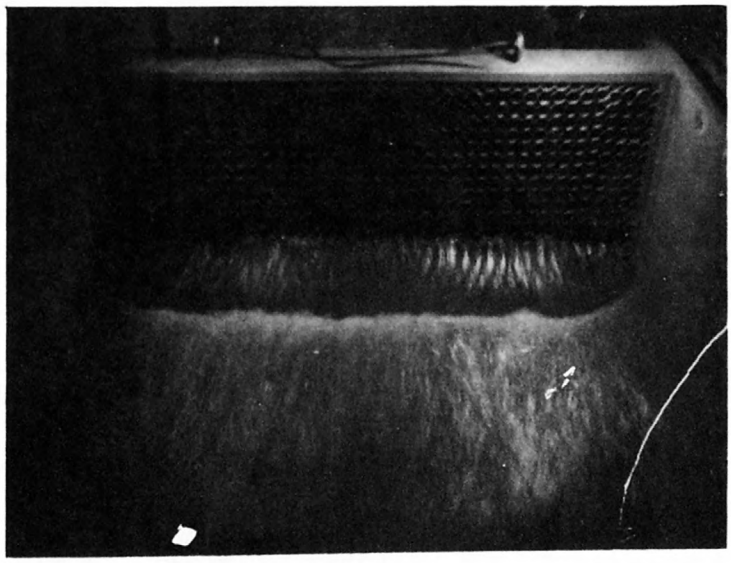

Figure 10.--Honeycomb grid in operation.

The following procedure was used to set up a given flow condition. The first step was to set the flume floor to approximately the desired slope. This slope was then accurately measured from floor elevations with the water in the flume. After a bottom slope had been determined a finger gate at the downstream end of the flume and the discharge were adjusted to give uniform flow conditions throughout the flume. Once the uniform flow conditions had been determined neither the bottom slope nor the finger gate were again moved until all runs for that flow condition had been completed. Measurements indicated that a given set of flow conditions could be reproduced to within ± 1%, on any given day by simply setting the discharge to the predetermined value.

All mean velocity measurements were made with a 5/16" outside diameter pitot tube. The differential pressure across the pitot tube was measured by a variable reluctance pressure transducer. The output of the transducer was recorded with a standard strip chart recorder. The calibration of the pitot tube was checked against previous calibrations and found to agree. The transducer was calibrated before and after each day of use. Point velocities were computed from three-minute time averages.

Velocity profiles were taken at various stations along the flume, to verify that the boundary layer was fully developed before reaching the test section. At one cross-section within the test reach, velocity profiles were taken at one foot intervals across the flume to determine the cross sectional distribution of velocity.

All turbulence measurements were made with a constant temperature anemometer. The sensing element was a parabolic shaped hot film. A detailed description of this equipment has been given by R. S. McQuivey (1967). The procedure used in making these measurements was the same as those developed by McQuivey for turbulence measurements in contaminated water. The turbulence signal was recorded on a frequency modulated magnetic tape recorder and later digitized and analyzed on a digital computer. See McQuivey and Richardson (1968) for the details of this procedure. All turbulence measurements were made at a distance of 1.5' to the left of the centerline. Measurements were made at several stations, however, the probe was always positioned six inches behind the center of a roughness cleat.

The slope of the flume floor was determined from a plot of floor elevations vs. distance. The floor elevations were measured to within ± .001' at 10 foot intervals along the centerline and sides of the flume. A precise level and a point gauge-target combination mounted on the flume carriage were used to determine the floor elevations. The water surface slope was determined by use of four stilling wells and point gauges connected to the flume at stations 75, 100, 125, and 150. The point gauges over the stilling wells and the precise level were permanently mounted to the laboratory wall so that all could easily be referred to a common base elevation. The depth of flow was computed as the difference between the water surface elevation and the floor elevation. The effect of the roughness cleats on the mean floor elevation was neglected. The discharge was measured with a calibrated side-contracted

orifice in the flume return line. The differential pressure on the orifice was determined with a water manometer. The temperature was measured by means of an ordinary glass mercury thermometer.

All experiments were completed in a time shorter than that required for the dispersant to complete one circuit in the system. This recirculation time was measured by continuously recording the concentration in the flow after dumping an instantaneous source of dye into the system. The time between successive rises on the concentration time curve was then taken as the recirculation time.

3. The Dispersants

In order to measure the mass transfer coefficient for fluid particles, dye was chosen as a dispersant. The dye used was Rhodamine W T fluorscent dye. Because this dye is soluble in water and the concentration of dye in the dosing solution was quite small, it was assumed that the fluid properties of the dosing solution were identical to those of the flume water.

The fine sediment used in this experiment consisted of uniformly sized spherical glass beads which were commercially available. The size distribution of the beads effectively simulated very fine sand as determined from the Wentworth scale. Smaller particles were not considered for the experiment because previous experiments (Sayre and Chang, 1968) indicated that particles within the Stokes range would behave very similarly to dye. The fine sediment particles chosen here have a fall velocity which is just above the Stokes range.

The coarse sediment dispersant was a uniformly sized natural quartz sand. It was classified as medium sand on the Wentworth scale. This size was chosen for two reasons. Previous experiments (Loyacano, 1967) indicate that this size will show a marked divergence in the diffusion characteristics from that of silt or dye. Also this size of sediment would make the experimental values of the Rouse number for the three flow conditions and two sediments progress approximately geometrically from 0.19 to 3.5.

Both sediments were sieved to obtain a uniform size. Measurements of the physical size were made by use of standard sieving techniques (Inter-Agency No. 4, 1941). The sieve size and gradation of both sediments are indicated on Figure 11. As can be determined from Figure 11, the median sieve diameter of the fine particles was 0.123 mm and the geometric mean size was about 0.122 mm. The geometric standard deviation of size was 1.08. The specific gravity of the fine sediment was found to be 2.42 by use of the pycnometer method. The manufacturer had guaranteed that at least 90% of these particles would be perfect spheres.

Figure 11 also shows the results of the sieve analysis of the coarse sediment. It can be determined that the median sieve diameter of the particles was equal to the geometric mean sieve diameter which was 0.390 mm. The geometric standard deviation of the particle sizes was 1.10. The specific gravity of the particles was found to be 2.65. The sediment was naturally worn river sand.

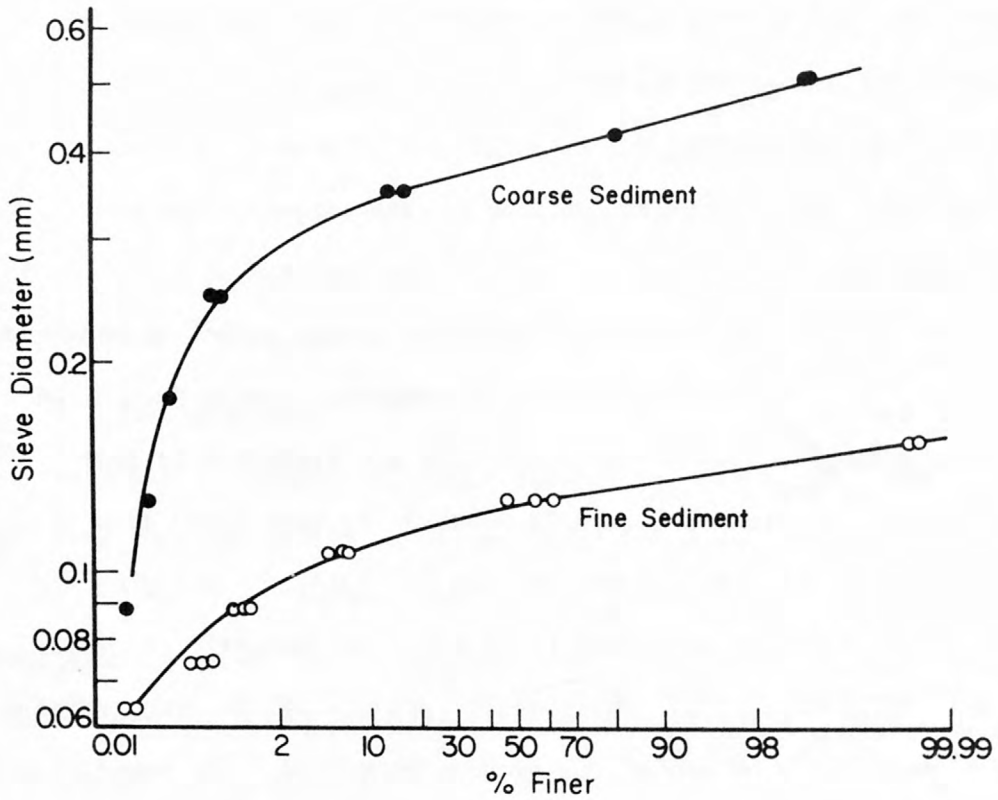

Figure 11.--Sieve analysis of sediments.

The fall velocity of the particles in a quiescent fluid was checked in two ways. The fall velocity of at least one hundred randomly chosen particles of each sediment was measured by dropping them individually into a column of water. The length of time required for the particle to fall a given distance was measured with a stop watch and the particle velocity was computed. After measuring the fall velocity of a particular particle, its nominal diameter was estimated from graphs given in report 12 (Inter-Agency, 1957) and the weight of each particle was computed. From the computed weight and the measured fall velocity of the particles a percent finer versus fall velocity curve was constructed and the median fall velocity was taken from this curve. The following are the important characteristics of the fall columns used in determining the individual fall velocities of the particles.

	Coarse	Fine
Inside diameter	14 1/2 cm	2.5 cm
Length of test section	97 cm	80 cm
Depth of water at beginning of test section	12 cm	16 cm

The fall velocities of the particles were also checked using a visual accumulation tube. The operation of the visual accumulation tube was as described in Report 11, (Inter-Agency, 1957). After comparing the results of the visual accumulation tube analysis, with those obtained by dropping single particles and those computed from the sieve analysis, it was decided that the results obtained from the visual accumulation tube were invalid. The error was attributed to the uniformity of the particle size in the sample. The visual accumulation tube analysis

gave fall velocities which were about 30-40% lower than those obtained by dropping single particles or from computations made from sieve size analysis for the coarse and fine sediments respectively.

4. Initial Conditions

The purpose of the dispersant injection system was to place a continuous line source of dispersant across the entire width of the flume either at the surface or at the bed. In order to eliminate the influence of turbulent diffusion in the transverse direction, the transverse injection rate was adjusted to match the transverse unit discharge of water. This made the quantity $\frac{\partial c}{\partial z} = 0$. In the case of the bottom injector this adjustment was not possible so an approximately uniform distribution was injected across the entire width of the flume. The injectors fed an array of closely spaced concentrated streams of dispersant into the flow. The stream spacings were about two inches when injecting at the surface and about one inch when injecting at the floor. To further simulate a line source the injector was oscillated back and forth during injection. Again this was not possible with the bottom injector. Actually an ideal inlet line source was not necessary because the computed values of the transfer coefficient and particle fall velocity depended only on the change in concentration from one measured profile to the next. Furthermore, the transfer coefficient is not constant for short diffusion times anyway. The first measured profile was always used as the initial condition for predicting subsequent profiles from the numerical solution.

When injecting dye a small amount of the flume water was diverted through a small pump and one hundred feet of 3/4" hose. A minute amount of concentrated dye solution (about 1-3 ml./sec.) was continuously added to the diverted flow. The dye was uniformly mixed with the diverted water while the mixture traveled through the one hundred feet of hose. The use of diverted flume water insured that the injected dye mixture and the flume water would have the same temperature. The rate of dye injection was always measured and compared with the measured flux of dye past the sampling stations. Checks indicated that the dye injector operated at a constant rate.

Figure 12 is a picture of the surface dye injector. The discharge through each outlet valve in the dye injector was adjusted for each run to insure that a proper distribution of discharge occurred. The following procedure was used for injecting dye through the top dye injector. Before the run was to begin the injector was placed in a trough across the top of the flume. This trough diverted the water from the injector into a drain. The injection of dye into the diverted water was then started. After about five minutes or until the dye appeared to be discharging uniformly from all nozzles the run was started by removing the injector from the trough and placing it in a rack just above the water surface.

The bottom dye injector consisted of an eight foot length of commercial lawn sprinkler hose fastened to the floor of the flume. This hose was only 1/4" high and the roughness cleats were 1 1/16" high, therefore, the hose did not disturb the velocity distribution appreciably. Since it was impossible to divert the injected water before a

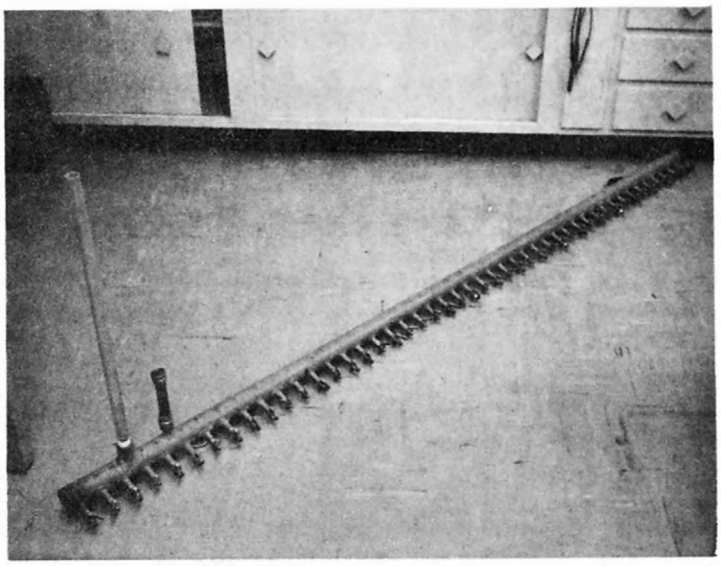

Figure 12.--Apparatus for injecting dye at the surface.

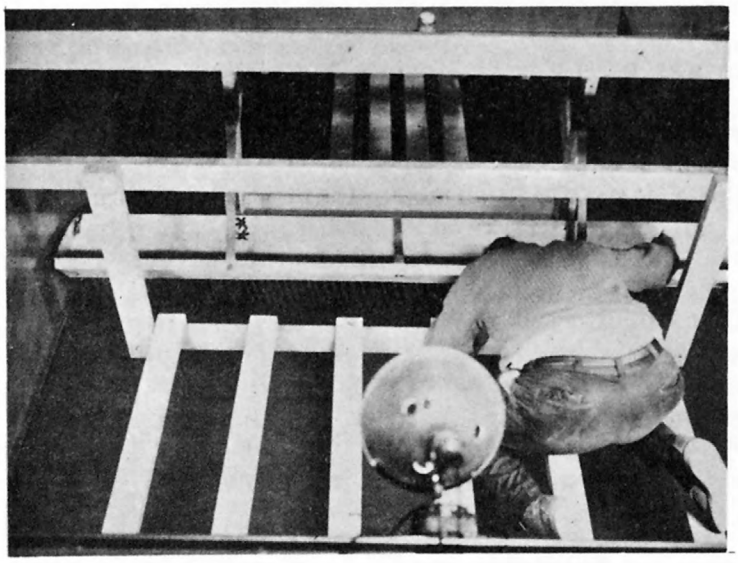

Figure 13.--Injection of sediment.

run was to begin as was done when the top dye injector was used, a different procedure was necessary. The dye was started several minutes before the run was to begin. The rate of increase of the background dye concentration in the flow was continuously monitored upstream of the injector. The run was started only after the rate of change of the background dye concentration became constant. It was then possible to subtract the background concentration from the measured concentrations.

The sediment was injected dry through a series of small holes in the bott m of a trough. Figure 8 shows a picture of this trough with no water in the flume. Figure 13 shows this trough in operation. The free fall distance of the sand was originally set at two inches but about 5% of the sand floated, thus the free fall distance was increased to about six inches and very little sand floated. The variation of the transverse sediment flux was controlled by the spacing of the holes in the bottom of the trough and the size of the holes regulated the mean sediment discharge. Previous calibrations had indicated that the discharge of sediment from a given size hole was a function only of the hole and sediment size and was independent of the depth of sand above the hole.

The procedure used when injecting sediment was as follows. Just before a run was to begin, the holes at the bottom of the trough were opened. A few minutes were allowed (1-3 minutes) in order for the sediment distribution to reach the steady state conditions after which the samples were taken. After all samples had been taken, the sand was shut off. The weight of sand in the trough was measured before and after each run and the injection time was recorded in order to determine the injection rate.

Following most of the sediment runs, the longitudinal distribution of the material deposited on the floor was determined by vacuuming up the sand in strips across the flume, and weighing the amount obtained from each strip. If there is no movement subsequent to initial contact with the bed, this deposition distribution and the mean stream velocity can be used to calculate the fall velocity of the material under flume flow conditions.

5. Sampling of the Dispersant

In order to determine point concentrations, samples were siphoned from the main flow through probes like the one pictured in Figure 14. The vertical spacing of the sample nozzles was two inches. The inlet velocities of the nozzles were adjusted to match the local mean stream velocity by adjusting the siphon heads (see Figure 15).

During most runs the vertical concentration profiles were determined at fixed transverse positions. When this type of sample was collected the probes were clamped to a rack that held them in a fixed position. The lateral position of probes were staggered to avoid interference from wakes of probes upstream. Certain runs were made in which the probe was traversed across the center six feet of the flume during the sampling period. These were called integrated samples because they gave a space averaged value of concentration. During the integral runs the siphon heads remained constant and the transverse variation in velocity was ignored. The longitudinal distances of the probes from the injection point varied from run to run. These distances for all runs are given in Table 2 of Appendix A.

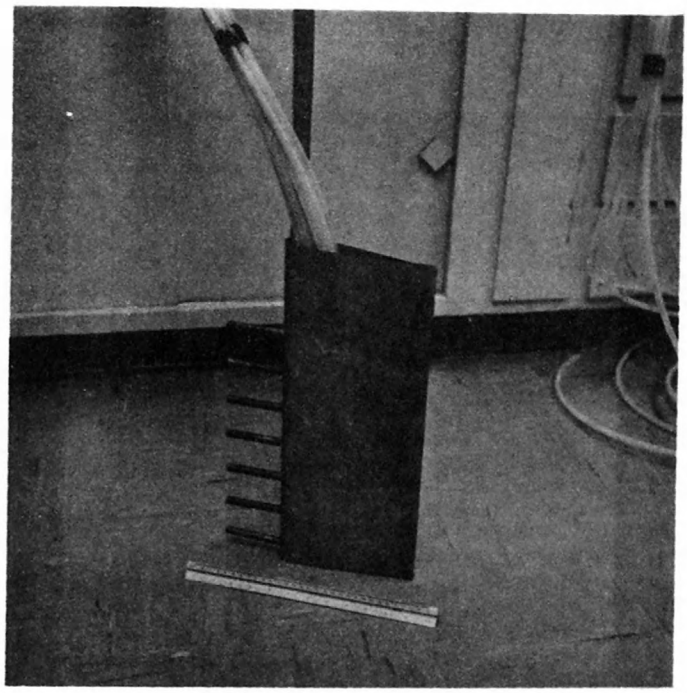

Figure 14.--The sample probe.

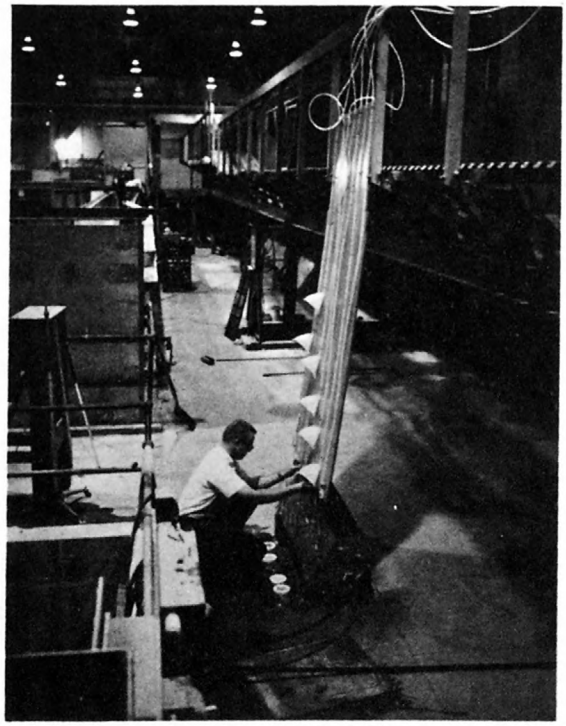

Figure 15.--The sample collection system.

The collection system for a sampler is shown in Figure 15. The four by eight foot sheet of plywood is hinged at the top so that the sample streams can be directed either into the sample containers or into the wasteway. The maximum sample size was one gallon. All samples were collected for the same length of time so the samples collected from near the bottom of the flume usually contain slightly more than one quart. The response time of the collection system was determined and it was found that the length of the tubing divided by the smallest tube velocity gave a satisfactory estimate of the time required for the dispersant to pass through the sampling system. The response time was needed for the integral runs, when the concentration of dispersant in the entire system was increasing uniformly with time (i.e. the bottom injection dye runs) and for determining the time required to reach equilibrium after the samplers were turned on.

6. Analysis of the Samples

Background samples were taken upstream from the injection point for all runs and this background concentration was subtracted from the other readings before further analysis. Samples were always analyzed for concentrations within one or two days after collection.

The concentration of Rhodamine W. T. fluroscent dye was measured with a Model 111 Turner fluorometer. Known concentration standards were prepared and the fluorometer was calibrated before analyzing the concentrations for each run. Measurements of dye concentrations were usually accurate to within ± 0.2 parts per billion (ppb).

Sediment concentrations were determined by decanting, drying, and weighing the sediment collected. Sediment weights were determined to within ± 0.001 gram and the mixture weights were determined to within ± 1 gram. The smallest samples collected consisted of about 1,000 grams and the amount of sediment collected per sample varied from 0 to 2 grams.

Chapter IV

PRESENTATION AND ANALYSIS OF DATA

A. Introduction and Summary of Data

1. Introduction

The purpose of this chapter is to present the data obtained and to describe the procedure used in the analysis of the data. The numbering system used in the runs will first be explained as well as the purpose of the individual runs. Then a description of tabulated data in the appendix will be given. This tabulated data includes the data taken which would be too voluminous to include in the text.

After describing the tabulated data, the data obtained in characterizing the flow field will be presented. First, will be the mean velocity measurements and then the turbulence measurements; after the turbulence measurements, the calculated momentum transfer coefficients will be presented.

After the flow field data has been presented then the dispersant fall velocities will be given.

Finally, the results of the diffusion experiments will be presented. First, the evaluation of the equations, second, the results of the mass transfer experiments, third, the results of the sediment transfer experiments, and finally, a numerical solution of the conservation of mass equation will be given. The numerical solution will allow further interpretation to be placed upon the experimental results.

2. Run Summary

The run numbers were designated so that the particular type of run could be determined from the run number. The first letter or first two

letters in the run number represent the type of dispersant used in that experiment. D, CS, FS, T stand for Rhodamine W. T. dye, coarse sediment, fine sediment and tracer particles respectively. After the type of dispersant has been given, then the injector location is represented by the next symbol, either T for injection at the surface, or B for injection at the bottom. All sediment particles were injected at the surface so no location symbol is used. Three flow conditions were used in this experiment. Flow conditions A, B, and C represent the low discharge, medium discharge and high discharge respectively. The digits in the run number can be used to determine which flow condition was used. For example, the numbers 0-9 represent flow condition A, numbers 10-19 are reserved for flow condition B and the numbers 20-29 are reserved for flow condition C. An A at the end of the run number indicates that this was the second run made on a particular day. The flow conditions were never altered between runs taken on the same day and no more than two runs were ever made on a single day. Finally, the sampling method can be determined from the number used in identifying the flow condition. The odd numbers indicate that the run was made with fixed probes and the even numbers designate the integral probe runs.

3. Description of Tabulated Data

Table 1 gives the hydaulic parameters which were held constant throughout a single run. The headings are symbols which have been described in the list of symbols with the units which were used to describe the parameters. Concentrations are always expressed in parts per billion (ppb) for dye and in parts per million (ppm) for sediment.

The recovery ratio (RR) is defined as the ratio of the flux of dispersant that remains in solution or suspension at any station to the injected flux. When the dispersant is something that remains in the solution such as dye, the recovery ratio is identically 1.0 for all stations. For sediment the recovery ratio decreases with increasing distance from the source because the sediment tends to settle and be deposited on the floor. The measured recovery ratio (RRM) is the ratio of the flux at a station, as determined from measured concentration and velocity profiles, to the injected flux. The recovery ratio is not necessarily equal to the measured recovery ratio because of possible unequal transverse injection distribution, lateral convective transport by secondary currents and errors in measurements of the concentration and velocity profiles.

In order to compare the concentration distributions obtained from different runs and different mean concentrations, all measured concentrations were normalized by use of a average concentration (C_b) defined as

$$C_b = \frac{\int_0^{Y_N} \gamma c_m u \, dy}{\int_0^{Y_N} \gamma u \, dy} = \frac{RRM \; FI}{\gamma U \; Y_N} \tag{38}$$

where U is the mean stream velocity computed from Figure 19, Y_N is depth, c_m is the measured concentration, and FI is the injected flux of dispersant per unit of width. The relative concentration was then computed by the expression

$$c = \frac{RR \; c_m}{C_b} \quad . \tag{39}$$

This expression insures that the relative concentration indicates a constant flux past any station for a particular flow condition.

The values of FI are given in Table 1 of Appendix A. Table 2 of Appendix A contains all concentrations obtained from the data. All concentrations included in Table 2 have had the background concentrations deducted and have been normalized. Table 3 in Appendix A gives the probe locations used during each run. The symbols R and L indicate whether the probe was located to the right or left of the centerline of the flume when looking downstream. Table 3 also gives all measured recovery ratios as well as the recovery ratios used in all calculations.

B. Flow Field Data

1. Spatial Velocity Distribution

Figures 16 and 17 show the isovels for flow conditions A, B, and C. Note the decrease in velocity at the center section of the flume which occurs for all three flow conditions. The wall effects are somewhat more pronounced for flow C then for the other flows. Measurements indicated that the cross-sectional distribution of velocity was symmetric with respect to the centerline of the flume, therefore, measurements from symmetric points on either side of the channel were averaged to obtain the curves presented in Figures 16 and 17. The scales are expanded vertically which makes the transverse variation appear more pronounced in these figures. The width-depth ratio was 6.0.

Figure 18 shows the variation of mean velocity across the channel. Again note the lower mean velocity indicated at the center of the flume. The injection rate of the dispersant was adjusted so that the unit discharge of the dispersant was proportional to the unit discharge of the water at any vertical section as determined from Figure 18.

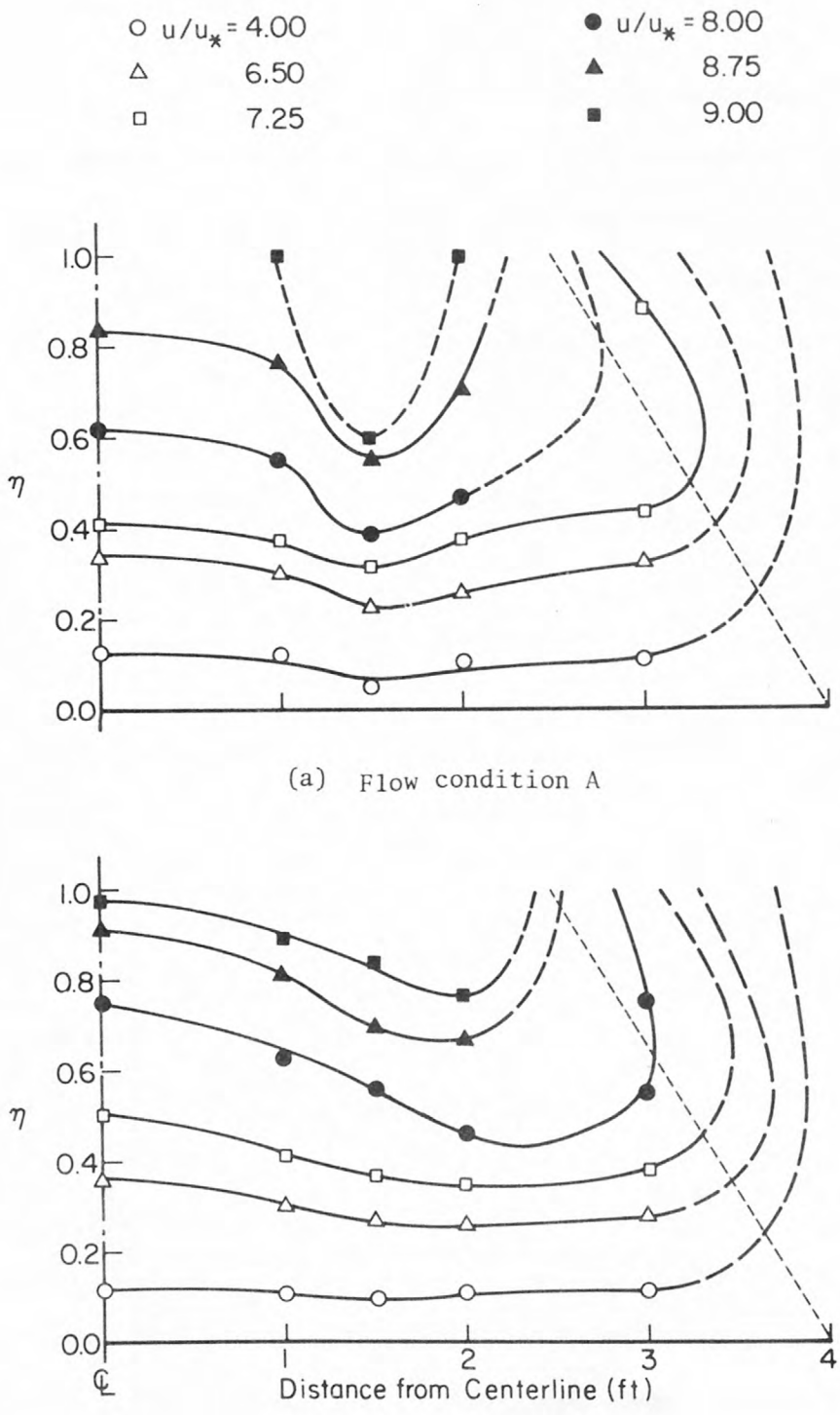

(a) Flow condition A

(b) Flow condition B

Figure 16.--Isovels for flow conditions A and B.

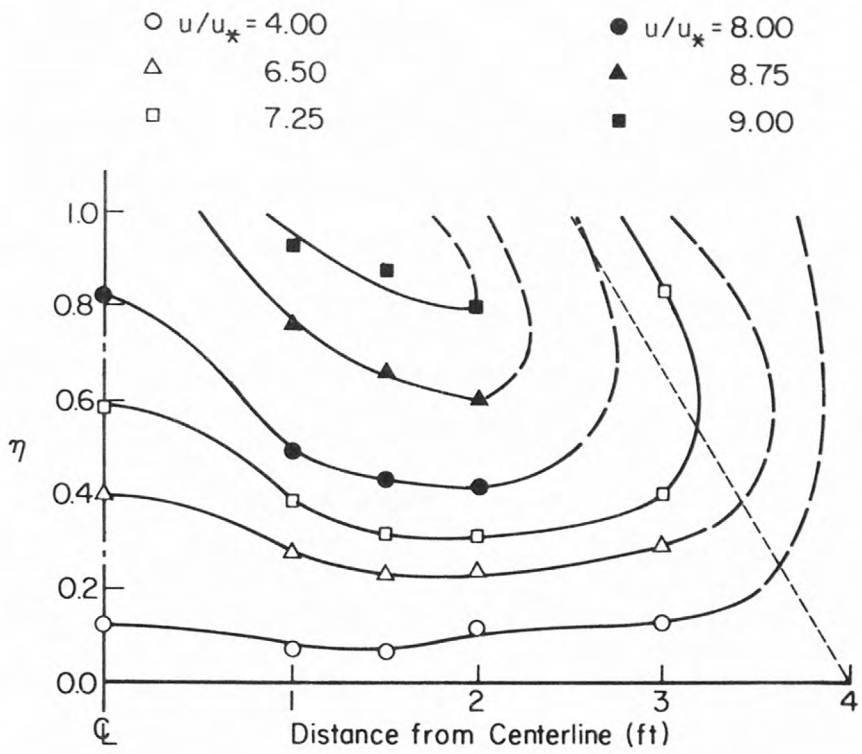

Figure 17.--Isovels for flow condition C.

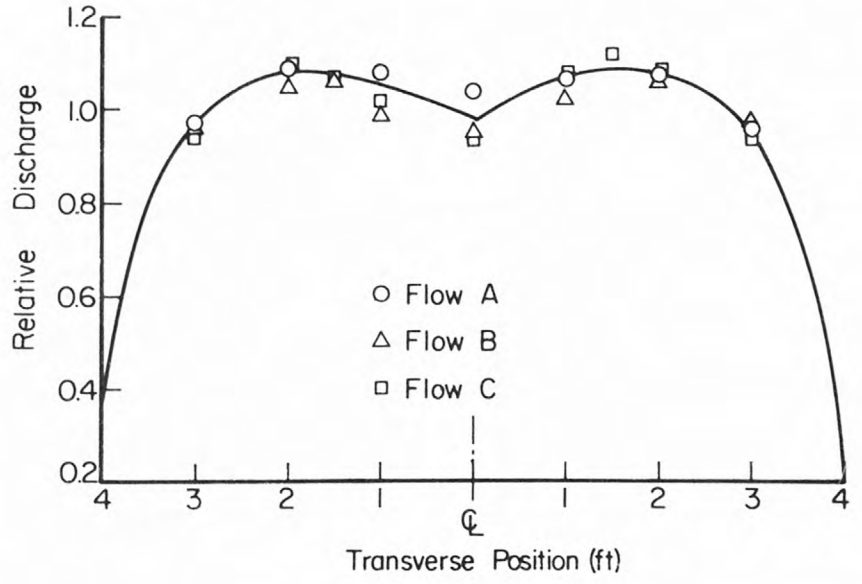

Figure 18.--Transverse velocity distribution.

Figure 19 shows the velocity profiles which were assumed to be representative of the flow in the test section for each of the three flow conditions. These profiles represent the average of all measurements below station 90, taken at positions 1, 1½, and 2 feet off the centerline of the flume. Measurements indicated that the boundary layer was fully developed before station 70. The dispersant was always injected at station 90. The curves shown in Figure 19 represent the average of six individual profiles. The value of the Von Karman coefficient (κ) was computed from the velocity distribution in the bottom 2/3's of the flow. The measured values of the constant were 0.389, 0.392, and 0.395 for flows A, B, and C respectively. Again note the wall effect causes a greater cut back in the velocity profile at the surface for flow condition C. The solid line in Figure 19 represents the average of all three flow conditions.

The density of the roughness cleats was small enough so that one might expect that they would cause local variations in the velocity profiles near the bottom. An experiment was performed for flow condition A to determine this variation. Sixteen profiles were measured at different positions relative to a roughness cleat. It was concluded from this experiment that the variation in mean local velocity was no more than 20% at a relative depth of 0.1 and that the variation decreased rapidly for greater relative depths. The maximum velocities occurred near the corners of the roughness cleats and the minimum velocities occurred about three inches behind the front of the center of each cleat. The average velocity profile should occur about six inches behind the center of any cleat. All subsequent velocity profiles were taken with the

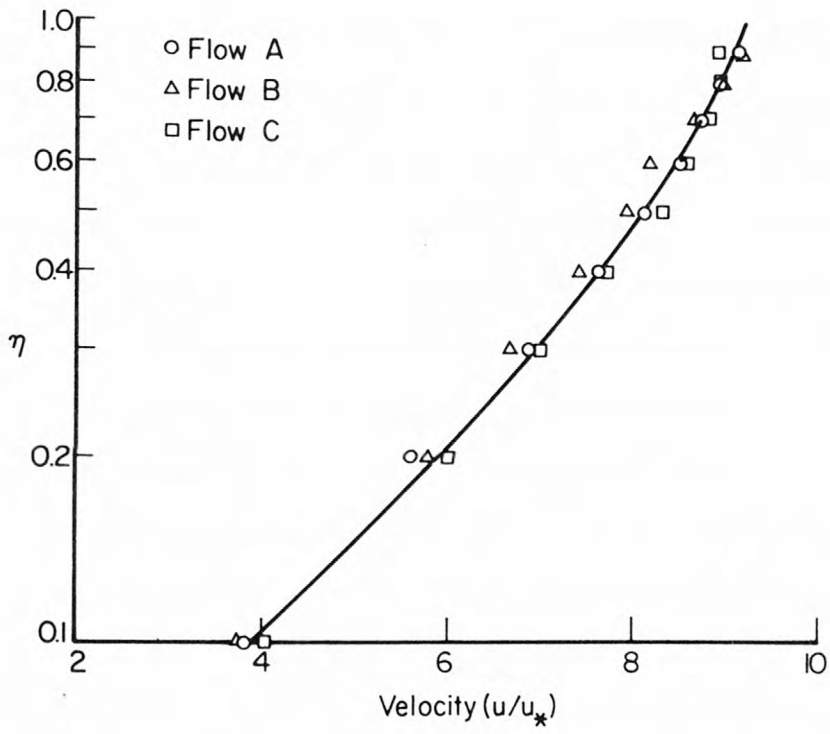

Figure 19.--Averaged velocity profiles in test section.

probes located six inches behind the center of a particular roughness cleat.

An experiment was also conducted to check the effect of the sample probes shown in Figure 14 on the local velocity distribution. The experiment was conducted only for flow condition C. The probe layout was the same as that used in Run DT21. In order to conduct the experiment, the probe furthest downstream was removed and a velocity profile was measured at the position where the probe had been. After this velocity profile had been measured the next to the last sample probe was removed and a velocity profile was measured in its position. The results of these profiles were then compared with previously measured profiles made near the same verticals but with no probes in position. It was concluded that the sample probes caused no major alteration in the local velocity profiles. The sample probes apparently reduced the mean velocity at the last probe position by about 3% and they reduced the mean velocity at the second to the last probe position by about 1%. The sample probes apparently decreased κ by 25% at the last probe position and increased κ by 4% at the next to the last probe position.

To insure that tests were made in a fully developed uniform flow, measurements were made of the mean velocity and turbulence intensities at various distances from the entrance. Some of these results are shown in Figure 20. The test reach extended from station 90 to roughly 122; however, one concentration profile was always measured at station 180. Only the results for flow condition B are presented, however, the rate of development of the boundary layer did not appear to be much different for the other flow conditions. All measurements shown in Figure 20 were taken eighteen inches to the right of the centerline of the flume.

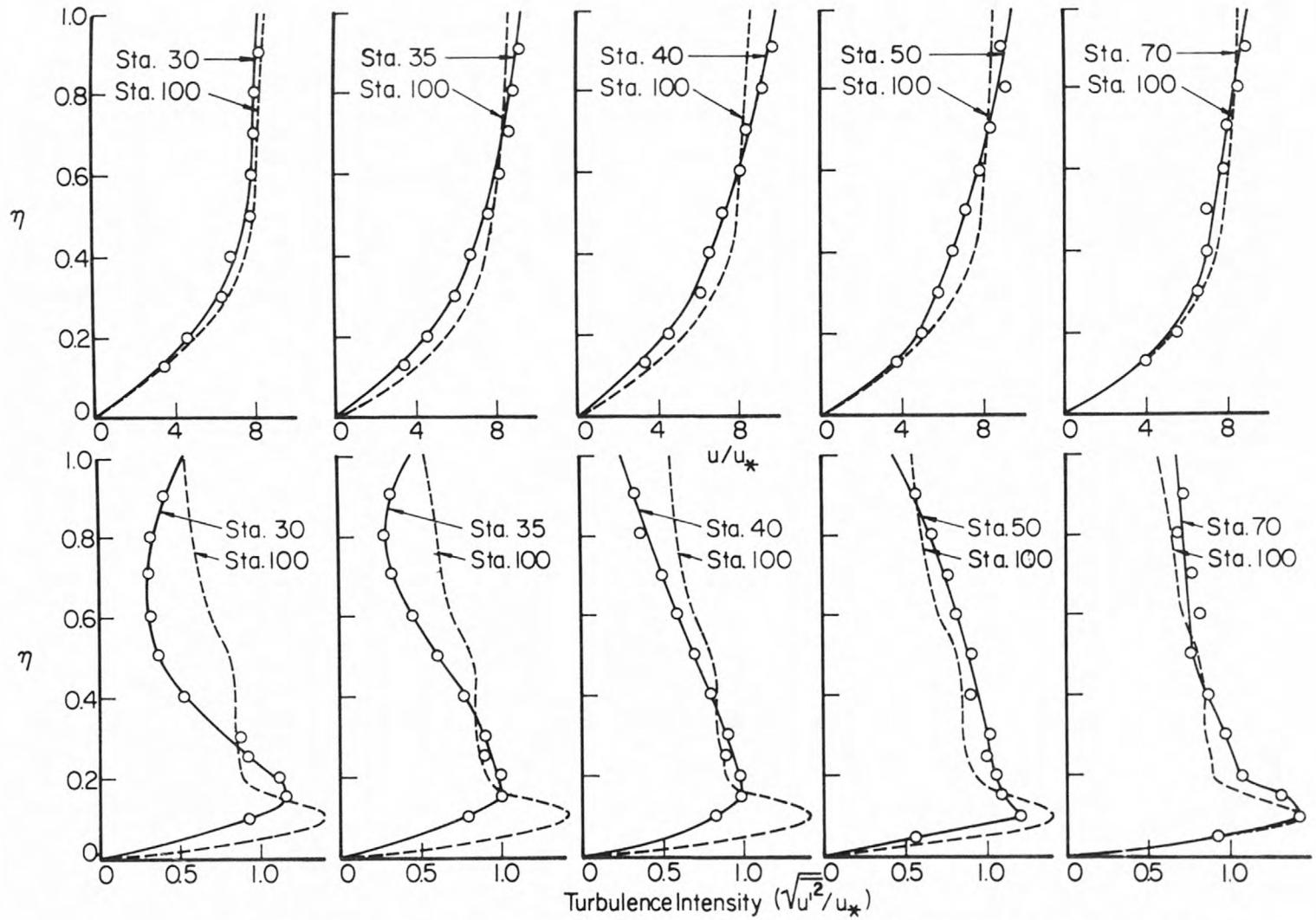

Figure 20.--Velocity and turbulence intensity profiles in the developing boundary layer; flow B.

2. Turbulence Properties

The Eulerian longitudinal turbulence intensities in the test reach are shown in Figure 21. These intensities show the typical distribution for open channel flow with a rough boundary (McQuivey, 1967). All turbulence measurements were made at station 100 with the probe eighteen inches to the left of the centerline. The probe was located six inches behind the center of a roughness cleat.

The Eulerian integral time scales are shown in Figure 22. Standard spectral analysis of the recorded data gave the spectral distribution of the turbulence. Data was digitized each 0.01 sec. The spectral distribution of the form

$$F(n) = \frac{4\,\Lambda_t}{[1 + (2\pi\, n\, \Lambda_t)^2]^{5/6}} \qquad (40)$$

suggested by Von Karman in 1948 (Robertson, 1967) seemed to fit the measured spectral distributions very well for all relative depths. In this equation n is frequency and Λ_t is the Eulerian integral time scale, which was computed from Equation 40 as ¼ the reciprocal of the cut-off frequency. Spot checks of the Eulerian integral time scale obtained by integrating the auto-correlation function showed that this approximation was satisfactory.

3. The Momentum Transfer Coefficient

The momentum transfer coefficient can be computed from its definition given in Equation 17. In order to evaluate the vertical component of the momentum transfer coefficient the shear stress was assumed to vary linearly from a maximum $\tau_o = \gamma\, Y_N\, S$ at the bed to zero at the surface so that

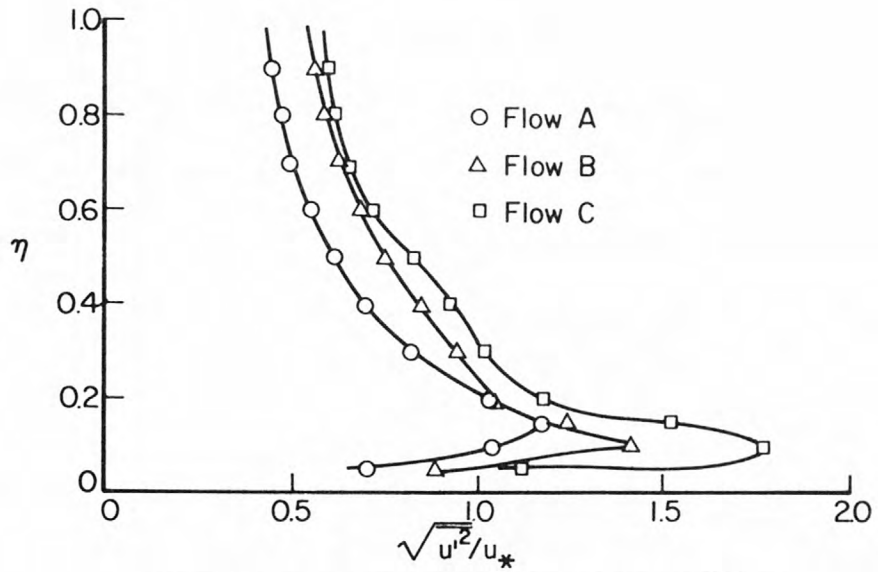

Figure 21.--Turbulence intensity profiles.

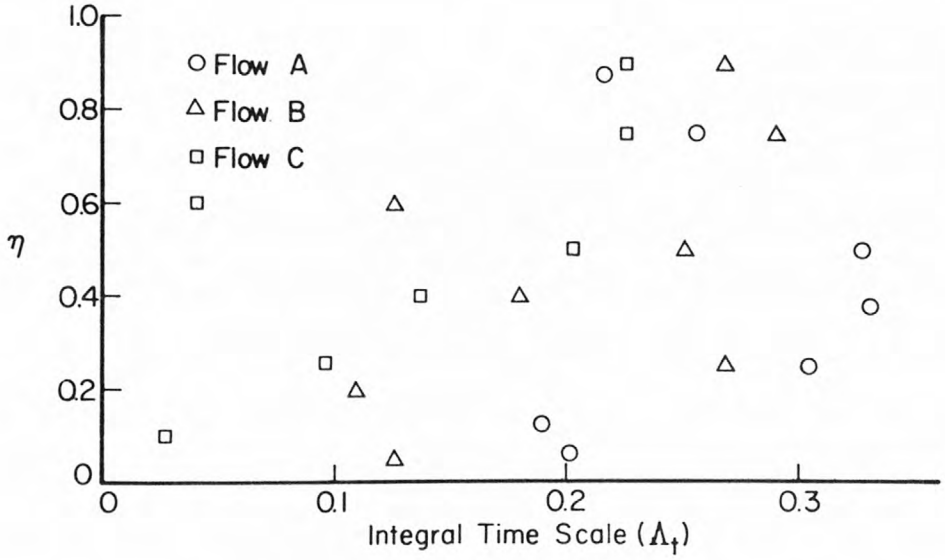

Figure 22.--Eulerian integral time scales of turbulence.

$$\tau_{xy} = \rho g \; Y_N \; S \; (1-\eta) = \rho u_*^2 (1 - \eta) \; . \tag{41}$$

Equation 41 has been verified by McQuivey for open channel flow at least on the center line. Solving Equation 41 and 17 one obtains the expression for the vertical component of the momentum transfer coefficient as

$$\frac{\varepsilon_m}{Y_N u_*} = \frac{1 - \eta}{\frac{d \left(\frac{u}{u_*}\right)}{d\eta}} \tag{42}$$

In order to compute the momentum transfer coefficient for the flow, the dimensionless velocity was first plotted as a function of the relative depth. This curve was graphically differentiated and the results of the differentation plotted and smoothed. From the smoothed graphical differentiation of the velocity profile and Equation 42, the dimensionless momentum transfer coefficient was calculated. Figure 23 shows the results of this calculation for the indicated conditions. The values shown in Figure 23 were computed from the dimensionless velocity which had been averaged for all three flow conditions as in Figure 19. The dashed line in Figure 23 shows the distribution of the momentum transfer coefficient as determined from Equation 22 with κ = 0.392. Calculations were made for individual flow conditions but they are not shown here. The variation between the computed momentum transfer coefficient as determined for the individual flow conditions was negligible in the bottom half of the flow. In the upper half of the flow, the computed transfer coefficient for the three flows diverged considerably. For example, flow condition C indicated an infinite momentum transfer coefficient at η = 0.9 which was apparently due to side wall effects. Flow condition A showed larger momentum transfer

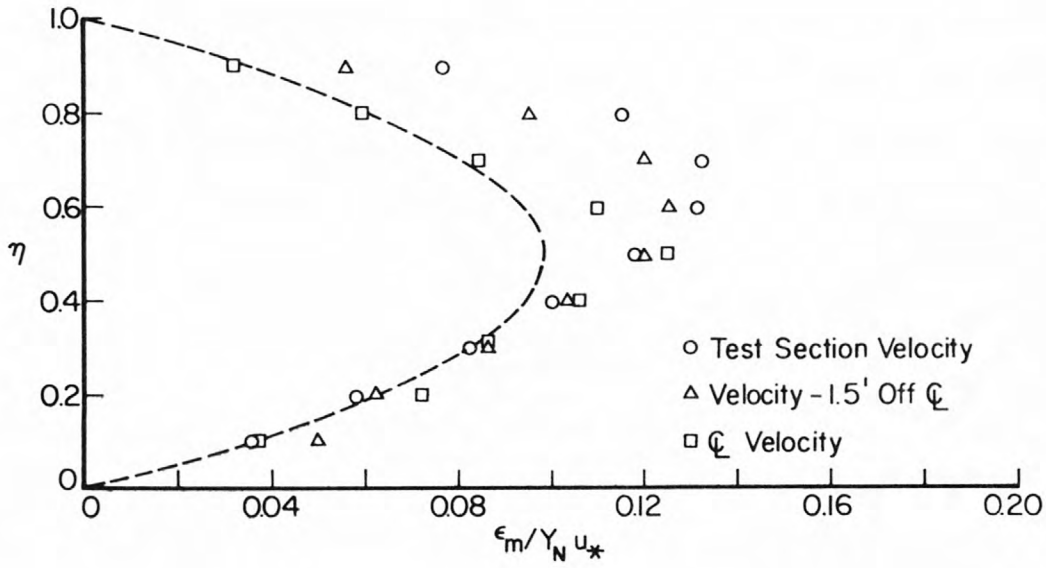

Figure 23.--Vertical distribution of the momentum transfer coefficient.

coefficient in the upper half of the flow than did flow B. The momentum transfer coefficient computed from the velocity profile for flow condition B looked considerably more like the dashed line shown in Figure 23. It was concluded that the sidewalls affected the apparent values of the momentum transfer coefficient considerably in the upper half of the flow and that the distribution of ε_m determined from Equation 22 with $\kappa = 0.392$ is probably a more representative measure of the value of ε_m than are the measured values presented in Figure 23.

C. Particle Fall Velocity

1. Fine Sediment, Quiescent Conditions

The standard fall velocity of the sediment particles was determined in at least two ways. The standard fall velocity of the glass beads was first computed from the median sieve diameter using Equation 16 and the value of C_D obtained from Report No. 12 (Inter-Agency, 1957, p. 20). The value of the median standard fall velocity obtained from these computations was 1.10 cm/sec. The distribution of the values of the single particle fall velocities obtained by dropping single particles is shown in Figure 24. The measured fall velocities were corrected to the standard fall velocity by use of tables given in Report No. 12 (Inter-Agency, 1957, p. 27). Figure 24 shows that the median standard fall velocity was equal to the geometric mean standard fall velocity which was 1.09 centimeters per second. The standard fall velocity of the fine sediment which is used in all subsequent calculations is 1.09 cm/sec.

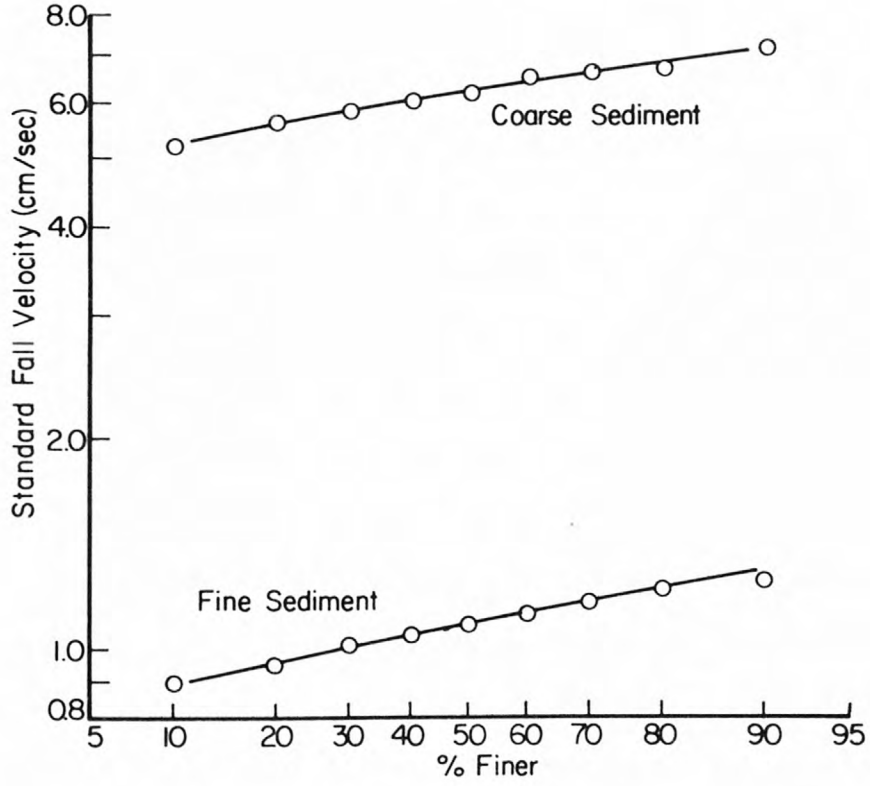

Figure 24.--Standard fall velocity distribution of sediments.

2. Fine Sediment, Turbulent Conditions

The magnitude of the turbulent fall velocity can also be determined in two separate ways. First, it can be calculated from the measured concentration profiles, and second, it can be determined from the distribution of deposited material on the floor of the flume, provided there is no movement after deposition. Information from the deposited material allowed the construction of the probability density function of the location of deposit as well as the cumulative distribution function as shown in Figure 25. For flow condition A, the sediment appeared to have moved very little after it was deposited on the floor. From Figure 25, it can be seen that 50% of the material was deposited above station 128.6 and 50% below station 128.6. Assuming that the sediment did not move once it came in contact with the floor, it was convected a median distance of 128.6-90 or 38.6 feet downstream while falling through a depth of Y_N. The mean stream velocity for run FS1 and FS 1A was 0.965 ft/sec computed from the discharge and the flow area. This mean velocity was used rather than the one measured in the test section because the sediment deposition data was sampled across the entire width of the flume, not just in the test area. From the mean stream velocity and the distance of convection, the median time that a sediment particle was held in suspension is computed to be 38.6/0.965 or 40.0 sec. Then the median rate of fall can be computed as 1.327 feet, divided by 40.0 sec. = 0.0332 feet/sec. at 72 1/2^{o} F. Correcting for temperature (Inter-Agency, No. 12, 1957, p. 27), this corresponds to 1.07 cm/sec @ 24 ^{o} C. Using the centroidal distance of the distribution curve instead of the median distance, one obtains a fall velocity

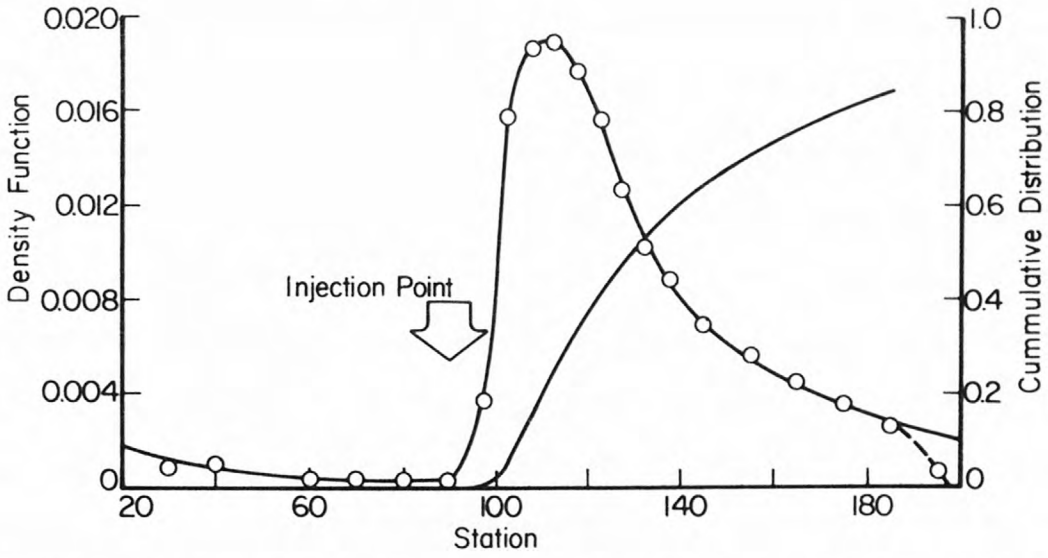

Figure 25.--Longitudinal deposition distribution of fine sediment; flow A.

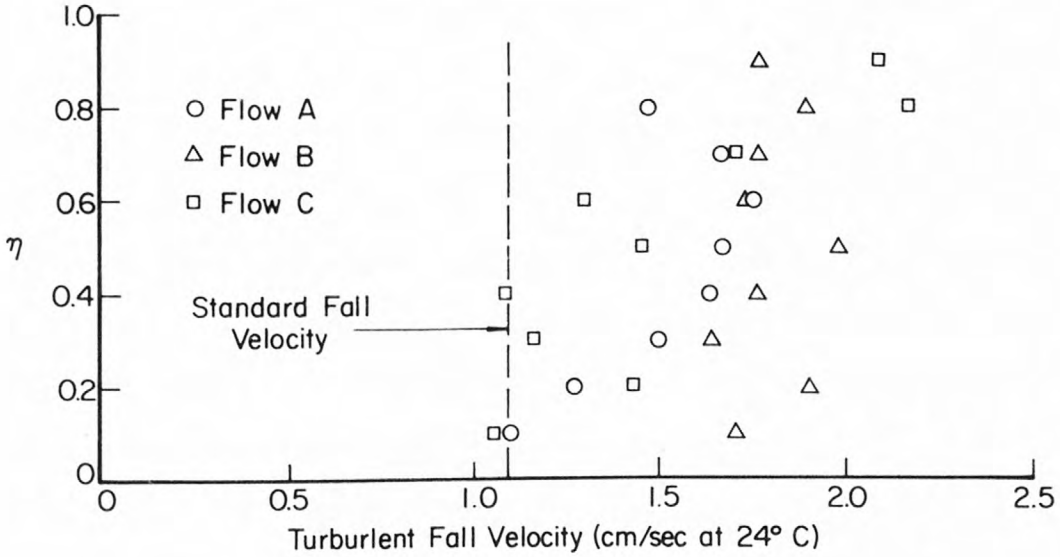

Figure 26.--Fine sediment turbulent fall velocities.

of 0.87 cm/sec @ 24^{o} C. Any movement of the sediment after the particles had first come in contact with the floor would cause the turbulent fall velocity as computed above to be too small. Approximately half of the sediment was injected for run FS1 and then after the flume had run for about three hours, the other half of the sediment was injected during run FS1A. Only about fifteen minutes lapsed between run FS1A and the time when the flow was stopped. The long tail on the frequency distribution curve as well as the small hump at about station 122 would seem to indicate that at least some of the sediment particles had moved after they were first deposited. The sediment deposition patterns for flow conditions B and C definitely indicated that the sediment had moved, probably many times, after it was first deposited. Since the sediment may have moved, this information serves only as an effective lower bound on the turbulent fall velocity. Ninety-six percent of the sediment injected was recovered from the floor of the flume and Figure 25 was normalized by the amount injected. It is assumed that the other four percent was in the flume tail box, pumps or return line at shut off time. It is suspected that the acceleration of the fluid as it approached the downstream finger gate caused the distortion at stations 185 and 195.

The particle fall velocities were also computed from the measured concentration profiles. The procedure which was used in this computation will be outlined in the next section. However, Figure 26 gives the results of the analysis. The tendency for the fall velocities to be greater near the surface is pointed out. It is believed that this is due to the particles falling as a group for some time before the turbulence diffuses the injected streams. The size of the hole through which

the sediment was injected and the rate of injection for each hole is given below.

Flow	Hole Size	Average Concentration	Injection Rate
A	3/32"	133 ppm	0.67 grams/sec/hole
B	1/8"	156 ppm	1.4 grams/sec/hole
C	5/32"	178 ppm	2.9 grams/sec/hole

The average turbulent fall velocities corrected to 24^{o} C as obtained from the concentration profiles were 1.51, 1.80, and 1.52 cm/sec. respectively for flow conditions A, B, and C. This gives ratios of V_{ST}/V_{sq} of 1.39, 1.65, 1.40 for flows A, B, and C respectively.

3. Coarse Sediment, Quiescent Conditions

From the median sieve diameter and Figure 6 of report no. 12 (Inter-Agency, 1957, p. 24) the standard fall velocity of the coarse sediment particles was computed. For a shape factor of 0.7 the standard fall velocity was computed as 5.9 cm/sec. For a shape factor of 0.9 the standard fall velocity was computed as 6.3 cm/sec.

The distribution of the values of the standard particle fall velocity as determined by dropping individual particles in a fall column is shown in Figure 24. The results shown in Figure 24 were for particles dropped from a submerged platform in the fall column. The standard fall velocity of each particle was computed from tables given in report no. 12 (Inter-Agency, 1957, p. 28). The median standard fall velocity from Figure 24 is 6.30 cm/sec. The value used for the standard fall velocity in all subsequent calculations is 6.30 cm/sec.

To determine the effect of injecting the particles dry, 100 dry particles were dropped through about eight inches of air into the fall column and their fall velocities were measured. The median fall velocity of the particles dropped through air was three percent less than that for the ones which were dropped from the submerged platform. The distribution of the dry particle fall velocities appeared to be identical to that shown in Figure 24 except it was lower by about three percent. The jetting action caused by injecting the particles through holes into the flume should reduce the amount of air trapped, and increase the particles fall velocity somewhat. It was therefore assumed that injecting particles dry would have a negligible effect on their average fall velocity.

One hundred particles which had been coated with a fluorescent dye were also dropped to determine the effect of the coating on the fall velocity. The dye coating had little if any effect on the fall velocity of the particles.

4. Coarse Sediment, Turbulent Conditions

The turbulent fall velocity of the coarse particles was determined both from the concentration profiles and from the distribution of deposited sediment. The procedure for picking up the deposited sediment was the same as that used for the fine sediment. Since it appeared that about 5% of the sand floated upon injection, the cumulative distribution curve was normalized by dividing by the quantity of material obtained from the bed rather than the amount which was injected. For flow condition A, the density function in Figure 27 virtually reaches a value of zero by station 110, and since the material was picked up completely to station

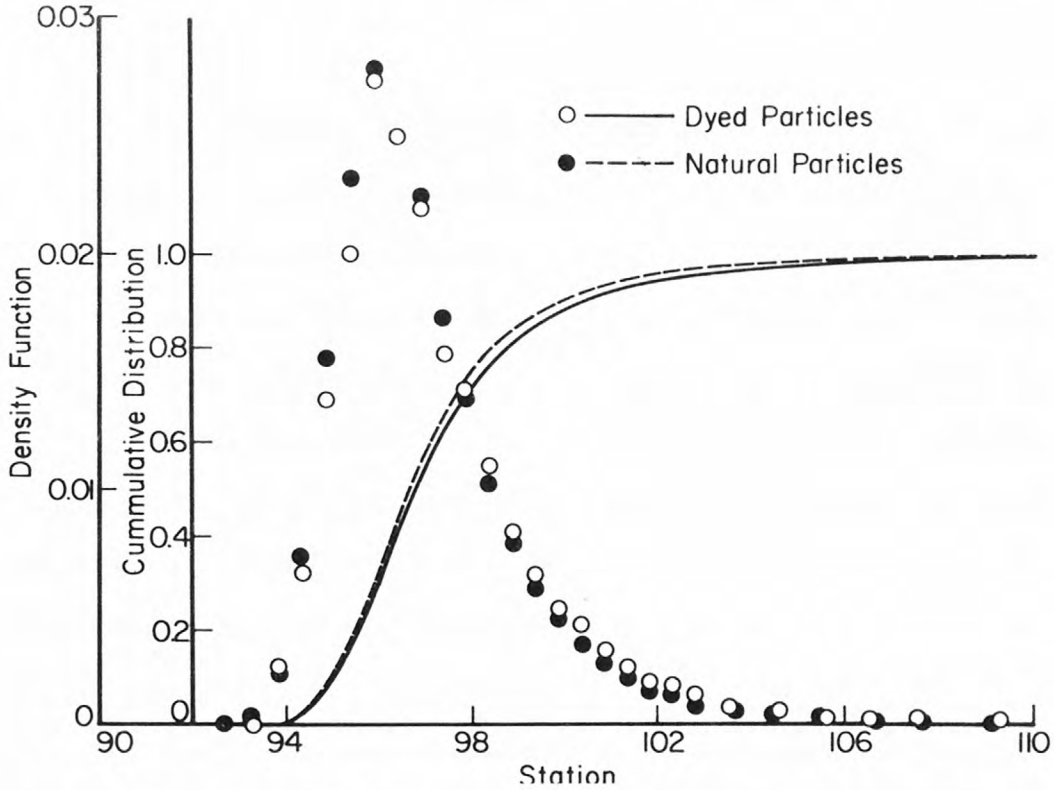

Figure 27.--Longitudinal deposition distribution of coarse sediment; flow A.

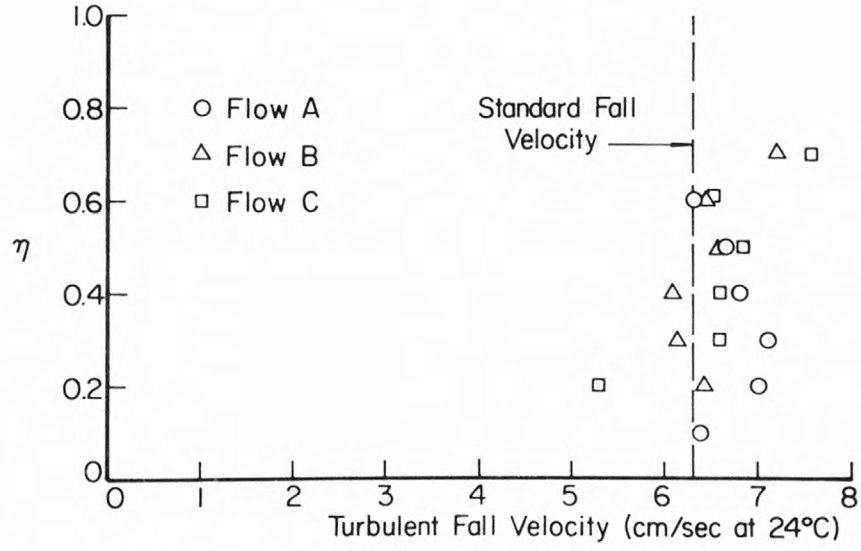

Figure 28.--Coarse sediment turbulent fall velocities.

180, all of the material which did not float should have been obtained from the floor. The procedure for the computation of fall velocity from the distribution of the deposited material was the same as that used for fine sediment. One preliminary run which will be called CSO was performed when the siphon tubes were not working properly. Fall velocities corrected to 24^{o} C computed from the median position of the deposited material were 6.32, 6.32 and 6.59 cm/sec., for runs CSO, CS1 & CS1A, and CS3 & CS3A respectively. The fall velocities corrected to 24^{o} C computed from the centroid of the deposited material were 6.00, 6.00 and 6.25 cm/sec, for these runs. The percentage of the injected material which was recovered was 98.0, 87.5 and 96.5 respectively for the three runs. The shapes of all distribution curves were almost identical with the one shown in Figure 27. The average injected concentrations were 162, 166 and 78.5 ppm respectively for runs CSO, CS1 & CS1A and CS3 & CS3A. The injected concentrations used in runs CS3 & CS3A was reduced by plugging half of the holes in the injector.

In order to determine the effect of the injection system on the resulting fall velocity, a special experiment was performed. Sand was injected in the usual manner for a length of time about equivalent to that of a normal run. Then one hundred and fifty grams of tracer particles which had been tagged by being coated with a fluorescent dye, were injected. These particles were injected wet with a salt shaker. The hole size in the lid of the shaker was such that no more than four or five particles would come out of each hole at a time. Care was taken to see that the particles entered the water with nearly zero initial

velocity. After the one hundred and fifty grams of tracer particles had been injected more sand was injected in the usual manner. The flow was then stopped soon after the second batch of normal sand had been injected and the water drained off. After the sand had dried, it was taken up in strips and the concentration of tracer particles was determined for each strip.

The concentration of the tracer particles in each strip was determined as follows. The average weight of a dyed particle was determined by counting out about one thousand grains and weighing them. The process was repeated five times. The average of all five measurements was 9,430 grains per gram with individual measurements ranging from 9,200 to 9,970 grains per gram. The sample from each strip was mixed thoroughly, then a sample of about one hundred grams was separated and the number of tracer particles were counted under an ultraviolet light. The size of the separated portion was determined in order that approximately 2,000 tracer particles should occur in each portion. From the weight of the sample, the number of tracer particles, and the average weight of a sand grain, the concentration of tracer particles was computed. From the concentration of tracer particles and the total weight of each strip, Figure 27 was constructed. From Figure 27 the mean turbulent fall velocity of each the dyed and the undyed particles was computed as was done for the fine sediment.

The average injected concentration was 191 ppm for the undyed sand. The percentage of the injected sediment which was recovered was 98.7 and 101.1 for the undyed and dyed particles respectively. The weight of tracer particles recovered was calculated by multiplying the concen-

tration computed in each strip by the total weight of sand recovered in that strip. The median turbulent fall velocity of these particles corrected at 24° C, was computed to be 6.30 and 6.40 cm/sec. for the dyed and the undyed particles respectively. The mean turbulent fall velocity corrected to 24° C was computed to be 5.89 and 6.08 cm/sec for the dyed and undyed particles. The average concentration of tracer particles in the strips increased more or less uniformly from twenty-five ppm at station 95 to forty-two ppm at station 105. It can be seen from the above experiment that the injection system did appear to increase the fall velocity of the particles, but that at least for flow condition A with coarse sediment this increase was relatively insignificant.

Figure 28 gives the turbulent fall velocities corrected to 24° C as determined from the measured concentration profiles. Pertinent information regarding the method of injection is summarized below.

Run	Hole Size	Injection Rate grams/sec/hole	ppm
CSO	1/8"	0.87	162
CS1-CS1A	1/8"	.87	166
CS3-CS3A	1/8"	.87	78
CS11-CS11A	5/32"	1.8	162
CS21-CS21A	3/16"	2.8	212
CS23-CS23A	1/8"	.87	51

For flow conditions A and C, runs were made on different days which were identical except for the injection concentration and minor variations in water temperature. No consistent difference could be detected in the concentration profiles for these runs. Even though no difference

could be detected, a five percent increase in the turbulent fall velocity was detected from the sediment deposition data for a decrease in mean concentration from 162 to 78 ppm for flow condition A. Two factors would affect the particle fall velocities in the two runs for flow condition C, the increase in mean concentration for CS21 could decrease the particle fall velocity, however, the increase in hole size may have caused the particles to fall faster due to a greater grouping effect. Thus it may be that the particle fall velocity for both runs in the flow condition C were nearly identical. Averaged turbulent fall velocities corrected to 24^{O} C computed from the concentration profiles were 6.72, 6.49 and 6.56 cm/sec respectively for flows A, B and C. This gives ratios of V_{ST}/V_{sq} of 1.06, 1.03 and 1.04 respectively for flow conditions A, B and C.

D. Results of the Diffusion Experiments

1. The Conservation of Mass Equation

The dimensionless form of the conservation equation which is used in this experiment was given in Equation 37 where it has been assumed that the effects of secondary currents are negligible. It will be discussed later why this assumption is approximately true for this experiment. Integrating Equation 37 from some arbitrary depth to the surface gives

$$\int_{\eta_1}^{1.0} \frac{u}{u_*} \frac{\partial c}{\partial X} \, d\eta = \int_{\eta_1}^{1.0} \frac{\partial}{\partial \eta} \left[\frac{\varepsilon_\Gamma}{Y_N u_*} \frac{\partial c}{\partial \eta} + \frac{V_{ST}}{u_*} c \right] d\eta$$

or

$$\frac{\partial}{\partial X} \int_{\eta_1}^{1.0} \frac{u}{u_*} c \, d\eta = \left[\frac{\varepsilon_\Gamma}{Y_N u_*} \frac{\partial c}{\partial \eta} + \frac{V_{ST}}{u_*} c \right] \Bigg|_{\eta_1}^{1.0} \qquad (43)$$

At $\eta = 1.0, \frac{\varepsilon_\Gamma}{Y_N u_*} \frac{\partial c}{\partial \eta} + \frac{V_{ST}}{u_*} c$ is the transport of dispersants across the surface which is zero except at the source. Therefore, Equation 43 can be evaluated as

$$\frac{\partial}{\partial X} \int_{\eta_1}^{1.0} \frac{u}{u_*} c \, d\eta = - \frac{\varepsilon_\Gamma}{Y_N u_*} \left| \frac{\partial c}{\partial \eta} \right|_{\eta_1} \Bigg|_{\eta_1} - \frac{V_{ST}}{u_*} \left| c \right|_{\eta_1} \Bigg|_{\eta_1} . \qquad (44)$$

The values of $\frac{\varepsilon_\Gamma}{Y_N u_*}$ and $\frac{V_{ST}}{u_*}$ were evaluated from Equation 44 and the measured velocity and concentration profiles. However, the procedure did not assume a constant value of velocity as did Al-Saffar (1964).

2. The Dye Transfer Experiments

These experiments included all runs in which fluorescent dye was used as the dispersant. It was assumed as did Elder (1959, p. 545) that the dyed fluid particles were hydrodynamically indistinguishable from the normal fluid particles. The flume roughness and the depth were held constant for all runs which should insure similarity of the velocity profiles. Provided that ε_d is proportional to $Y_N u_*$ then the measured concentrations should be functions only of X and η and not a function of U. Measurements indicated that ε_d was proportional to $Y_N u_*$ because the measured concentration profiles for the dye runs were independent of U.

After all profiles had been normalized to give a constant flux, as previously described, a single averaged profile for each station was determined from all runs. A few of the integrated profiles for distances greater than fifteen depths which showed obvious divergent tendencies were not averaged. All other runs were given equal weight and the concentration and relative depths averaged. The average points were plotted

and a smooth curve drawn through the points. Figures 29 and 30 show some of these averaged measured profiles. Also shown in these figures are the measured points and computed profiles which will be discussed later. The profiles for distances X = 10 and X = 14 are not shown in Figure 29.

Some divergence occurred between the concentration profiles measured with the fixed and integrating probes. When the dispersant was injected at the surface, the integrated samples indicated more rapid mixing for distances greater than fifteen normal depths from the source. When the dye was injected at the floor the integrated samples indicated a positive concentration gradient for distances greater than twelve normal depths. This anomaly was attributed to the effects of secondary currents and will be discussed later. Fixed probe samples were considered to be the least affected by secondary currents since they were not located in the updraft and downdraft regions of the secondary currents.

The following procedure was used to determine the transfer coefficient from the measured concentration profiles. From the averaged profiles the values of the concentration were read at equal intervals $\Delta\eta$ = 0.05 and from these values both $\frac{\partial c}{\partial \eta}$ and $\int_{\eta_1}^{1.0} \frac{u}{u_*}\, c\, d\eta$ were computed. In computing $\int_{\eta_1}^{1.0} \frac{u}{u_*}\, c\, d\eta$ the value of $\frac{u}{u_*}$ which had been averaged for all three flow conditions was used. The values of $\frac{\partial c}{\partial \eta}$ and $\int_{\eta_1}^{1.0} \frac{u}{u_*}\, c\, d\eta$ were then plotted versus η and the results smoothed. The smoothed values of $\frac{\partial c}{\partial \eta}$ and $\int_{\eta_1}^{1.0} \frac{u}{u_*}\, c\, d\eta$ were then plotted as a function of X and a smooth curve drawn through the points. Intervals of $\Delta\eta$ = 0.1 were used when plotting $\frac{\partial c}{\partial \eta}$ and $\int_{\eta_1}^{1.0} \frac{u}{u_*}\, c\, d\eta$ as functions of X. The value of $\int_{\eta_1}^{1.0} \frac{u}{u_*} c\, d\eta$

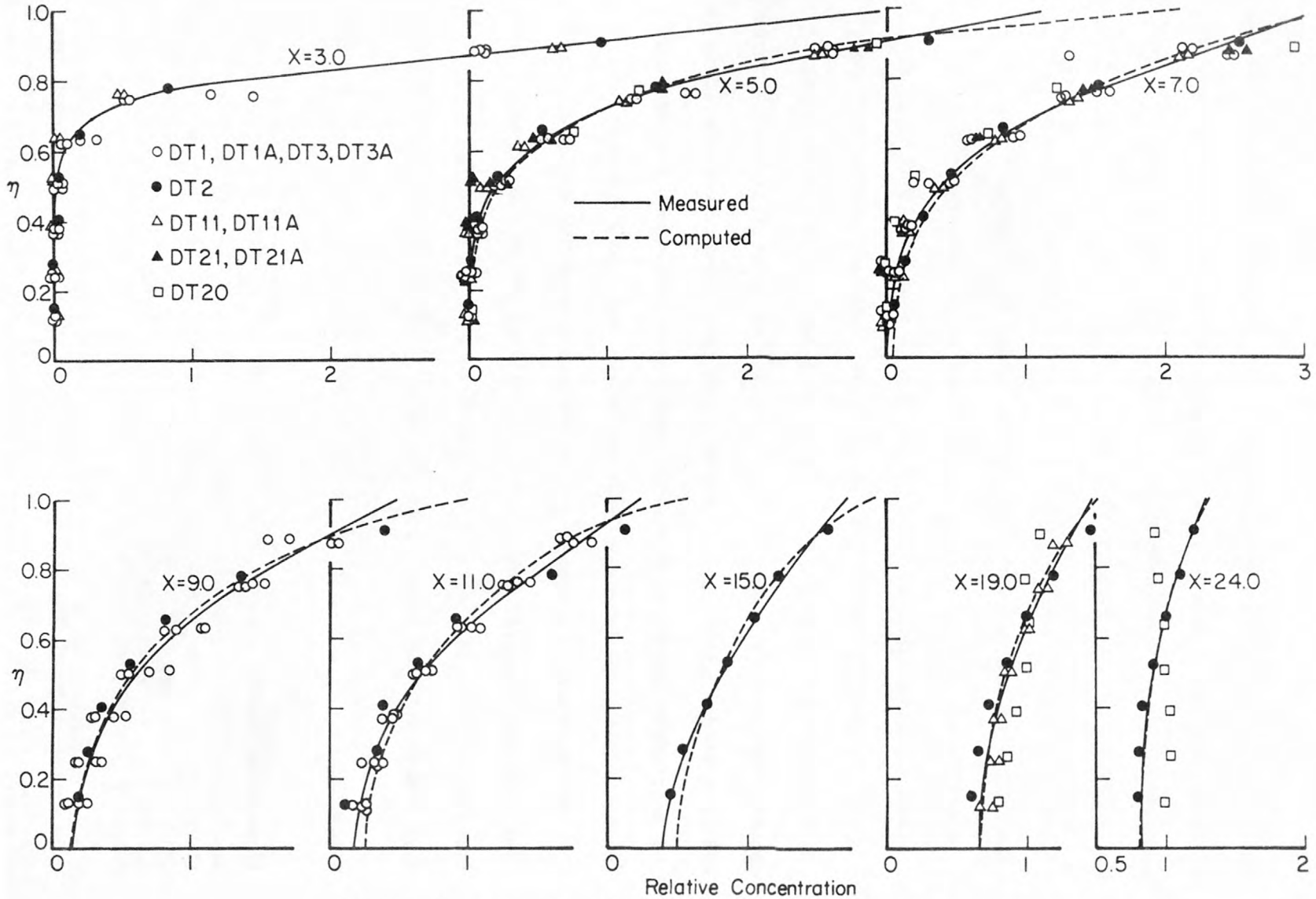

Figure 29.--Concentration profiles; dye injected at water surface.

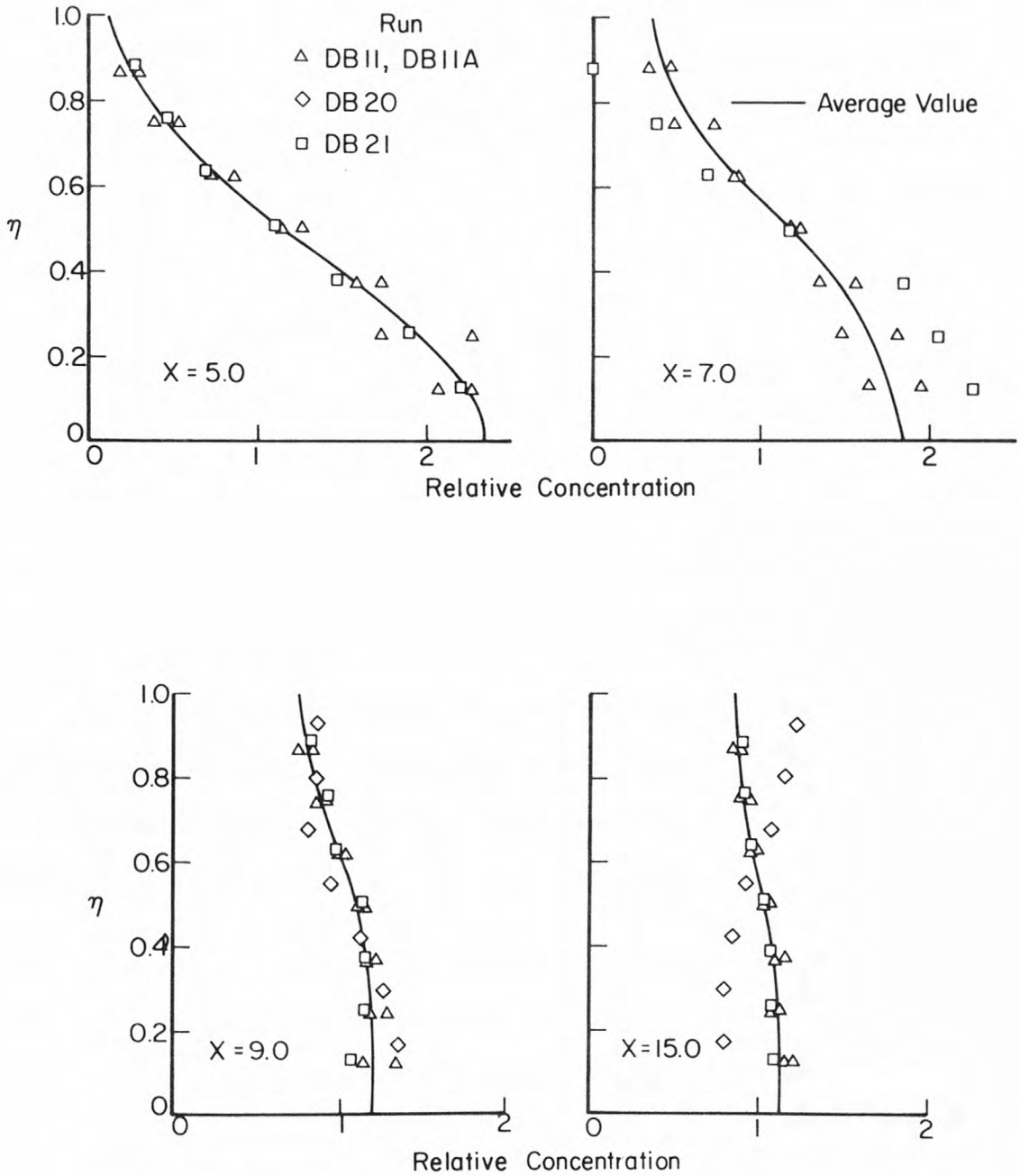

Figure 30.--Concentration profiles; dye injected at bed.

was then graphically differentiated with respect to X to give the vertical dispersant flux.

With $V_{ST} = 0$, Equation 44 can be solved for the mass transfer coefficient as

$$\left.\frac{\varepsilon_d}{Y_N u_*}\right|_{\eta_1} = - \frac{\frac{\partial}{\partial X}\int_{\eta_1}^{1.0} \frac{u}{u_*}\, c\, d\eta}{\left.\frac{\partial c}{\partial \eta}\right|_{\eta_1}} \quad . \tag{45}$$

Since the flow is uniform $\frac{\varepsilon_d}{Y_N u_*}$ is not a function of X and plots of $\left.\frac{\partial c}{\partial \eta}\right|_{\eta_1}$ and $\frac{\partial}{X}\int_{\eta_1}^{1.0} \frac{u}{u_*}\, c\, d\eta$ should have the same shape when they are plotted on semi-logarimithic paper. Figures 31 and 32 show these plots for the top dye experiment with $\eta_1 = 0.6$. The value of $\frac{\varepsilon_d}{Y_N u_*}$ was determined by finding the ratio of the ordinates which would make graphs like Figures 31 and 32 most nearly agree. This was done by plotting both graphs on tracing paper and then visually alining the curves. The degree of fit between $\frac{\partial}{\partial X}\int_{\eta_1}^{1.0} \frac{u}{u_*}\, c\, d\eta$ and the $\left.\frac{\partial c}{\partial \eta}\right|_{\eta_1}$ curves improved near the surface for the top dye runs and near the floor for the bottom dye runs. The top dye experiments were given the most weight in determining the values of $\frac{\varepsilon_d}{Y_N u_*}$ in the top part of the flow and the bottom dye experiments were given the most weight in determining the value of $\frac{\varepsilon_d}{Y_N u_*}$ in the bottom part of the flow. Actually since many more experiments were conducted by injecting dye at the top and since the initial conditions were hard to control for the bottom dye experiments,

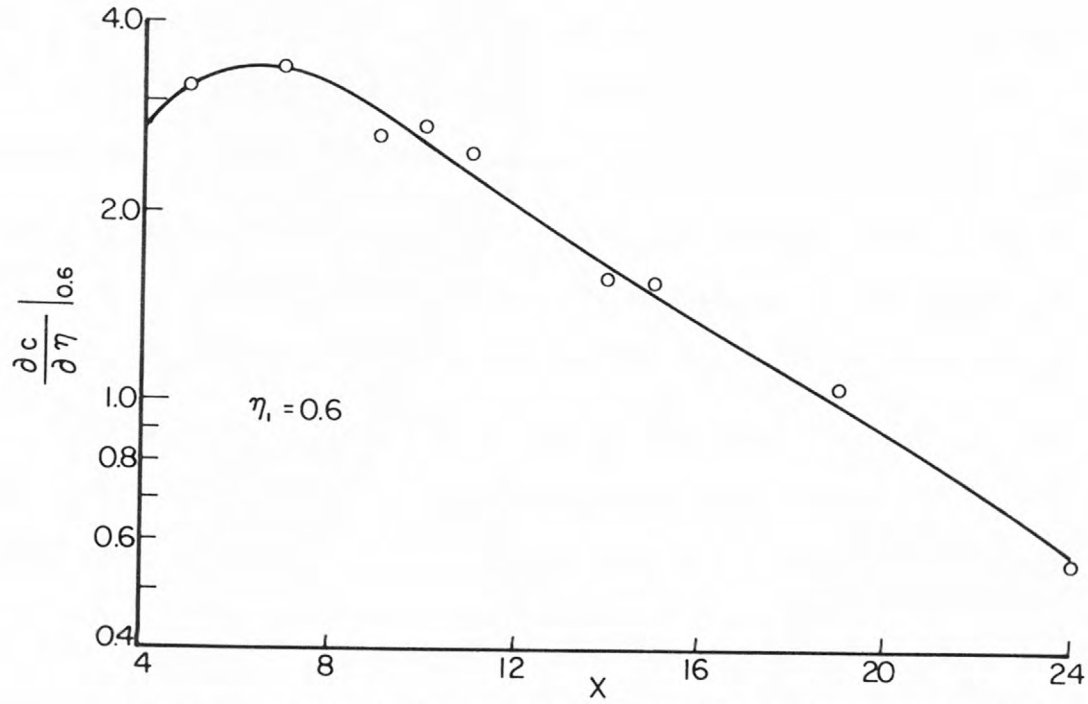

Figure 31.--Longitudinal distribution of vertical concentration gradient at $\eta_1 = 0.6$; dye injected at top.

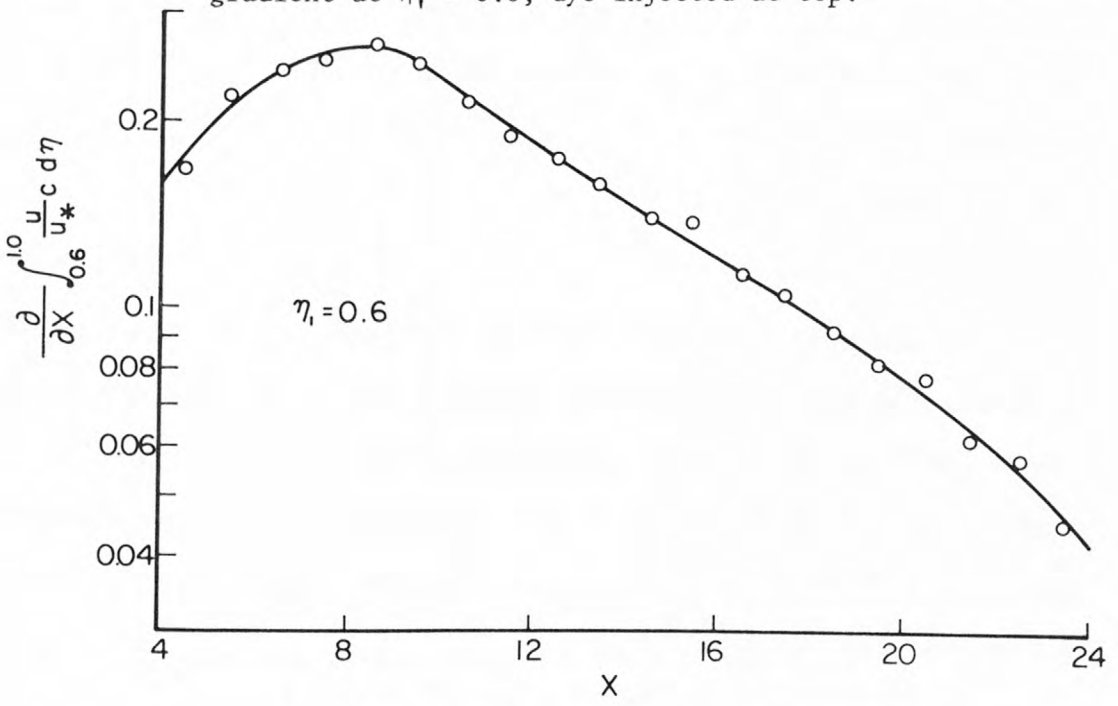

Figure 32.--Longitudinal distribution of vertical flux at $\eta_1 = 0.6$; dye injected at top.

the top dye experiments were used exclusively for determining $\frac{\varepsilon_d}{Y_N u_*}$ in all except the bottom thirty percent of the flow. Three values of $\frac{\varepsilon_d}{Y_N u_*}$ were determined for each relative depth, one which was considered to be the most probable value (mpv) and two values which were considered to represent the confidence limits on the measured values. The data points shown in Figure 33 are the most probable value of $\frac{\varepsilon_d}{Y_N u_*}$ as determined from Figures like 31 and 32. The cross hatched area in Figure 33 indicates what is believed to be the range of at least ninety percent confidence in the value of $\frac{\varepsilon_d}{Y_N u_*}$. The dashed line represents the momentum transfer coefficient assuming $\kappa = 0.392$ computed from Equation 22. The smooth curve in Figure 33 represents the most probable value of $\frac{\varepsilon_d}{Y_N u_*}$ used in all subsequent calculations. The mean of the most probable value of $\frac{\varepsilon_d}{Y_N u_*}$ is then computed to be 0.0633 giving a turbulent Schmidt number of $Sc = \frac{0.0653}{0.0633} = 1.03$ where ε_m is computed from Equation 22 with $\kappa = 0.392$.

An estimate of the significance of the longitudinal diffusion terms in Equation 5 was determined from measured data. The measured concentration profiles allow the determination of the concentration as a function of both X and η. The steady two dimensional diffusion equation was assumed in which the fall velocity was zero. Equation 5 in non-dimensional form then reduces to

$$\frac{u}{u_*} \frac{\partial c}{\partial X} = \frac{\varepsilon_{dx}}{Y_N u_*} \frac{\partial^2 c}{\partial X^2} + \frac{\partial}{\partial \eta} \left[\frac{\varepsilon_{dy}}{Y_N u_*} \frac{\partial c}{\partial \eta} \right] .$$

From this equation it can be seen that the longitudinal diffusion term is truly negligible if

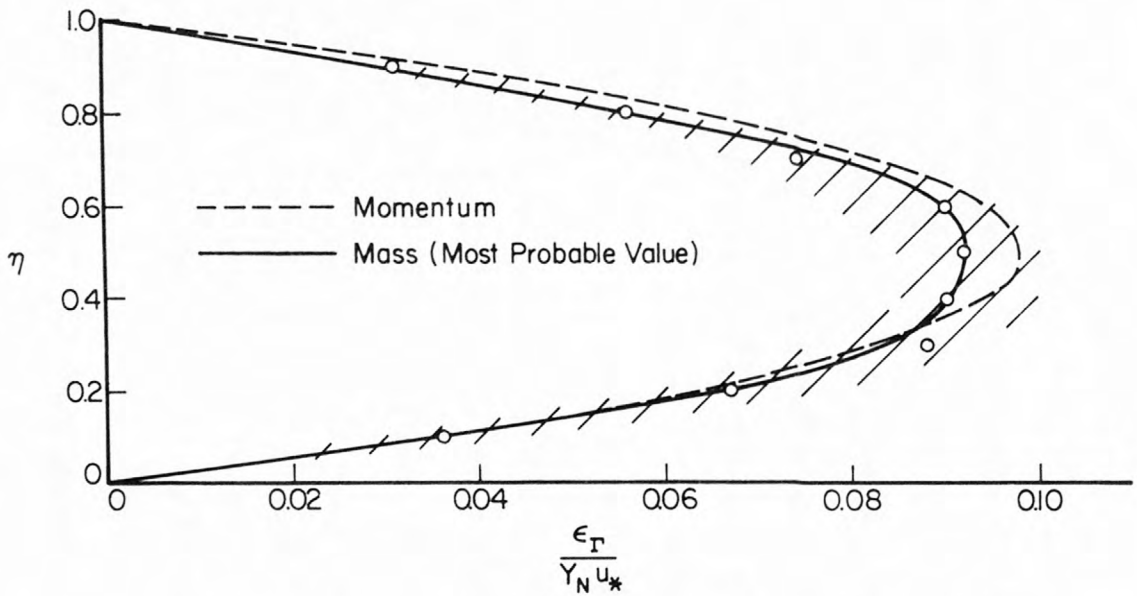

Figure 33.--Measured mass transfer coefficients for dye.

$$\frac{\varepsilon_{dx}}{Y_N u_*} \frac{\partial^2 c}{\partial X^2} << \frac{\partial}{\partial \eta}\left(\frac{\varepsilon_{dy}}{Y_N u_*}\right) \frac{\partial c}{\partial \eta} + \frac{\varepsilon_{dy}}{Y_N u_*} \frac{\partial^2 c}{\partial \eta^2}$$

In order to evaluate the significance of the longitudinal diffusion, a logarithmic velocity distribution and an analogy between mass and momentum transfer were assumed valid. Then from Equation 22 the mass transfer coefficient can be computed

$$\frac{\varepsilon_{dy}}{Y_N u_*} = 0.392\ \eta\ (1-\eta)\ 0.97\ .$$

The longitudinal transfer coefficient was also assumed to be equal to the vertical transfer coefficient. Actually ε_{dx} is larger than ε_{dy} because of the greater longitudinal intensities and scales of turbulence, however, the difference should not be more than two or three hundred percent. With these assumptions than the effect of longitudinal diffusion is small if

$$\frac{\partial^2 c}{\partial X^2} << \frac{\partial c}{\partial \eta} \frac{(1-2\eta)}{\eta(1-\eta)} + \frac{\partial^2 c}{\partial \eta^2}\ . \qquad (46)$$

All terms in this expression were evaluated approximately from the measured concentration profiles for values of η = 0.1, 0.5 and 0.9 and for all values of X in the test reach. The measurements indicated that the longitudinal transfer due to diffusion was on the order of one per cent of the vertical transfer. This was considered a negligible quantity.

3. The Sediment Transfer Experiments

The transfer of sediment is a much more complex phenomenon than the transfer of dye. Because only limited data were available and because of the increased complexity of the process a different procedure was used when analyzing the results of the sediment experiments.

The flux of dispersant past any section is not constant in the sediment transfer experiments as it was in the dye experiments because the material tends to settle out and be deposited on the bed. The rate of decrease in the flux of sediment depends upon the turbulent fall velocity and the probability of deposit once a particle encounters the bed. The recovery ratio (RR) is the percentage of the original flux remaining in suspension at any station. The concentration profiles were normalized using the same procedure as outlined in Chapter IV-A-3.

The following procedure was used to determine RR as a function of X. The measured concentrations were plotted and a smooth curve drawn through the points. The flux past each station was then computed by graphical integration, using ten increments in the vertical. The measured recovery ratio was computed as the ratio of the measured flux to the injected flux. The measured recovery ratios were plotted as a function of X for all runs at a given flow condition and sediment size and a smooth curve was drawn through the plotted points. The recovery ratio then was read from this smooth curve and used in all subsequent calculations.

When runs were made on separate days, for example, the coarse sediment runs for flow conditions A and C the variation of mean concentration and small changes in water temperature did not appear to significantly affect the measured concentration profiles so the results were combined. After all profiles had been normalized the concentrations and relative depths were averaged and plotted as a function of relative depth. A smooth curve was then drawn through the average concentration points. Figures 34 through 39 show all data points as well as the averaged smooth

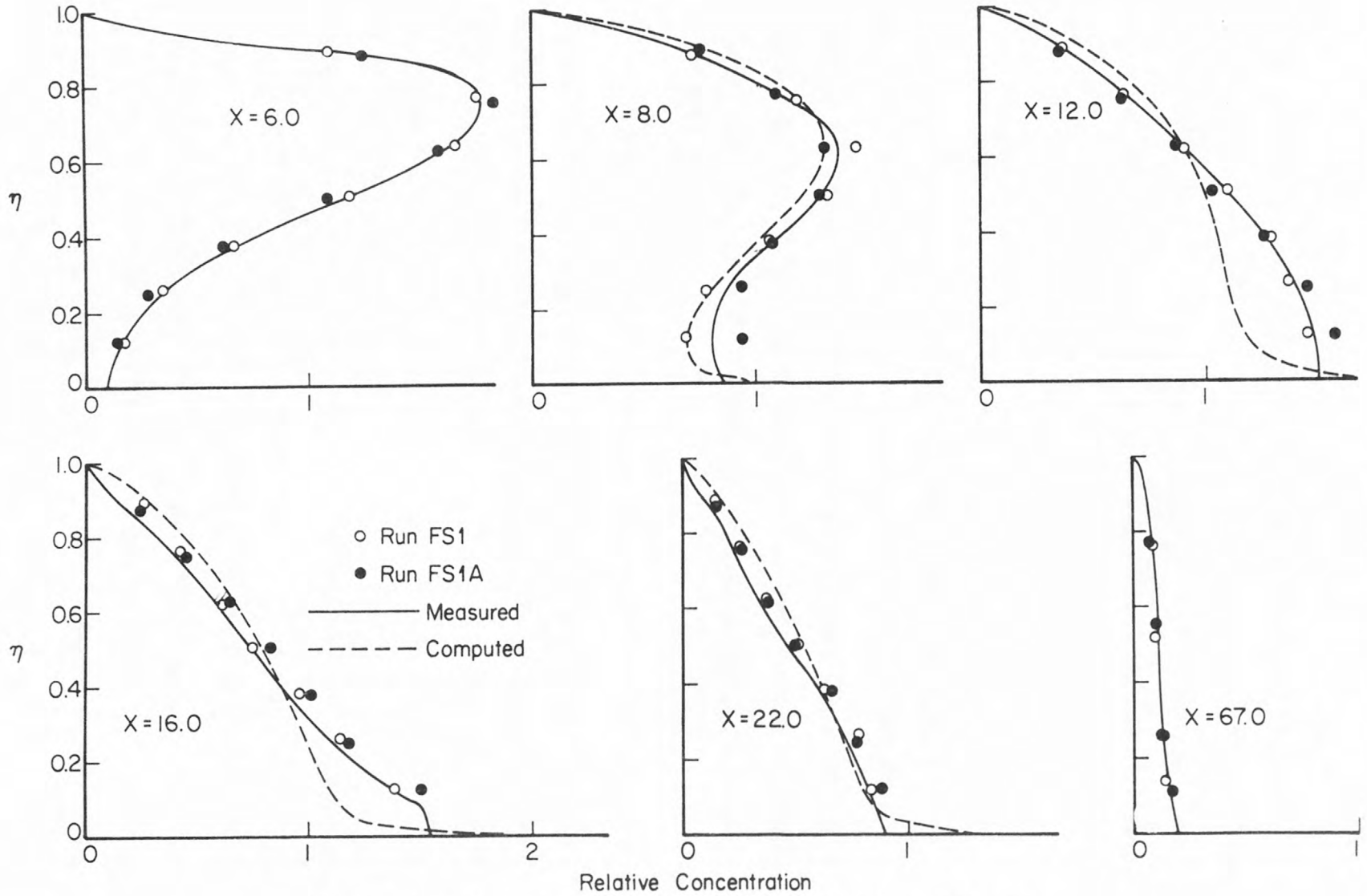

Figure 34.--Concentration profiles; flow A, fine sediment.

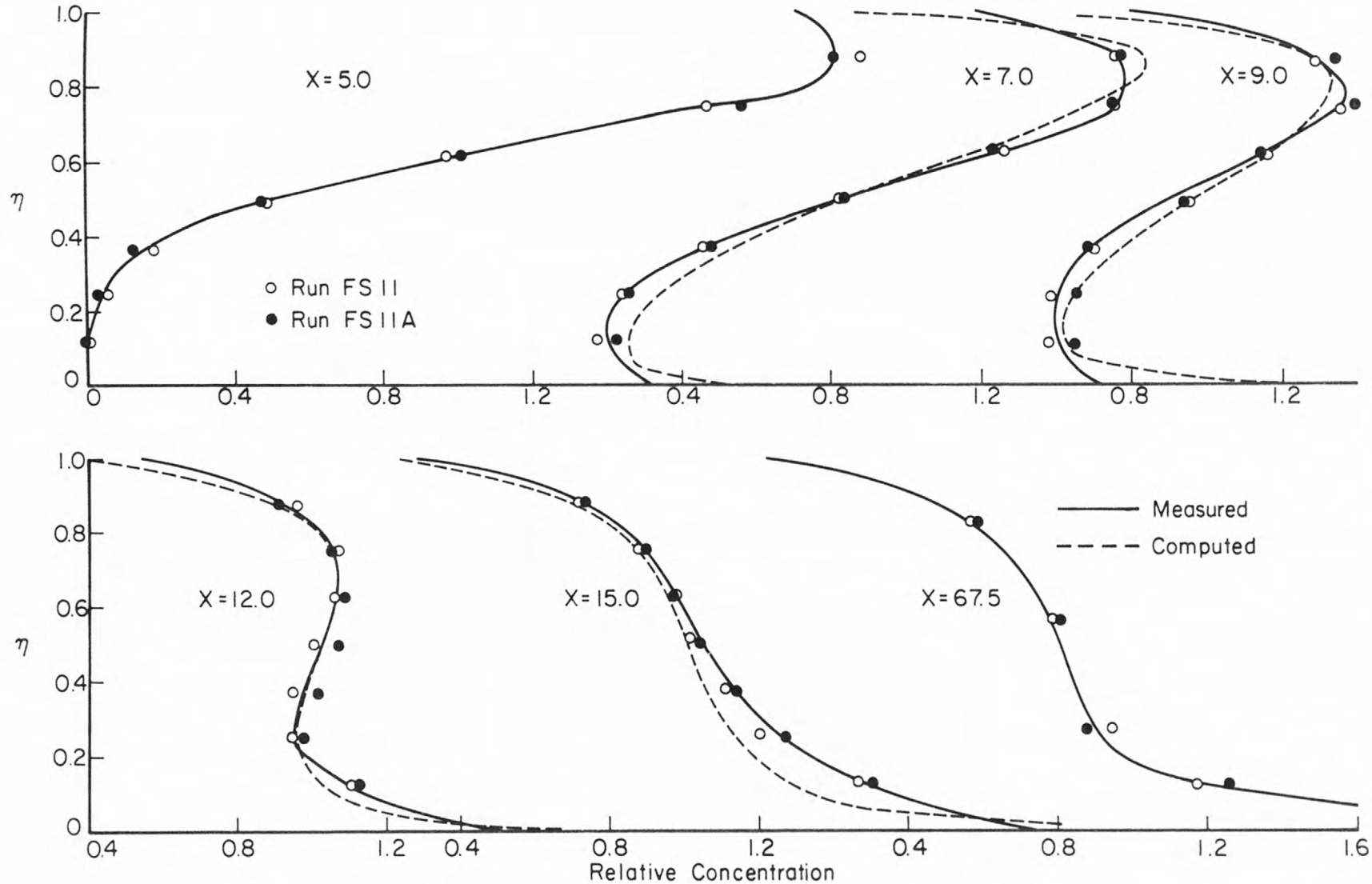

Figure 35.--Concentration profiles; flow B, fine sediment.

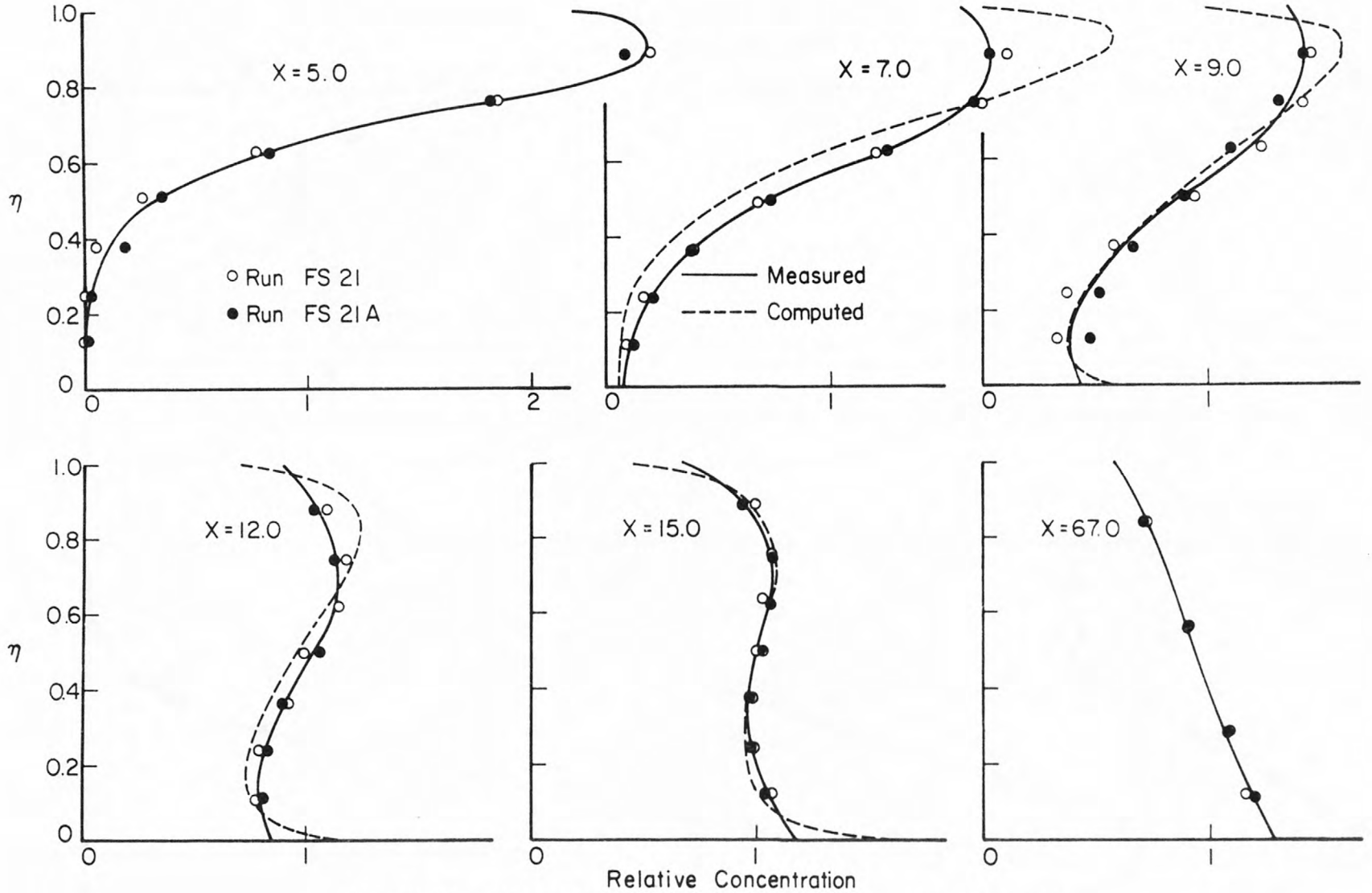

Figure 36.--Concentration profiles; flow C, fine sediment.

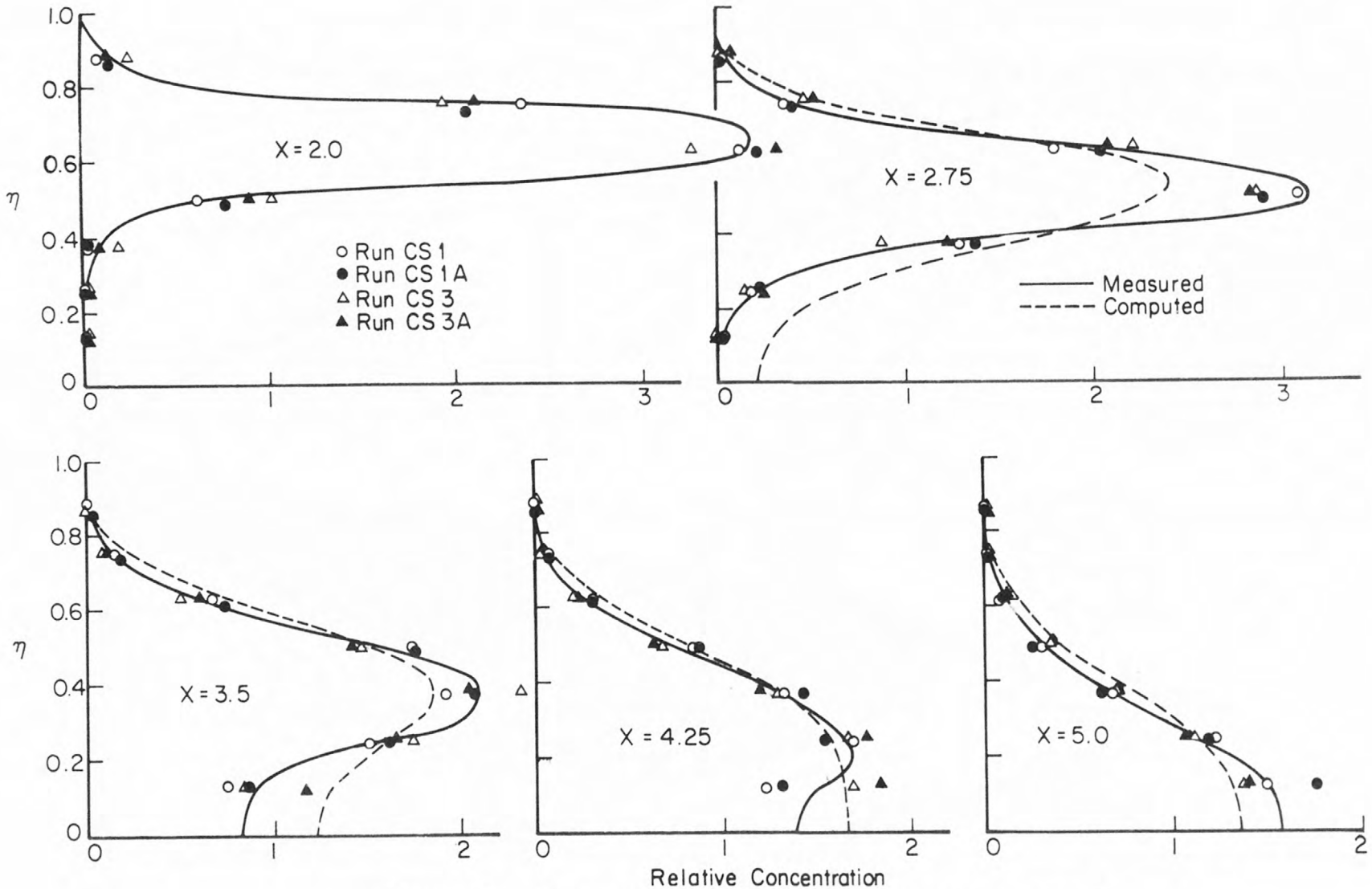

Figure 37.--Concentration profiles; flow A, coarse sediment.

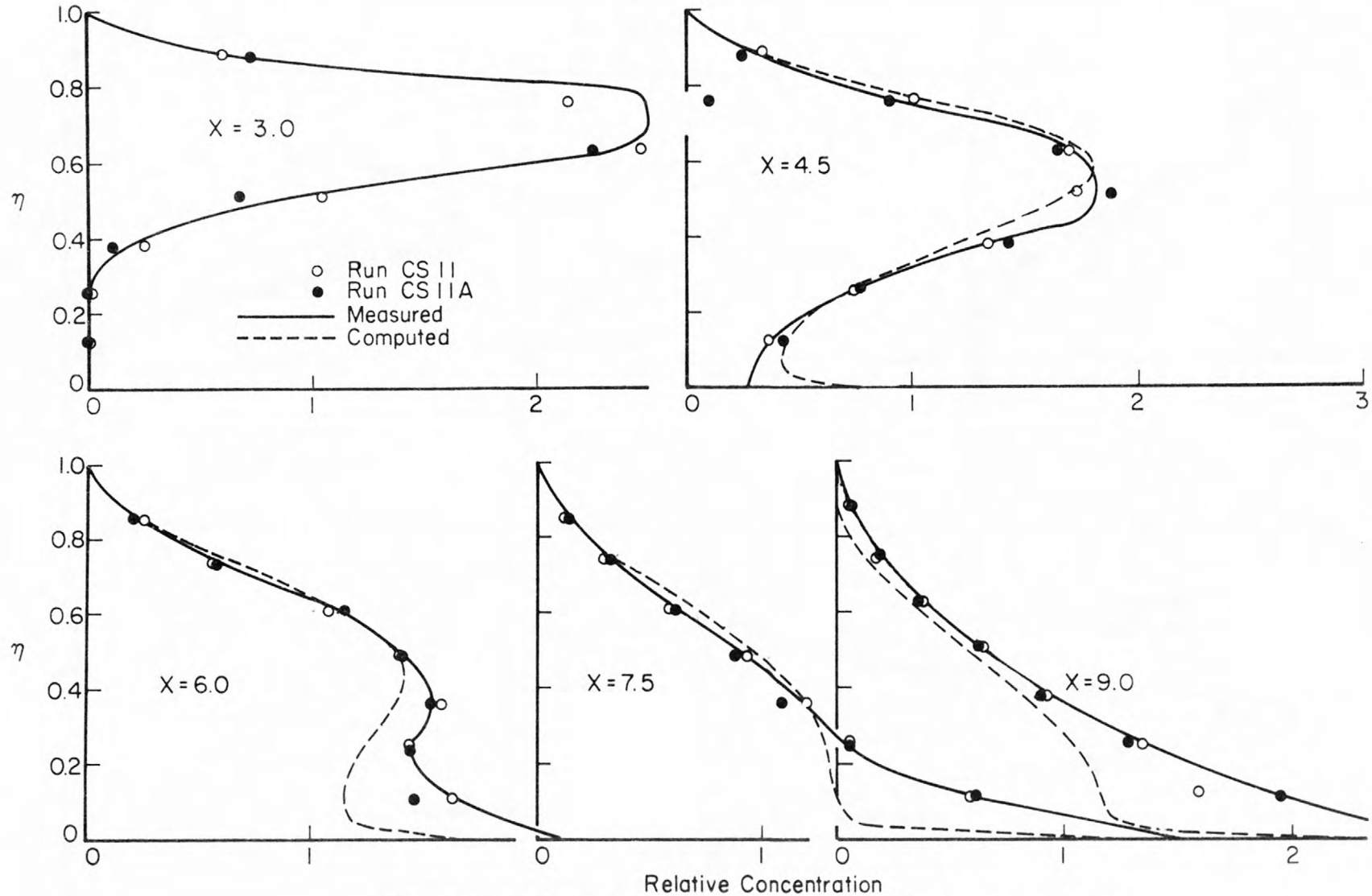

Figure 38.--Concentration profiles; flow B, coarse sediment.

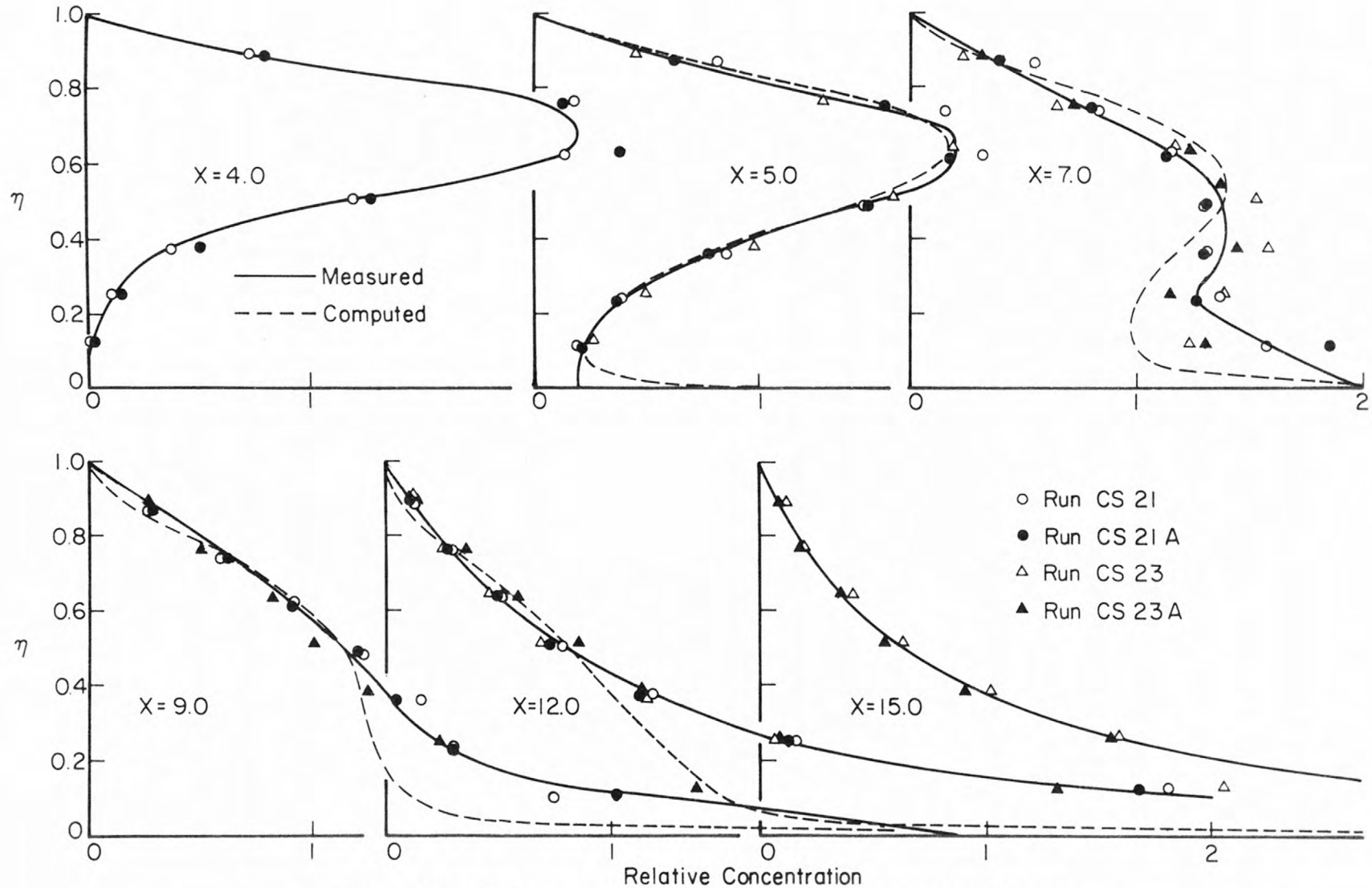

Figure 39.--Concentration profiles; flow C, coarse sediment.

curves drawn through the points. The averaged smooth curves are representated by the solid lines. The dashed lines in these figures represent the computed profiles and will be discussed later.

The procedure used to compute the dye mass transfer coefficient cannot be applied directly to determining the sediment transfer coefficient for two primary reasons. First, with sediment there are two unknowns in Equation 44 instead of only one. To use the previous procedure one would have to assume one of the unknowns and then compute the other. The second reason is that the concentration gradient and the vertical flux change signs which make plotting on log paper difficult. For these reasons a different approach was used for the analysis of the sediment profiles.

A close look at Equation 44 reveals that three terms are functions of X and two are not. In order to simplify notation the three terms that are functions of X will be renamed as follows:

$$\left.\begin{aligned} \Sigma &= \frac{\partial c}{\partial \eta}\Big|_{\eta_1} \\ \psi &= c\Big|_{\eta_1} \\ \Omega &= \frac{\partial}{\partial X}\int_{\eta_1}^{1.0} \frac{u}{u_*}\, c\, d\eta \quad . \end{aligned}\right\} \tag{47}$$

All of these terms are functions of X and η, however in all cases only one value of η will be considered at a time. Therefore, effectively they will be functions of X only. With this notation Equation 44 can be written

$$\Omega + \frac{\varepsilon_{se}}{Y_N u_*}\,\Sigma + \frac{V_{ST}}{u_*}\,\psi = 0 \quad . \tag{48}$$

The terms Ω, Σ, and ψ can be evaluated from measured profiles and for a given value of η_1, both $\frac{\varepsilon_{se}}{Y_N u_*}$ and $\frac{V_{ST}}{u_*}$ are assumed to remain constant. If measured values of Ω, Σ, and ψ and constant values of $\frac{\varepsilon_{se}}{Y_N u_*}$ and $\frac{V_{ST}}{u_*}$ are used in Equation 48, the right side probably will not be exactly zero. The value of the right side of Equation 48 will be called E_r. If the true values of $\frac{\varepsilon_{se}}{Y_N u_*}$ and $\frac{V_{ST}}{u_*}$ are used in Equation 48 then E_r represents an error in measurements. Equation 48 can then be written

$$\Omega + \frac{\varepsilon_{se}}{Y_N u_*} \Sigma + \frac{V_{ST}}{u_*} \psi = E_r \ . \tag{49}$$

When the values of Ω, Σ and ψ are evaluated from the data, various numerical curve fitting techniques can be used to compute $\frac{\varepsilon_{se}}{Y_N u_*}$ and $\frac{V_{ST}}{u_*}$ such that the value of E_r has specified properties. Two curve fitting techniques, the least squares and the method of averages, which were used to evaluate $\frac{\varepsilon_{se}}{Y_N u_*}$ and $\frac{V_{ST}}{u_*}$ from the measured values of Ω, Σ and ψ, will be presented.

The value of $\psi = c \big|_{\eta_1}$ can be taken directly from Figures 34 through 39. The values taken from these figures were then plotted as functions of X as demonstrated in Figure 40 for data taken from Figure 39.

The value of $\Sigma = \frac{\partial c}{\partial \eta}\Big|_{\eta_1}$ was also computed directly from the information in Figures 34 through 39. Values taken from the figures were first plotted as a function of η for each value of X and a smooth curve was drawn through the points. Then from the set of smooth curves of $\frac{\partial c}{\partial \eta}$ vs η, curves like those in Figure 41 were plotted.

To determine the value of $\Omega = \frac{\partial}{\partial X} \int_{\eta_1}^{1.0} \frac{u}{u_*} c \, d\eta$ the following procedure was used. First values of $\int_{\eta_1}^{1.0} \frac{u}{u_*} c \, d\eta$ were determined from the averaged velocity and concentration profiles by numerical integration with

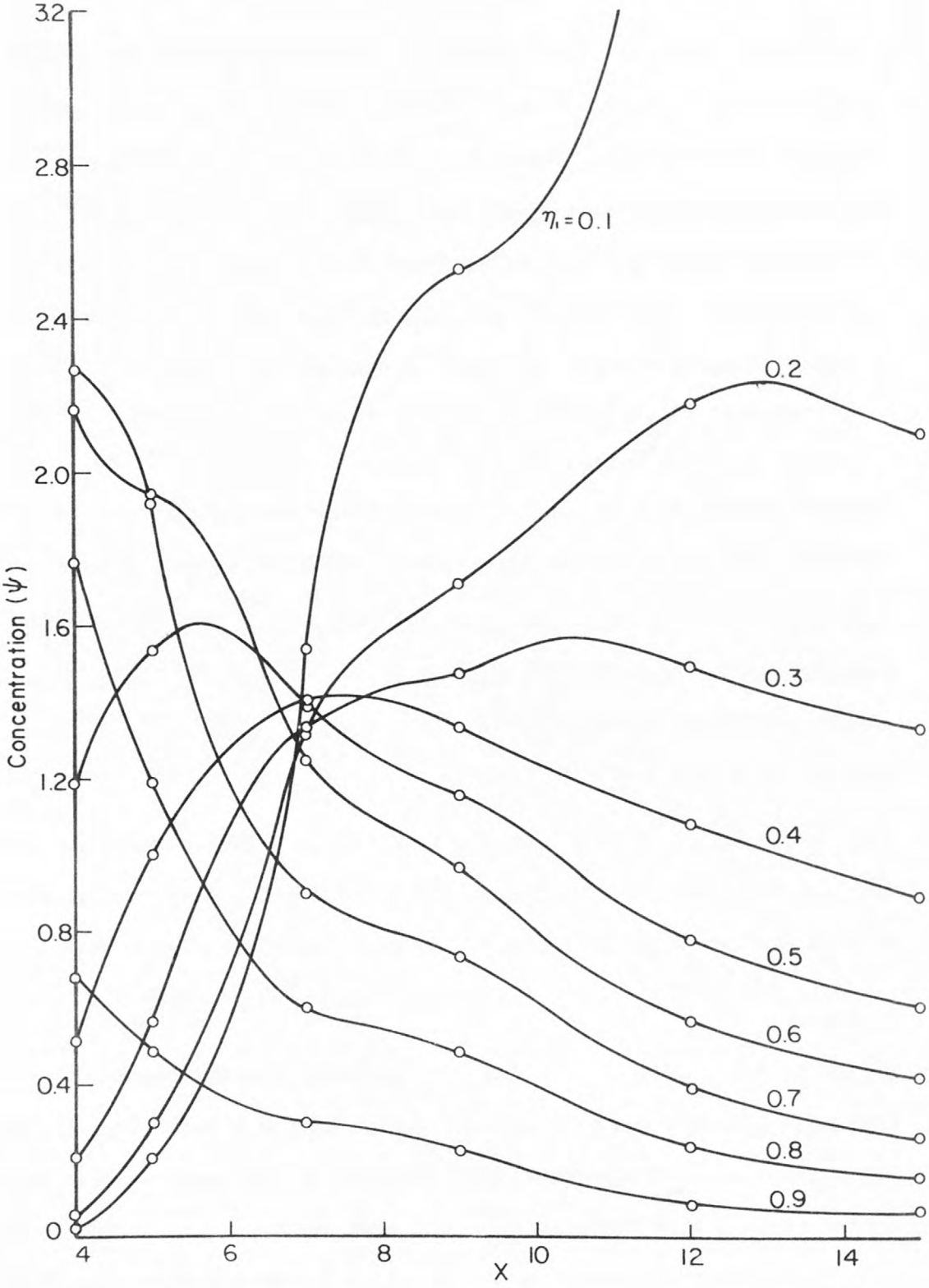

Figure 40.--Longitudinal concentration distribution; flow C, coarse sediment.

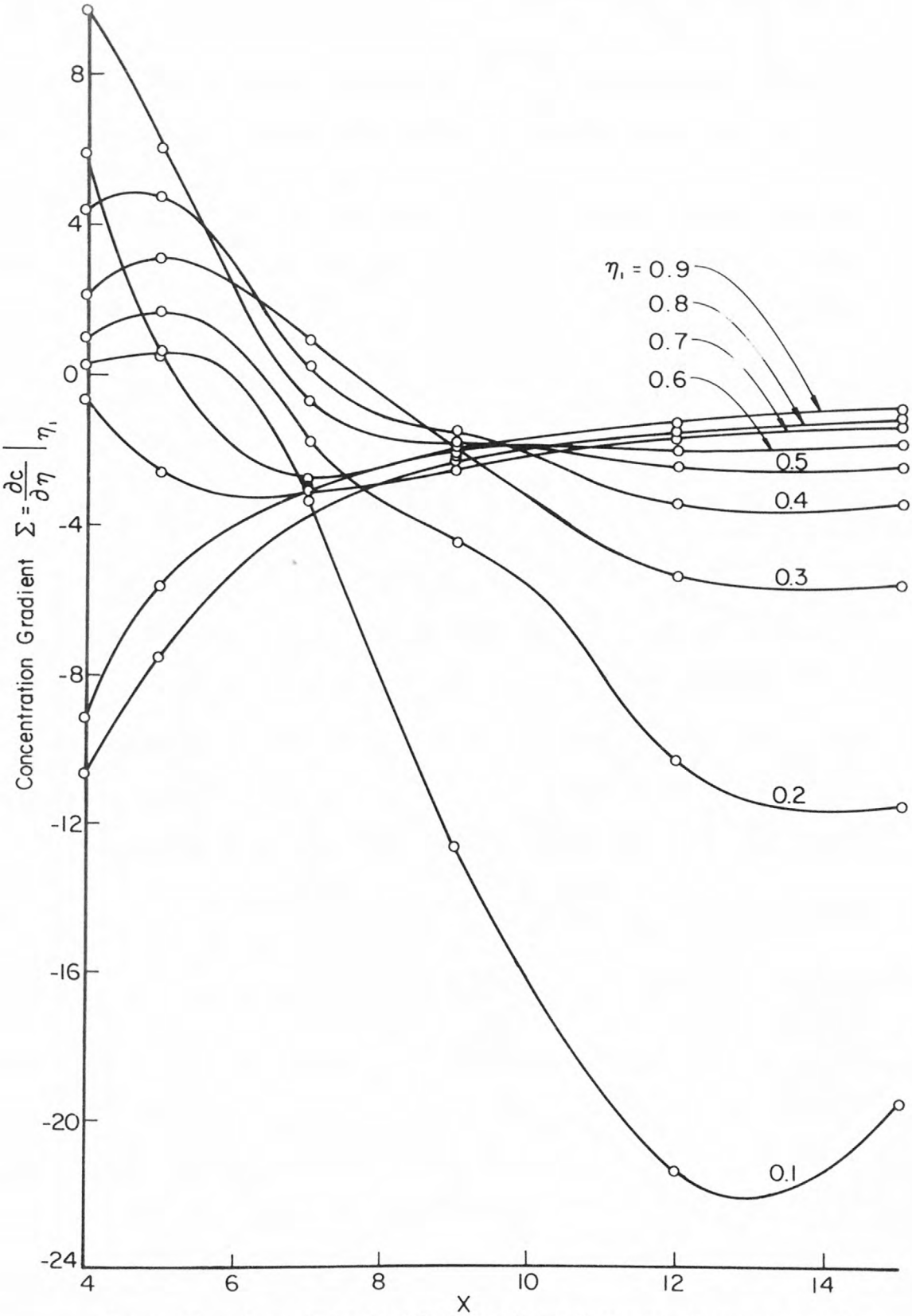

Figure 41.--Longitudinal distribution of vertical concentration gradient; flow C, coarse sediment.

$\Delta\eta = 0.05$. The values of $\int_{\eta_1}^{1.0} \frac{u}{u_*}\, c\, d\eta$ were plotted as a function of η for each value of X and smoothed. The smoothed values of $\int_{\eta_1}^{1.0} \frac{u}{u_*}\, c\, d\eta$ were plotted as a function of X for the nine values of η_1. Smooth curves were then drawn through the points and the curves were graphically differentiated. Plotting the values of $\int_{\eta_1}^{1.0} \frac{u}{u_*}\, c\, d\eta$ for all values of η_1 on one sheet of paper gave some help in drawing smooth curves through the plotted points. The resulting values of Ω for one flow condition are shown on Figure 42. To avoid confusion, Ω for all values of η_1 are not plotted on Figure 42.

The values of Ω, Σ, and ψ were read from curves like those shown in Figures 40, 41, and 42 at about thirty equally spaced values of X. In the standard least squares technique, values of $\frac{\varepsilon_{se}}{Y_N u_*}$ and $\frac{V_{ST}}{u_*}$ are determined such that the value of E_r^2 summed over the different values of X is minimized. This is done by first, squaring Equation 49 to obtain $(E_r)^2$, and then finding $\frac{\varepsilon_{se}}{Y_N u_*}$ and $\frac{V_{ST}}{u_*}$ corresponding to the minimized value of $\Sigma\,(E_r)^2$ by setting $\frac{\partial \Sigma (E_r)^2}{\partial (\varepsilon_{se}/Y_N u_*)}$ and $\frac{\partial \Sigma (E_r)^2}{\partial (V_{ST}/u_*)}$ equal to zero and solving these equations simultaneously for $\frac{\varepsilon_{se}}{Y_N u_*}$ and $\frac{V_{ST}}{u_*}$. This procedure was repeated for each value of η_1 and for all six combinations of sediment and flow conditions.

In the other curve fitting technique, the method of averages, the values of Ω, Σ and Ψ were divided into two groups, and $\frac{\varepsilon_{se}}{Y_N u_*}$ and $\frac{V_{ST}}{u_*}$ were determined such that the sum of the values of E_r was zero for each group. Equation 49 was applied to each set of values of Ω, Σ and ψ and

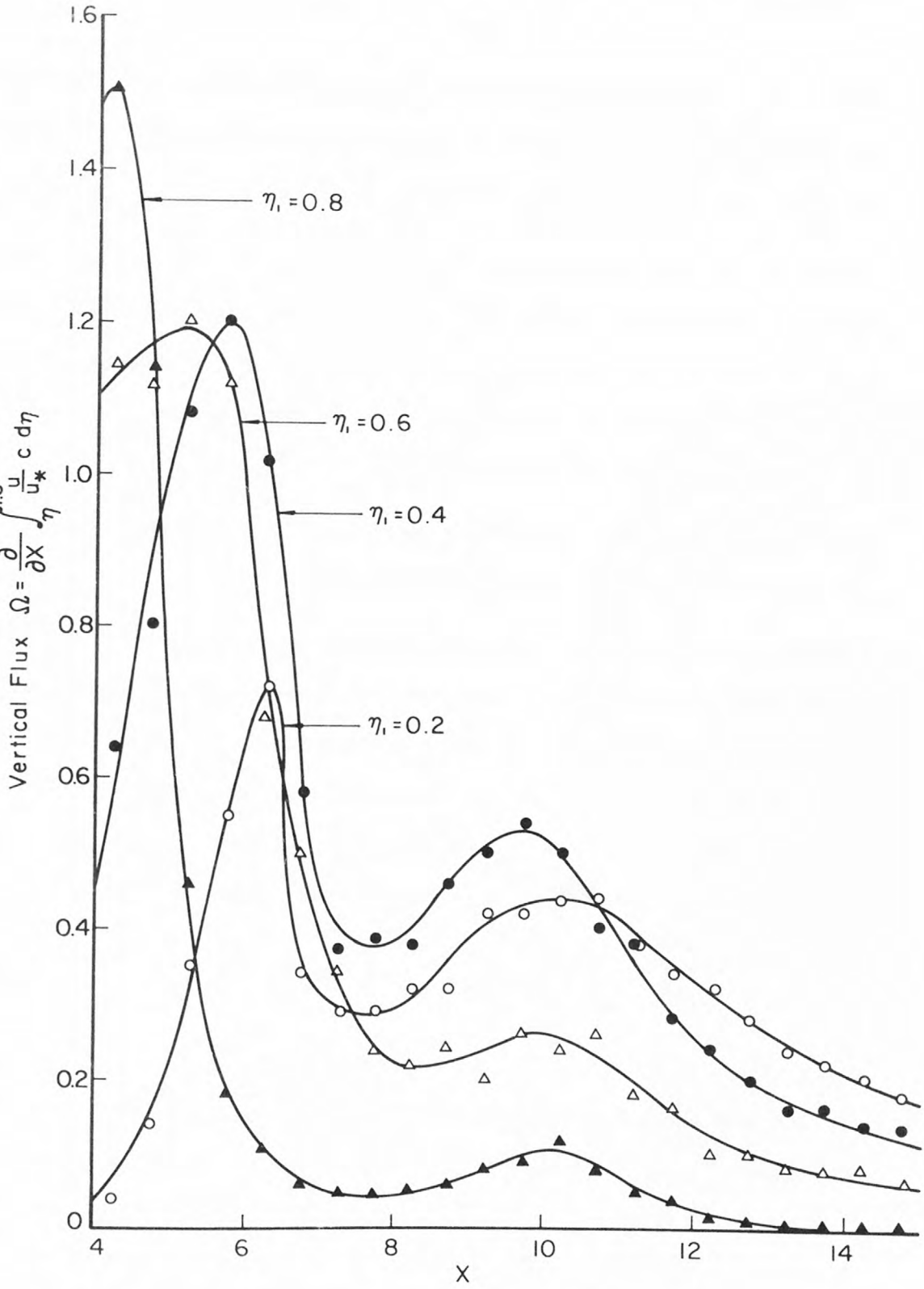

Figure 42.--Longitudinal distribution of vertical flux; flow C, coarse sediment.

these equations were summed for each group and the sum of the error terms set equal to zero. This resulted in two equations from which the values of $\frac{\varepsilon_{se}}{Y_N u_*}$ and $\frac{V_{ST}}{u_*}$ could be determined. The values of $\frac{\varepsilon_{se}}{Y_N u_*}$ and $\frac{V_{ST}}{u_*}$ determined by this method depend upon how the points are divided into groups. To determine the groups, the points were numbered consecutively with increasing X and the even numbered points were assigned to group one and the odd numbered points were assigned to group two.

Figure 43 shows the computed values of $\frac{\varepsilon_{se}}{Y_N u_*}$ for the fine sediment and for all three flow conditions. Since no functional form of the distribution of $\frac{\varepsilon_{se}}{Y_N u_*}$ was discernible from Figure 43, the following procedure was employed to determine a distribution which could be used in the numerical solution. In chapter II it was pointed out that the value of ε_{se} could be divided into two components as indicated in Equation 35, where ε_T is the result of tangential turbulent fluctuations and ε_c is the result of the curvature of the fluid particle paths. It was assumed that there is an analogy between ε_T and ε_m so that

$$\frac{\varepsilon_T}{Y_N u_*} = \alpha_1 \kappa (1-\eta) \eta \qquad (50)$$

where α_1 is a proportionality constant.

The most intense shear zone should occur at approximately $\eta = 0.1$. The value of ε_c was assumed to be a maximum there. It was assumed, furthermore, that ε_c would decrease in proportion to the cube of the distance from $\eta = 0.1$ in such a manner as to reach zero at both the surface and the floor. This is somewhat equivalent to assuming that the eddy peripheral velocity decreases linearly and that the diameter

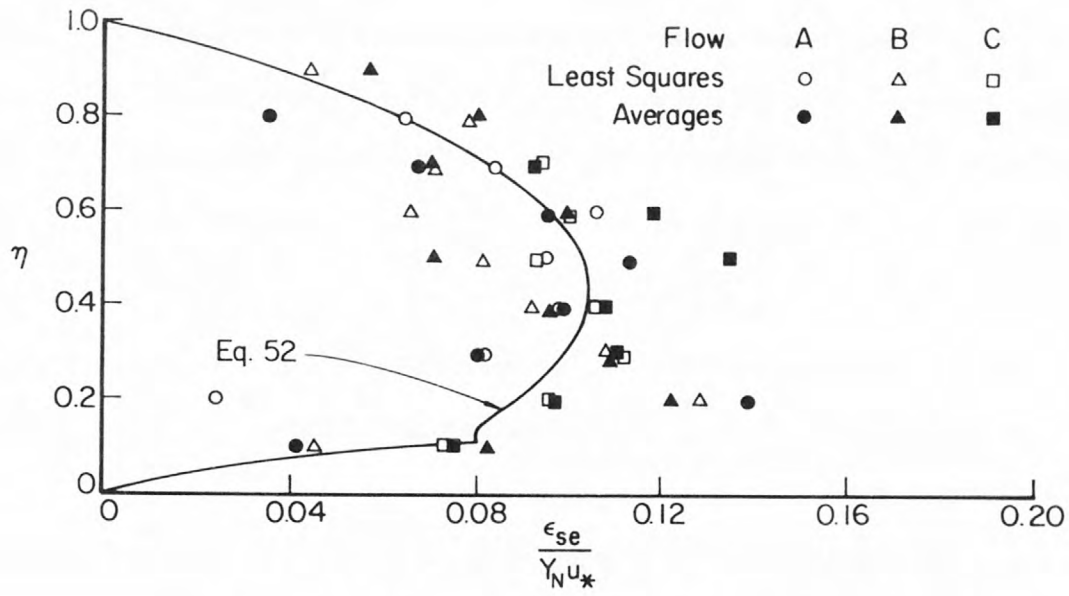

Figure 43.--Fine sediment transfer coefficient.

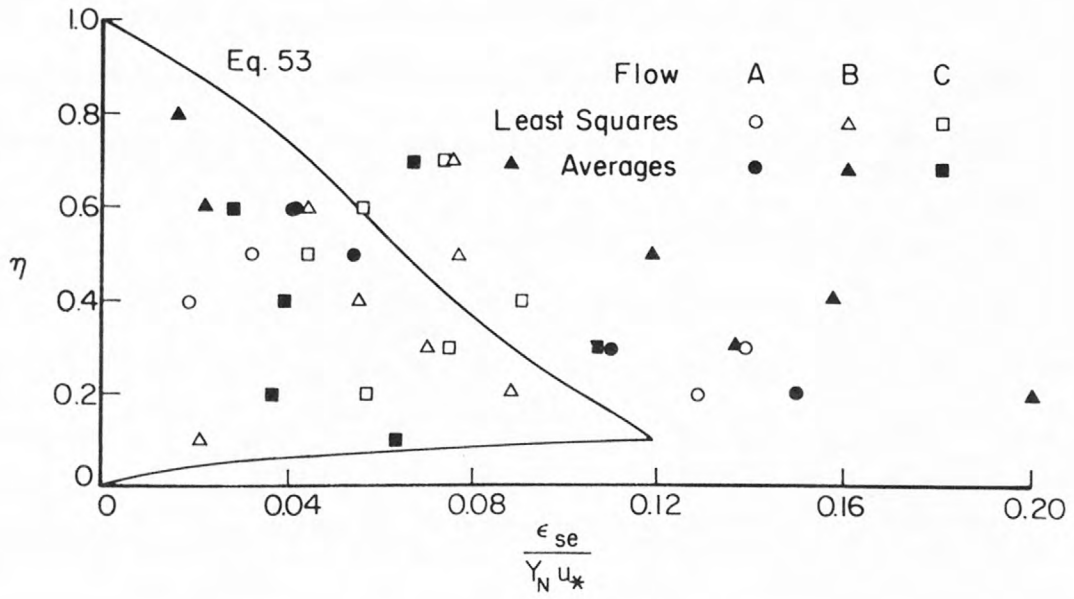

Figure 44.--Coarse sediment transfer coefficient.

of the eddies increases linearly with distance from the most intense shear zone. These assumptions give the functional form of ε_c as

$$\left.\begin{aligned} \frac{\varepsilon_c}{Y_N u_*} &= \alpha_2 \left(\frac{1-\eta}{0.9}\right)^3 \qquad \eta \geq 0.1 \\ \frac{\varepsilon_c}{Y_N u_*} &= \alpha_2 \left(\frac{\eta}{0.1}\right)^3 \qquad \eta \leq 0.1 \end{aligned}\right\} \tag{51}$$

where α_2 is a constant. It is assumed here for convenience that ε_c is proportional to $Y_N u_*$. The data neither supports nor refutes this assumption.

The measured values of $\frac{\varepsilon_c}{Y_N u_*}$ were then divided into two groups and the values of α_1 and α_2 were determined by the method of averages. The points in the upper part of the flow were assigned to group one, points in the lower part of the flow were assigned to group two. For the fine sediment the values of α_1 and α_2 were then computed to be 0.985 and 0.0376 respectively, giving the assumed functional form for $\frac{\varepsilon_{se}}{Y_N u_*}$ as

$$\left.\begin{aligned} \frac{\varepsilon_{se}}{Y_N u_*} &= 0.985 \kappa \quad (1-\eta)\,\eta + 0.0376 \left(\frac{1-\eta}{0.9}\right)^3 \quad \eta \geq 0.1 \\ \frac{\varepsilon_{se}}{Y_N u_*} &= 0.985 \kappa \quad (1-\eta)\,\eta + 0.0376 \left(\frac{\eta}{0.1}\right)^3 \quad \eta \leq 0.1 \end{aligned}\right\} \tag{52}$$

Equation 52 is plotted on Figure 43 for comparison with the measured data.

Computation methods used for the evaluation of the coarse sediment data were identical with those used for the fine sediment data and the resulting measured values of the transfer coefficient are shown on Figure 44. The same procedure was also used to obtain the functional form of $\frac{\varepsilon_{se}}{Y_N u_*}$ for the coarse sediment. It was determined that $\alpha_1 = 0.492$ and $\alpha_2 = 0.102$. This gives an expression for $\frac{\varepsilon_{se}}{Y_N u_*}$ as

$$\left.\begin{aligned} \frac{\varepsilon_{se}}{Y_N u_*} &= 0.492\,\kappa\,(1-\eta)\eta + 0.102\left(\frac{1-\eta}{0.9}\right)^3 \qquad \eta \geq 0.1 \\ \frac{\varepsilon_{se}}{Y_N u_*} &+ 0.492\,\kappa\,(1-\eta)\eta + 0.102\left(\frac{\eta}{0.1}\right)^3 \qquad \eta \leq 0.1 \end{aligned}\right\} \quad (53)$$

The values determined for $\frac{V_{ST}}{u_*}$ have previously been presented in Figures 26 and 28. The values presented in these figures represent the average of the values obtained by the two curve fitting techniques.

4. The Numerical Solution of the Conservation of Mass Equation.

A computer program was written to solve Equation 37 numerically. This solution was useful for three reasons. First, it could serve as a valuable guide in the planning of the experiment. Second, it could be used to further indicate the validity of the diffusion equation as a mathematical model of the turbulent transfer process, and finally it could be used to check the accuracy of the transfer coefficients and turbulent fall velocities as computed from the measured concentration profiles.

Equation 37 was solved by the explicit four point forward difference scheme (Richtmyer, 1957, p. 91). For this scheme the flow domain is divided into N layers in the vertical and M columns in the horizontal per unit of length, i.e. the flow domain is divided into N x M differential areas per unit length. The concentration and the fluid velocity were assumed constant in each differential area. The subscripts i and j identify the layer and column of the differential area respectively. The layers are numbered from the floor to the surface and the columns numbered from the source of the dispersant downstream. $E(i) = \varepsilon_\Gamma/Y_N u_*$ is the value of the dimensionless transfer coefficient at the bottom of the i^{th} row. $UI(i) = u_*/u$ is the reciprocal of the dimensionless velocity at the center of the i^{th} row and $VS = \frac{V_{ST}}{u_*}$.

With this scheme the general finite difference form of Equation 37 becomes

$$[DX\ UI(i)]^{-1}\ [c(i,j+1)-c(i,j)] = \frac{1}{DY^2}\left\{E(i+1)[c(i+1,j)-c(i,j)] - E(i)\ [c(i,j) - c(i-1,j)]\right\} + \frac{VS}{DY}\left[c(i+1,j)-c(i,j)\right] \quad (54)$$

where $DY = Y_N/N$, $DX = Y_N/M$. Double subscripts are not used where the variables are not functions of X. Equation 54 can be solved explicitly for

$$C(i,j+1) = C(i,j) + \frac{DX\ UI(i)}{DY^2}\left\{E(i+1)[c(i+1,j)-c(i,j)]-E(i)[c(i,j) - c(i-1,j)]\right\} + \frac{VS\ DX\ UI(i)}{DY}\ [c(i+1,j)-c(i,j)]\ . \quad (55)$$

The solution for the differential areas along the boundaries cannot be determined from Equation 55 but must be solved individually from boundary conditions. When i = N, the terms involving E(i+1) and VS c(i+1,j) on the right side of Equation 55 represent the flux of dispersant into the projected differential area from the layer above. Since the flux across the surface of the flow is zero, except at the source, then these terms must be zero for the top row of differential areas. The equation for the top row then becomes

$$c(N,j+1) = c(N,j) - \frac{DX\ UI(N)}{DY^2} E(N)[c(N,j) - c(N-1,j)]$$

$$- \frac{VS\ DX\ UI(N)}{DY}\ c(N,j)\ . \qquad (56)$$

The boundary condition at the floor is more complicated than the one at the surface. Since the sediment in the bottom layer can fall out and be deposited on the floor of the flume the transport at the floor may not be zero. It was assumed that all particles in the bottom layer would come in contact with the floor at some time. It was also assumed that there was some probability ($0 \leq A \leq 1$) that any particle coming into contact with the floor would be deposited. The transport out of the bottom layer to the floor is then seen to be the product of A, VS, c (1,j) and DX. The difference equation for the bottom layer becomes

$$c(1,j+1) = c(1,j) + \frac{E(2)\ DX\ UI(1)}{DY^2} [c(2,j) - c(1,j)]$$

$$+ \frac{VS\ DX\ UI(1)}{DY} [c(2,j) - A\ c(1,j)]. \qquad (57)$$

The complete program is given in appendix B.

A critical step in the numerical solution of a partial differential equation by the finite difference method is the selection of the mesh or grid size (the values of DX and DY). The subjects of stability and rate of convergence are very complex and no conditions have ever been derived analytically which apply strictly to Equation 55 (Sayre, 1968, p. 17). However, two criteria are of basic importance. They are the absolute size of the grid and the ratio of the sides of the grid (DX/DY). In general the absolute size of the grid controls the rate of convergence of the numerical solution to the true solution. If the absolute size of the mesh gets too small, truncations can cause errors in the numerical solution to increase with decreasing grid size. Thus, the error in the numerical solution would be expected to decrease with the absolute grid size to a certain point, say the critical mesh size, and then to start increasing again due to truncation errors. In this program it was believed that the grid size was always larger than this critical grid size and that the computer cost dictated the smallest practical grid size. The ratio of DX/DY in general controls the stability of the numerical solution. One rule seems immediately apparent from Equation 55. This rule is that DX/DY must be chosen such that all the coefficients of the concentration difference terms in Equation 55 must be less than 1.0. Since these coefficients basically determine the flux of dispersant into the area C(i, j+1), if the coefficients are larger than one it means that mathematically one has transferred more dispersant out of the differential area than was originally there. As a result of this, the concentration differences in column j+1 can be larger than those in column j, and the solution soon bounds out of

reason. A rule of thumb which was always found to work for the writer was not to permit the sum of the absolute values of the coefficients of the concentration difference terms in Equation 55 to exceed a value of 1.0.

To check the accuracy of the finite difference program its solution was compared with the analytical solution given by W. E. Dobbins (1944). Dobbins obtained a solution to Equation 37 for the condition that both the velocity and the transfer coefficient do not vary with depth. The finite difference equation would be expected to be least accurate for large sediment fall velocities and small fluid velocities. The finite difference equation was checked against Dobbin's solution for three cases. These cases correspond approximately to the most accurate, intermediate and least accurate conditions anticipated for the finite difference equation. Figures 45 and 46 show the results of these comparisons. Since the comparisons for the run with $V_{ST} = 0$ agreed better than the one shown in Figure 46 this graph is not shown. All predicted profiles were run with DY = 0.02 since the computer cost went up rapidly with decreasing values of DY.

The results of the program will be discussed relative to its success in fulfilling the three purposes for which it was written.

There were two main concerns in the project planning stage. First, could Equation 44 be solved for ε_Γ and V_{ST} with any degree of accuracy given reasonable accuracy in the physical measurements of the concentrations? The other question was where should the concentration profiles be measured in order to maximize the accuracy in computing the desired quantities. In order to see if Equation 44 could be solved graphically,

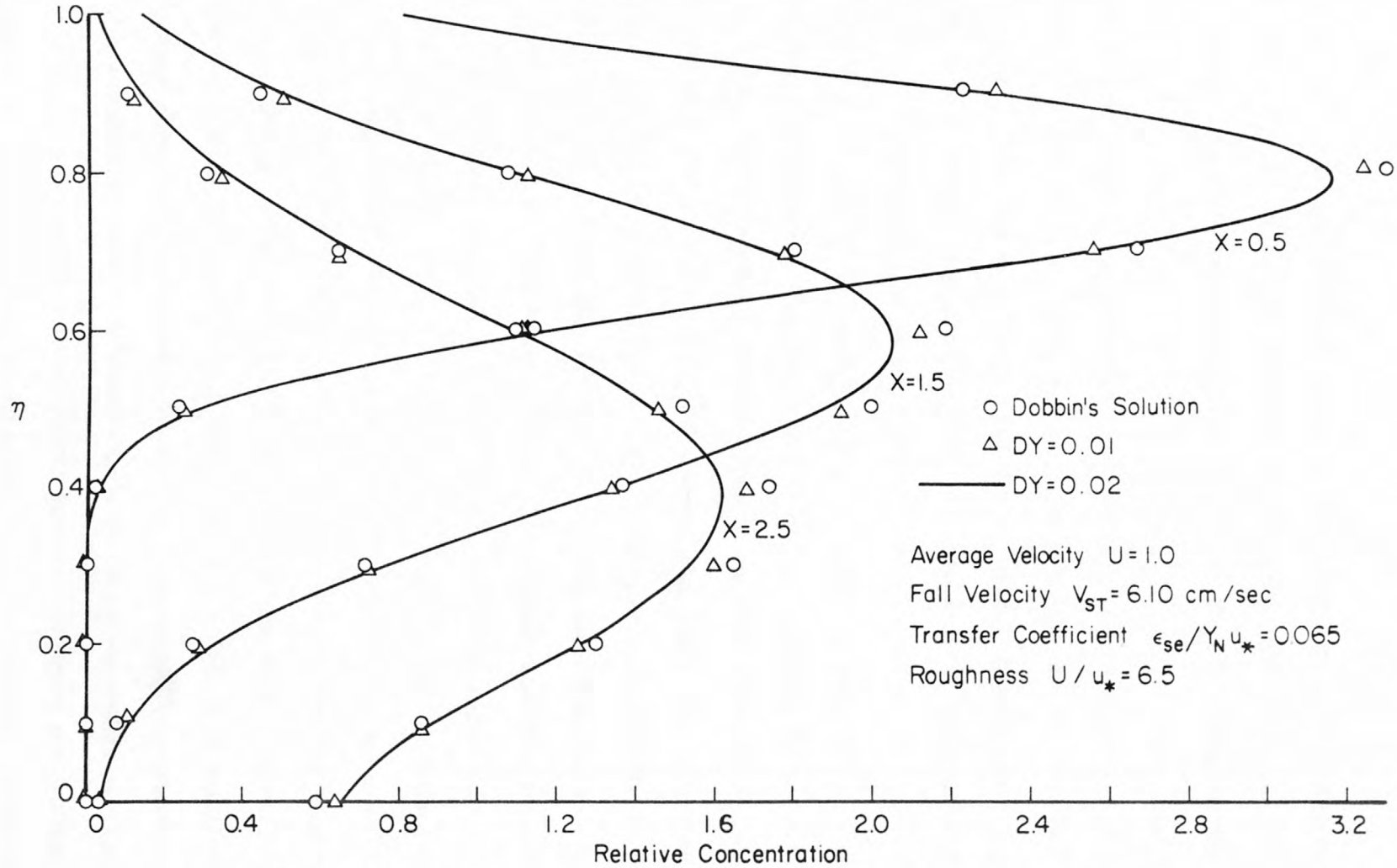

Figure 45.--Comparison of numerical and analytical solutions; flow A, coarse sediment.

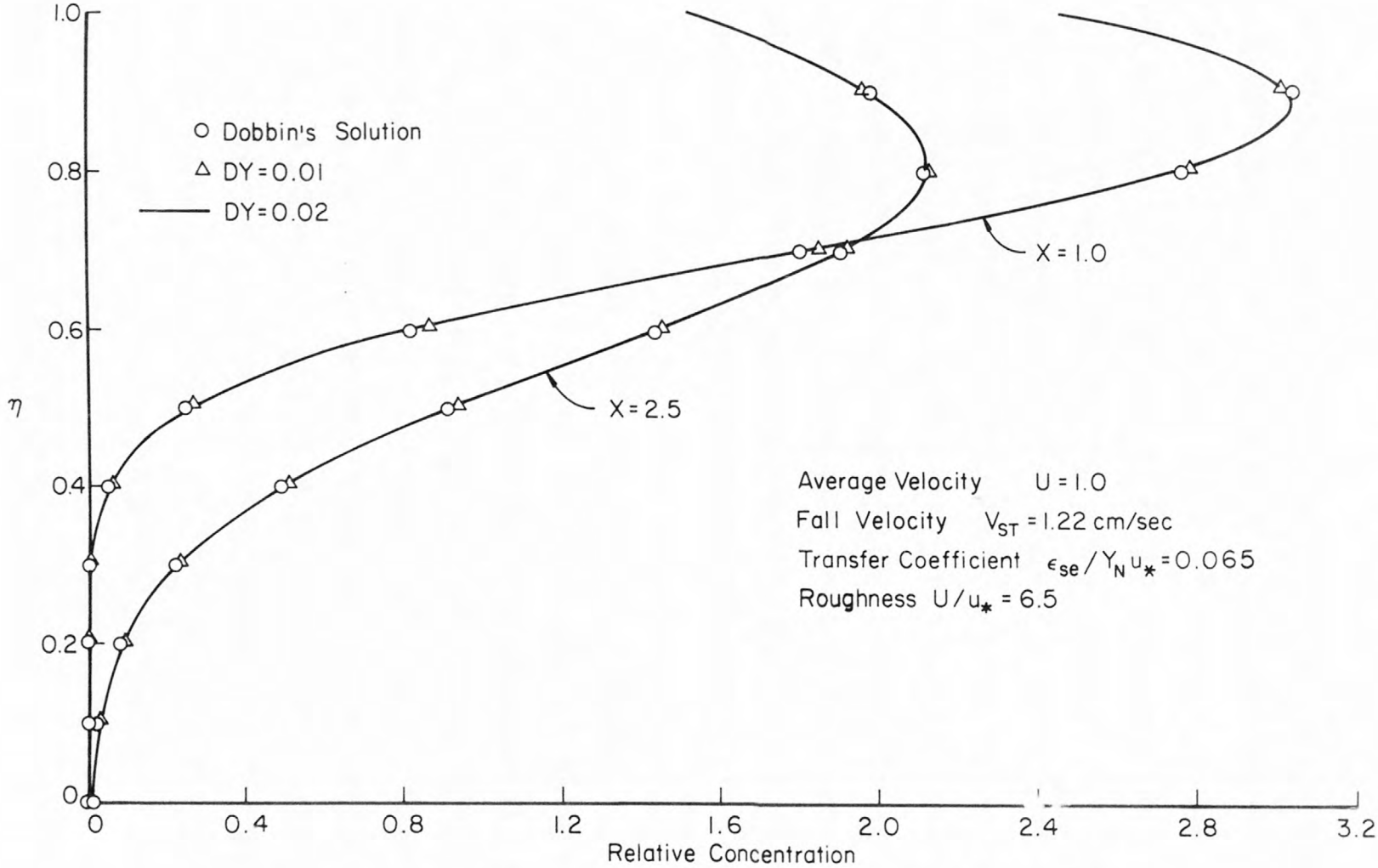

Figure 46.--Comparison of numerical and analytical solutions; flow A, fine sediment.

the concentration profiles were predicted for various design conditions. From these predicted profiles the values of ε_Γ and V_{ST} were computed using Equation 44 and checked against the input values. It was found that a much greater accuracy could be expected for dye or for very fine sediment than for coarse sediment. For example, if V_{ST} was zero, it was found that Equation 44 would give the original values of ε_Γ to within ten percent provided that the concentration profiles were accurate to three significant figures, and the distance between the predicted profiles was about one normal depth. Profiles measured near the source in general gave better accuracy for the evaluation of ε_Γ near the surface. The closer the predicted profiles were together the more accurate were the results. The accuracy deteriorated rapidly with increasing particle size.

It was realized at this time that the accuracy of the sediment runs would be relatively poor unless many closely spaced profiles were taken. It was decided that a reduced accuracy would be accepted and that a wider range of conditions would be investigated rather than improving the accuracy for a small range of conditions by more profiles at each condition. The longitudinal spacing of the probes reduced to a compromise between practicality and desirability. For the dye runs many profiles were possible because the concentration profiles were not a function of the stream velocity. For the sediment runs the probes were spaced so that the probe furthest downstream would be at a point where median sized particles would just hit the floor and the probe nearest the source would be at a point where a measurable concentration existed throughout a major portion of the flow depth.

It was found that the predicted profiles were not very sensitive to minor local changes in the velocity distribution.

The initial conditions used in the numerical solution were always the first measured concentration profile. It was found that the measured profiles could not be predicted from initial conditions that appeared to be reasonable approximations of the actual source conditions. Some observations and measurements were made to try to define the actual source condition in the flume. It was concluded that either Equation 3 or 37 or both must be invalid for the sharp concentration gradients that occur initially. Recall that Taylor's theory by continuous movements as well as the measurements of Pien (1941) and others indicate that ε_Γ is not constant for short diffusion times. By comparing the measured concentration distributions to the concentrations predicted using the actual initial conditions at the source, it was determined that dye diffused less rapidly in the first few normal depths of flow than would be predicted by Equations 3 and 37. This is in qualitative agreement with Taylor's theory which states that ε_Γ initially increases proportional to time before attaining a constant value. For dye, the predicted concentration profile at two normal depths was roughly equivalent to the concentration profile measured at three normal depths. Agreement between a set of measured concentration profiles and a set of profiles predicted for a particular combination of V_{ST} and ε_Γ, is a strong indication of the validity of Equations 3 and 37. The degree of fit between the measured profiles and the predicted profiles can be seen in Figures 29, 34, 35, 36, 37, 38, and 39.

The third purpose of the numerical solution to the diffusion equation was to verify the parameters computed from the concentration profiles. If the values of the turbulent fall velocity and the transfer coefficient computed from measured concentration profiles can be used in conjunction with the conservation equation to reproduce the measured profiles then this helps to verify the computed values of the fall velocity and the transfer coefficient.

Predicted profiles for the dye runs were made with the values of $\frac{u}{u_*}$ which had been averaged for all three flow conditions. All predicted profiles used the measured profile at X = 3.0 as the initial condition. All profiles were predicted with V_{ST} = 0 and with DY = 0.02 and DX = 0.005. In order to illustrate the validity of the computed values of $\frac{\varepsilon_d}{Y_N u_*}$, concentration profiles were predicted using the most probable value of $\frac{\varepsilon_d}{Y_N u_*}$ obtained from Figure 33. Some of these profiles are shown in Figure 29.

In order to give the reader a feel for the sensitivity of the concentration profiles to changes in the mean value of $\frac{\varepsilon_d}{Y_N u_*}$, Figure 47 is shown with profiles which have been predicted with different values of the coefficient. Except for the values of the transfer coefficient all conditions were identical in predicting the profiles shown on Figure 47.

Figure 48 should give the reader some indication of the sensitivity of the concentration profiles to the variations in the distribution of the transfer coefficient. All distributions of the transfer coefficients used in predicting the profiles in Figure 48 have the same mean value.

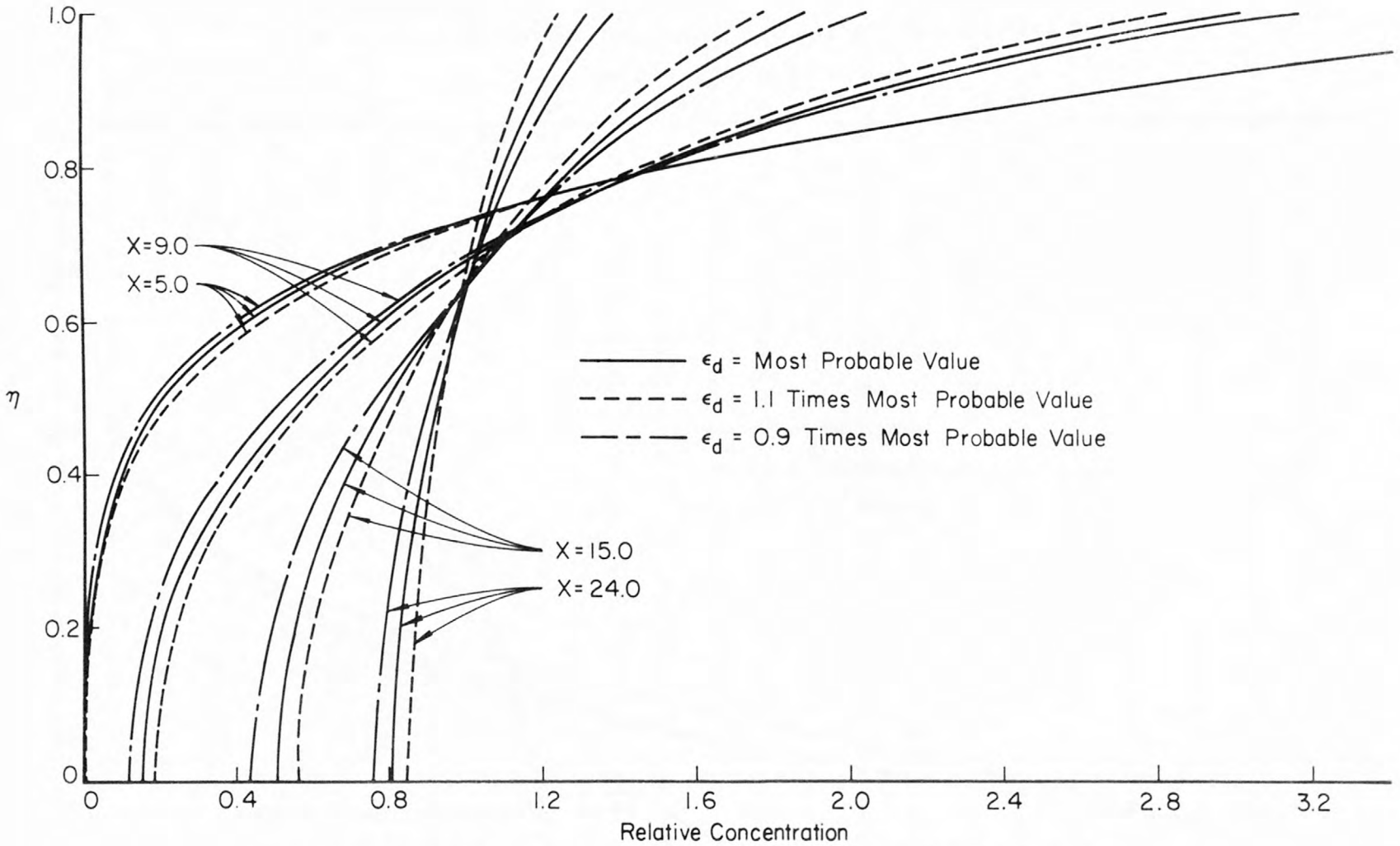

Figure 47.--Predicted dye concentration profiles for different magnitudes of mass transfer coefficients.

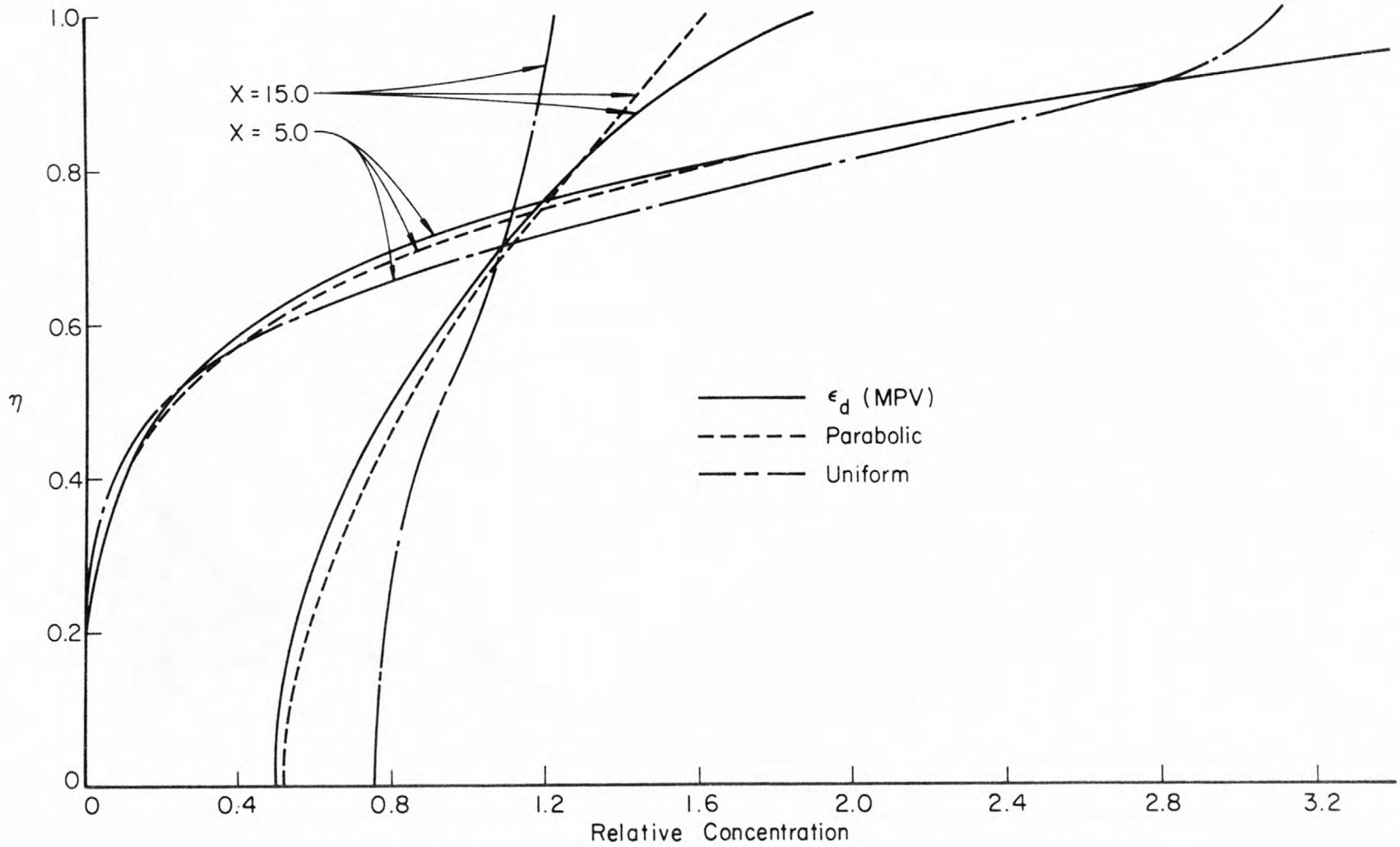

Figure 48.--Predicted dye concentration profiles for different mass transfer coefficient distributions.

Predicted concentration profiles are shown for all sediment runs on Figures 34 through 39. All of these predicted profiles were computed with the following things in common. The values of $\frac{u}{u_*}$ used in predicting each profile was that value of $\frac{u}{u_*}$ which applied to the particular flow condition. Profiles were predicted using Equations 52 and 53 to represent the sediment transfer coefficients. The turbulent fall velocity was assumed constant throughout the depth of flow and equal to that value obtained by averaging the results from the measured concentration profiles. The probability of deposit (A) was assumed to be constant for all values of X. The value of A used in predicting these profiles was determined mainly from intuition after observing the measured concentration profiles and the deposition data. The initial conditions were always assumed to be the first measured concentration profile at (X_o). The following table shows other pertinent information concerning the predicted profiles.

Flow	Sediment	DX	DY	X_o (depths)	V_{ST} (cm/sec)	A
A	Fine	0.0008	0.02	6.0	1.46	0.5
B	Fine	0.0008	0.02	5.0	1.70	0.2
C	Fine	0.0012	0.02	5.0	1.46	0.1
A	Coarse	0.0005	0.02	2.0	6.64	1.0
B	Coarse	0.0006	0.02	3.0	6.35	0.5
C	Coarse	0.0008	0.02	4.0	6.26	0.2

Predicted profiles are shown as dashed lines on Figures 34 through 39 to allow a direct comparison with the measured concentration profiles.

In order to give the reader a feel for the effect of the distribution of the transfer coefficient on the predicted profiles, Figure 49 shows profiles predicted using both a uniform and a parabolic distribution of $\frac{\varepsilon_{se}}{Y_N u_*}$. Conditions similar to those of flow C with the coarse sediment was chosen for this comparison not only because it was felt that the fine sediment would behave like the dye, but also because the confidence in the computer program was not too great for flow condition A with the coarse sediment (See Figure 45). The mean values of the total sediment transfer coefficient is the same for all distributions shown in Figure 49. The dashed curves shown in Figure 49 are nearly identical to the dashed curves shown in Figure 39. However, the values of α_1 and α_2 are 0.640 and 0.105 respectively.

Figure 50 was constructed in order to give the reader some feel for the effect of the magnitude of the transfer coefficient on the predicted profiles. The dashed profiles shown in Figure 50 are identical to the dashed profiles shown in Figure 49. The relative distributions of the transfer coefficient used in predicting all profiles shown in Figure 50 were identical. In addition all other conditions such as the fall velocity and the probability of deposit were the same for all profiles shown in Figure 50.

The effect of the probability of deposit on the predicted concentration profiles is shown in Figure 51. All conditions used in predicting the profiles in Figure 51 are identical to those used in predicting the dashed profiles in Figure 49 except for the probability of deposit.

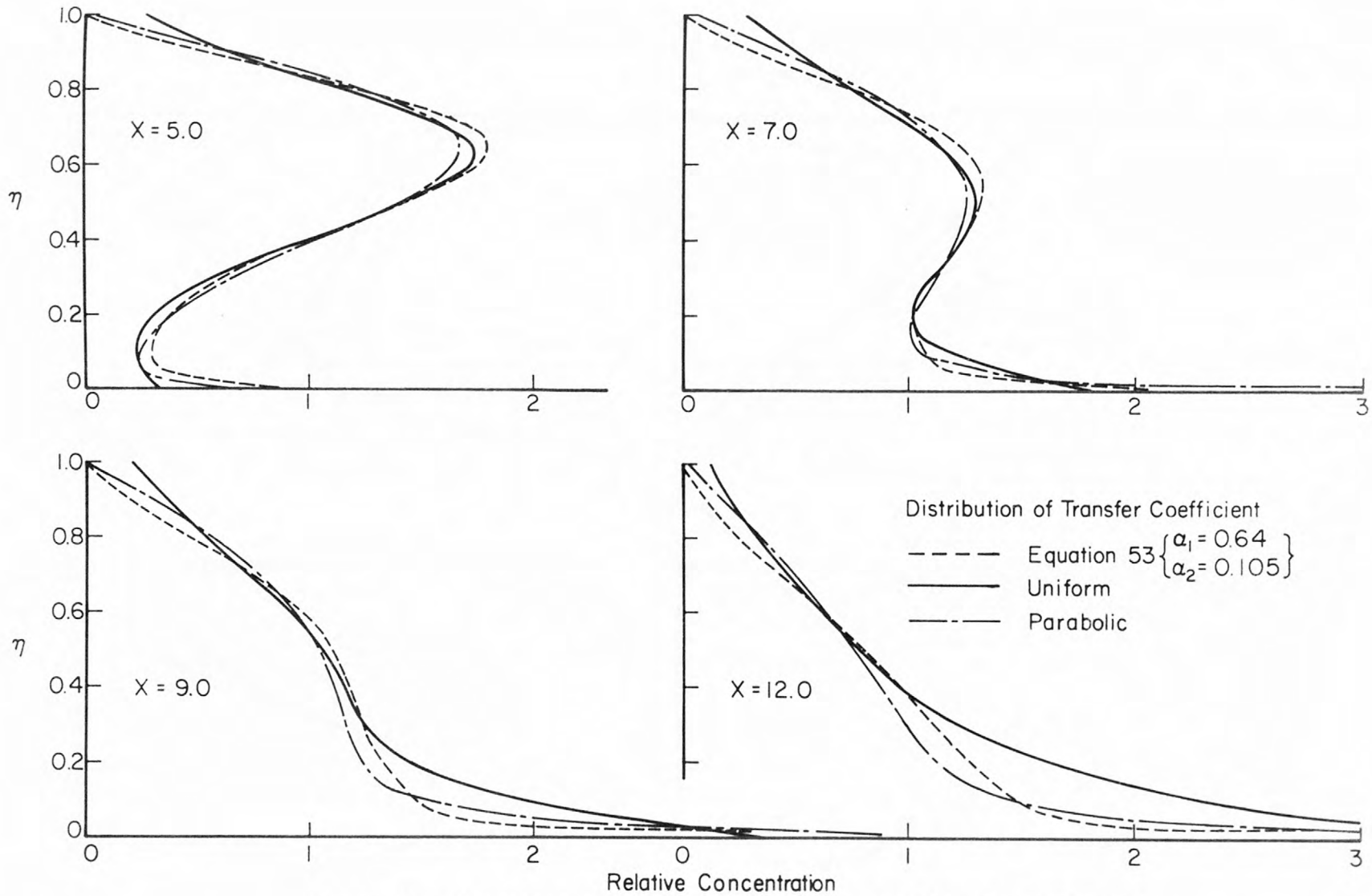

Figure 49.--Predicted sediment concentration profiles for different transfer coefficient distributions; flow C, coarse sediment.

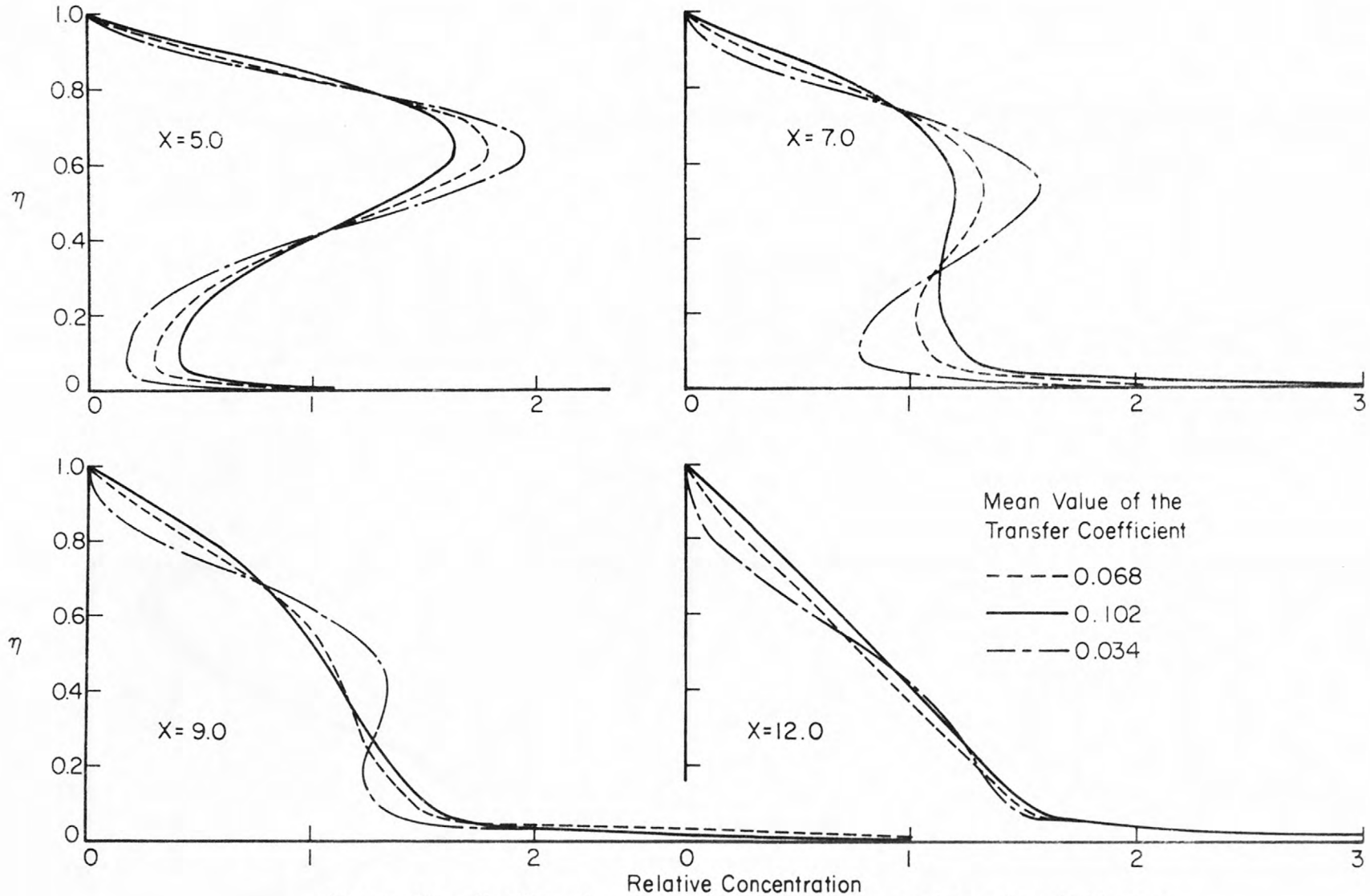

Figure 50.--Predicted sediment concentration profiles for different magnitudes of transfer coefficients; flow C, coarse sediment.

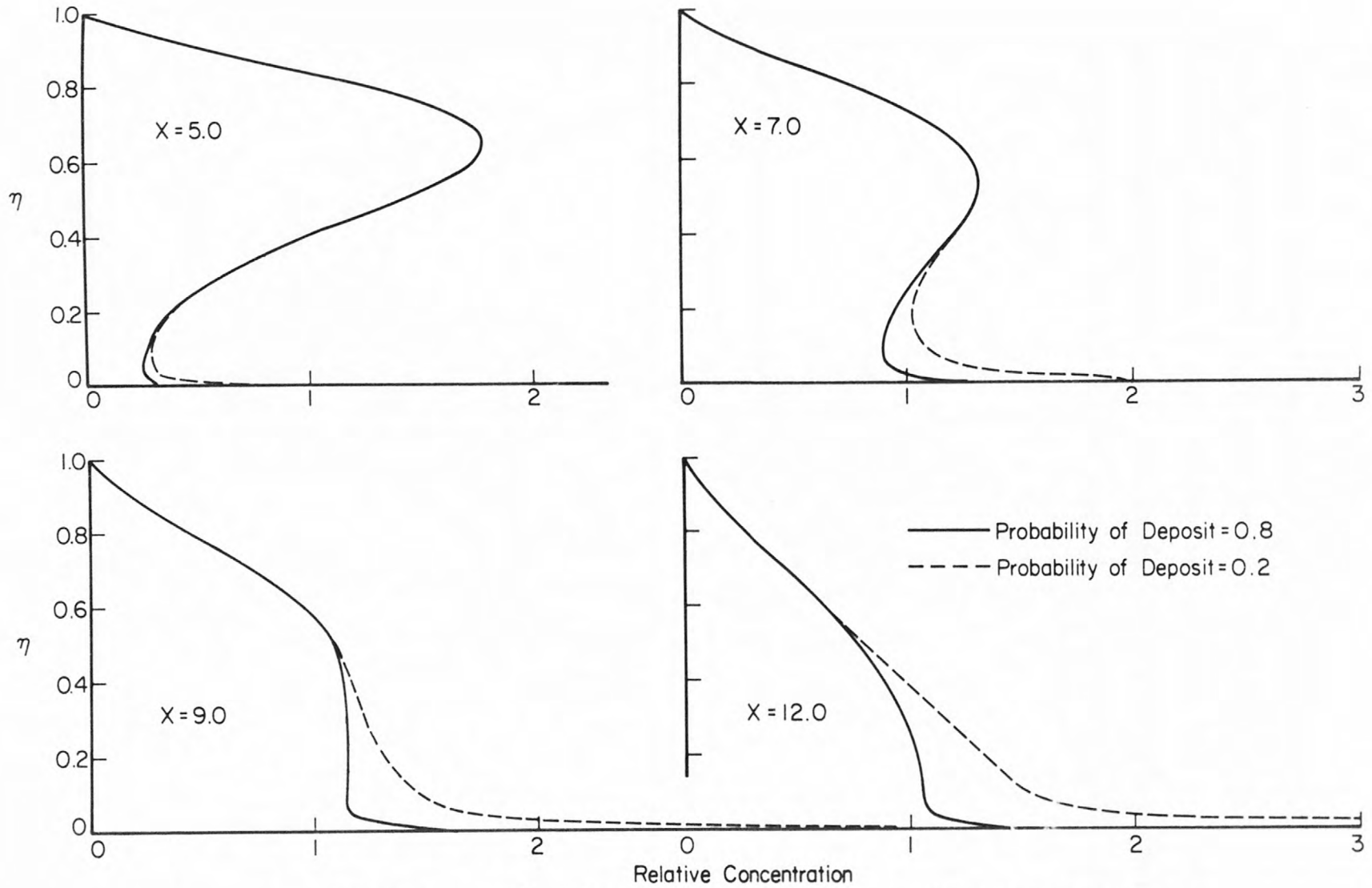

Figure 51.--Predicted sediment concentration profiles for different deposition probabilities; flow C, coarse sediment.

Finally, Figure 52 gives profiles which have been predicted with various fall velocities. The dashed profiles shown in Figure 52 are identical with the predicted profiles shown in Figure 35. The solid line profiles shown in Figure 52 have been predicted using the standard fall velocity of the fine sediment corrected to the flume temperature.

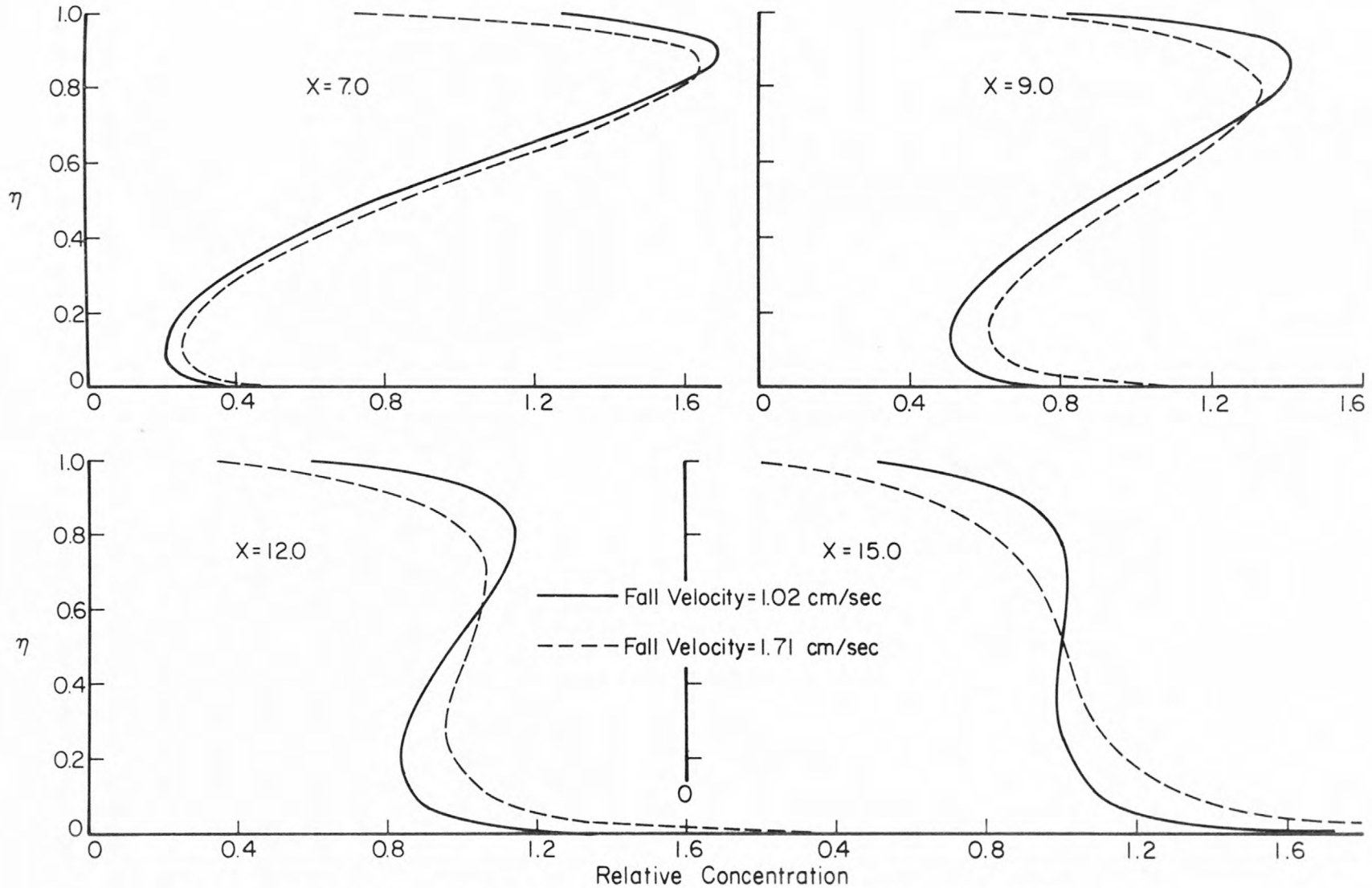

Figure 52.--Predicted sediment concentration profiles for different turbulent fall velocities; flow B, fine sediment.

Chapter V

DISCUSSION OF RESULTS

A. The Flow Field

1. Distribution of Primary Velocity Components

The velocity profile within the test area (1-2' off the center line) showed some cutback at the surface due to the effects of the side walls and/or secondary currents. This cutback at the surface could not be detected on the centerline velocity profile. The Von Karman coefficient computed in the test section was reasonably constant from flow condition to flow condition and had an average value of 0.392. This value was determined from the bottom two-thirds of the velocity profile. Velocity profiles were never taken while injecting sediment into the flow but the average concentration of sediment never exceeded 213 ppm. It was believed that this small amount of sediment would have negligible effects on the mean velocity profile. For flow condition A with the coarse sediment the material tended to deposit in a pile and the sediment tended to build up on the floor, in some cases building up to a depth equal to half the height of the roughness blocks (See Figure 53). This buildup of sand on the floor could have caused the roughness characteristics of the flume floor to be altered locally, however, this effect was ignored.

The density of the roughness cleats on the floor was such that some spatial variation in the mean velocity occurred up to about 2/10's of the depth. This variation was believed to have an insignificant effect on most concentration profiles. The variation could, however, cast some

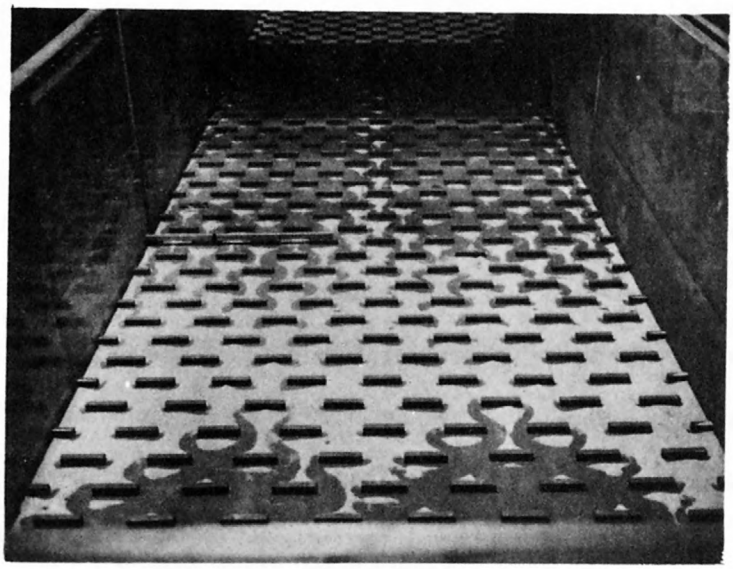

Figure 53.--Sediment deposition pattern after special tracer study.

doubt on the sediment concentrations measured at the bottom most relative depth. The probes themselves caused small variations in the local velocity profiles, but again this effect was considered to be minor.

As for the overall characteristics of the flow field, the value of the Chezy coefficient shown in Table 1, Appendix A was nearly constant for all three flow conditions. This is in accord with the resistance law for turbulent flow near a rough boundary according to which the Chezy coefficient should be independent of the Reynolds number. Also, velocity profiles and turbulence intensity measurements (Figure 20) indicate that the boundary layer was fully developed before reaching the test section. This indicates that the flow and turbulence structure was uniform with respect to the longitudinal direction in the test reach.

2. Turbulence Structure

The measured turbulence intensities show the usual variation for open channel flow over a rough boundary (McQuivey, 1967). The measured Eulerian integral time scales show much variation with depth. The significance of these variations have been discussed elsewhere (McQuivey and Richardson, 1968).

3. Secondary Currents

Indications were that the secondary circulation pattern in this flume was of the same type as that shown in Figure 3-b. There are two reasons for this assertion. The first is that the isovels shown in Figures 16 and 17 do not show local distortions at the quarter points as do the ones shown in Figure 3-c, and the centerline distortions are concave downward indicating an updraft area unlike the ones shown in

Figure 3-c. It is also pointed out that the isovels measured in this experiment are very similar to those measured by Tracy (1965), near the end of a wide closed conduit (Figure 2). The width-depth ratio in this experiment was about the same as in the experiments of Delleur and McManus (1959) and Vanoni (1946), however, in both of these previous experiments, the bottom was much smoother relative to the walls than was the case in this experiment. The work of Elder (Hinze, 1967) indicated that roughening one boundary would increase the size of the cell near that boundary. The second reason for believing that there were only two primary cells is indicated in Figures 53 and 54. Figure 54 shows two views of the flume floor immediately following the fine sediment experiment for flow C. Note that the sediment is deposited on the floor in three streaks. The three streaks can barely be seen in Figure 53. These streaks correspond exactly to the assumed vertical draft areas. Vanoni (1946, p. 99) observed five streaks in his flume which would correspond to the vertical draft areas indicated in Figure 3-c.

For these two reasons it is believed that the secondary currents in these tests consisted of two primary cells of the general shape shown in Figure 3-b. It is suggested that the extremely rough floor is one reason for two primary cells being formed rather than the four that were previously observed for flows of approximately the same width depth ratio. When flow condition C was first set up the measured isovels were similar to those shown in Figure 3-c. But the entrance conditions were improved by the removal of the upstream weir, after which the isovels assumed the form shown in Figure 17. Thus, it appears that at a width depth ratio of about six, four primary cells may be more common than

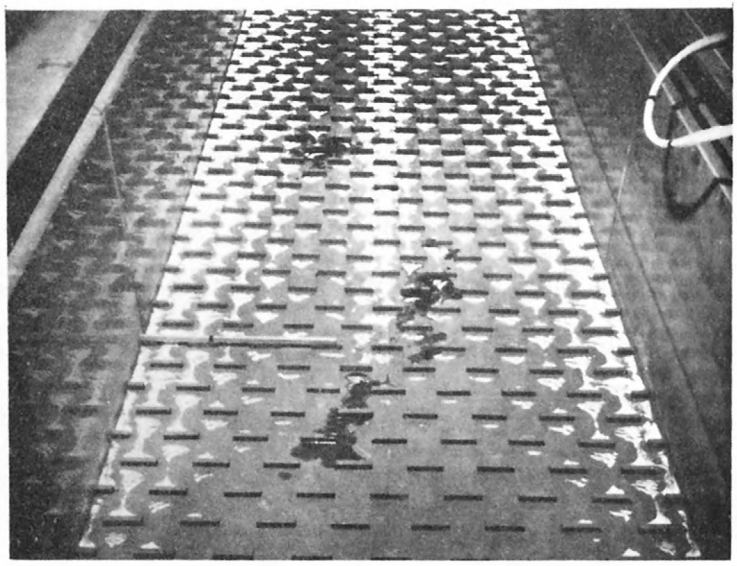

(a) Flume floor looking downstream.

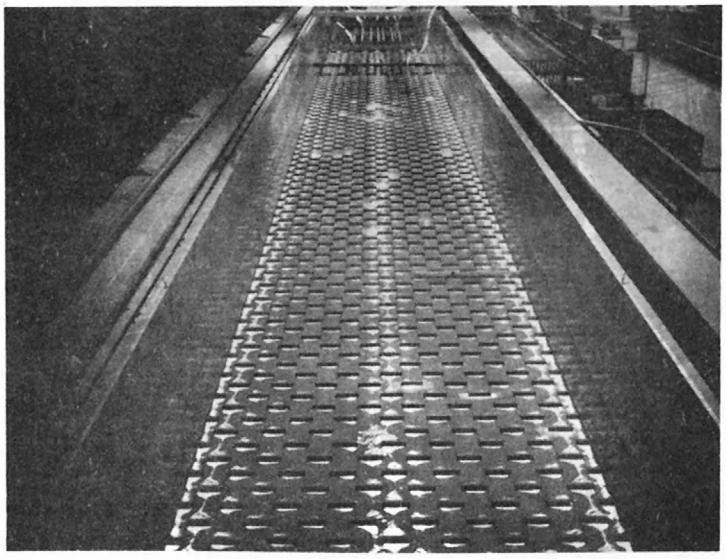

(b) Flume floor looking upstream.

Figure 54.--Sediment deposition pattern after run FS21A.

two, however, two can be obtained for a very rough floor with smooth walls provided the entrance conditions are nearly ideal.

The secondary currents were thought to have little or no effect on the fixed-probe measured concentration profiles in this experiment for the following reasons. All fixed-probe samples were taken in a region where the secondary current should have been primarily horizontal in direction. Recall that these measurements were taken between twelve and twenty-four inches off the centerline of the flume. The dispersant particles should be convected transversely with the mean secondary current velocity. That is, their path lines should make angles with the centerline of the flume approximately equal to or less than that of the secondary current angle. If only a few of the particles in the samples had experienced any strong updraft or downdraft currents in their history, then the measured vertical concentration gradients should not be affected much by the secondary currents, provided that the transverse concentration gradient is small. The experiment was designed to fulfill this last condition. The isovels and sediment deposition pattern indicated that the strong updraft region was concentrated near the center of the channel. Thus so long as the samplers did not pick up particles which at some time had been near the center of the channel, the measured concentration profiles would have been relatively unaffected by the secondary currents. The angle of drift due to secondary currents has been estimated as varying from 0.6 to 3.0 degrees (Liggett, et al, 1965, p. 109). With the exception of the sampler at X = 67, the angle subtended by the flume centerline and a line passing through the centerline of the source and any one of the sampling positions was never less than 3.8°.

The vertical draft region must, of course, have some width, say 6 inches to 1 foot, but the calculation carried out above was for the extreme case. Little weight was placed on measurements made in locations where the above analysis would indicate that they may have been affected by vertical draft regions. It is therefore believed that the measured values of the mass transfer coefficient were relatively free from the influence of secondary currents. Unfortunately the same cannot be said of the velocity profiles which were used to compute the momentum transfer coefficient. It is again pointed out that any measurements of equilibrium conditions will be affected by secondary currents.

B. Particle Fall Velocity

1. Quiescent Fall Velocity

The visual accumulation tube was found to be inadequate for determining the fall velocities of uniformly sized sand in that it indicated a sediment fall velocity of from thirty to forty percent lower than its actual value. The uniformity of size apparently kept the sample from dispersing properly so that the particles fell as a group in a closed container. In effect they experienced hindered settling, which no doubt explains the small fall velocities indicated by the visual accumulation tube.

The standard fall velocity determined by dropping single particles agreed well with the standard fall velocity computed from the sieve analysis. A Corey shape factor of 0.9 instead of the usual 0.7 appeared to be more representative of the coarse sediment. The larger shape factor should indicate that the coarse sand was more spherical than "normal" sand. Dropping single particles was considered to be the most

accurate way of determining the standard fall velocity for sediments having these size distributions.

2. Evaluation of the Sediment Injection System

An ideal sediment injector would have provided a continuous line source of sediment at the surface of the flow which was free from effects such as concentration, group action, etc. In practice, where the ideal could not be achieved, it was suspected that four factors could cause trouble. First, because the particles were injected dry, they could have air bubbles clinging to them causing retardation or even floating. Second, the time required for the particles to decelerate from their initial velocity to terminal fall velocity could be significant. Third, the mean concentration could affect the resulting fall velocity by causing hindered settling. Finally, the grouping action resulting from concentrated streams of sediment passing through the holes in the injection trough could affect the fall velocity.

Tests in quiescent fluids seemed to indicate that the first two of these effects were relatively minor. The median fall velocity of particles dropped dry through six to eight inches of air was only three percent less than that of those dropped with zero initial velocity from a submerged position. Few if any of the particles were found to float if the injector was more than four inches above the water.

Ideally, the experiments should be performed with very small concentrations, however, the length of sampling time available, the size of the sample nozzles and the quantity of sediment needed for accurate analysis combined to dictate a required mean concentration of about 150 ppm. The result of Camp (1946, p. 899) indicates that a mean concentration of

200 ppm should reduce the fall velocity by considerably less than one percent. The maximum point concentration ever measured in these experiments was about 550 ppm which occurred in run CS21. Camp's figures indicate that even this concentration should affect the fall velocity by less than one or two percent. It can be concluded from previous work that the effects of concentration on the fall velocity in these experiments should indeed have been negligible. Computations of the actual turbulent fall velocity from the analysis of the deposition data are subject to challenge because there is no assurance that particles did not move after they first came in contact with the floor, even for flow condition A with coarse sediment. However, this data should give quite accurate indications of the relative variation in the fall velocity due to different injection system conditions. The distance to which fifty percent of the particles had been deposited could easily be determined to within ± 0.1' or better than 1.6%. Fall velocities measured in this way for runs CS0 and CS1 & CS1A agree exactly and the injection condition were exactly the same. In runs CS3 & CS3A half of the holes in the injector were plugged, thereby reducing the mean concentration to half of that in runs CS0 and CS1 & CS1A; all other conditions were identical. The fall velocity computed from the deposition data for runs CS3 & CS3A was 4.5 percent larger than that computed for runs CS0 and CS1 & CS1A. These measurements then indicate that reducing the mean concentration from 160 to 80 ppm increased the fall velocity by 4.5 percent. This is much more than what would have been predicted from Camp's curves. Since only three measurements were obtained it is possible that this difference is entirely due to experimental error. In any case it was

assumed that for the mean concentrations used in this experiment (less than 213 ppm), hindered settling effects would be negligible.

If there is any significant increase in fall velocity due to the particles falling as a group, this effect should be much more pronounced near the surface and should decrease as the turbulence spreads out the injected streams of sediment. The obvious way to note this effect is to look at the distribution of the fall velocity in the vertical. The concentration profiles provided the only data from which the distribution of the fall velocity in the vertical could be computed. For the fine sediment, the results indicate a definite trend from a higher fall velocity near the surface to a lower fall velocity near the floor. This trend is not apparent for the coarse sediment, except possibly for flow condition C and even there it is not great. Measurements were not possible in the uppermost region of the flow for the coarse sediment runs because the sediment fell out of the upper portion of the flow almost before it could be sampled. The concentration profiles definitely suggest that there is a significant grouping effect for the fine sediment. Due mainly to the smaller ratio of the sediment particle diameter to the injector hole diameter used for the fine sediment experiments, it is not surprising that the grouping effect was more pronounced for the fine sediment. For example, for flow condition A the injector hole was 19.8 times as large as the average fine sediment particle but only 8.2 times as large as the average diameter of the coarse sediment particle. Thus, the coarse sediment particles were discharged in a less concentrated stream of fewer particles which could be scattered or dispersed more easily. The fine particles, on the other hand, tended to run out

of the hole more like a fluid. It was observed that the streams from the fine sediment injector were much better defined than for the coarse sediment; there was even a vena contracta. The angularity of the coarse sediment particles probably caused these particles to spread and tumble as they came out of the injector, at least more so than the spherical fine sediment particles. The sediment streams were spaced only about two inches apart and the injector trough was continuously oscillated back and forth along its axis during the injection. It was anticipated that the turbulence would almost immediately break up the streams, but this apparently did not happen as quickly as was hoped.

The special tracer particle experiment conducted with the coarse sediment permitted an evaluation of the combined effect of all four factors discussed above. The undyed sand was injected in the usual manner. The tracer particles were injected wet, with zero initial velocity, in very small groups and with effectively zero mean concentration, in short, under essentially ideal conditions. The results of this experiment indicated that at least for flow condition A with the coarse sediment, the combined effect of all four factors increased the fall velocity by not more than about 1.5 percent. Since measurements from the concentration profiles indicated that the group effect was small for flow condition A with the coarse sediment, the quiescent fall velocity experiment indicated that the effects of dry injection with finite initial velocities were insignificant, it is concluded that the concentration effect was also insignificant as predicted by Camp.

3. Turbulent Fall Velocity

If turbulence has an effect on the fall velocity this effect should be greatest near the floor of the flume where the turbulence levels are the greatest. It is not suggested that data obtained in this experiment are complete enough to detect this variation. However, the same procedure possibly could be used to determine this effect. The effect of turbulence was considered to be constant throughout the depth for this entire discussion.

The fall velocity computed from the concentration profiles include both the effects of the injection system and the effects of turbulence. Unfortunately, these two effects cannot be differentiated for the fine sediment runs. The grouping effect is believed to be the only significant factor to be considered as a result of the method of injection. The combined effects of turbulence and grouping as determined by the averaged results from the concentration profiles were to increase the particle fall velocity in the flume by 39, 65 and 40 percent respectively for flows A, B & C with the fine sediment. Since there appears to be a trend toward lower fall velocity with increasing dispersion time in Figure 26, one must conclude that at least a large portion of the increase in fall velocity must be attributed to the grouping effect and not to turbulence. The only question remaining is how much can be attributed to the grouping effect and how much must be attributed to turbulence. Even in the bottom layers, where the concentration profiles indicated that there must have been considerable dissipation of the original grouping effect, measurements indicated large particle fall velocity. Therefore, one would appear justified in concluding that a

significant portion of the increase was actually due to turbulence. For flow condition A, measurements from the deposition data indicate a particle fall velocity which is about equal to the standard fall velocity. However, these measurements really only indicate a lower bound to the particle fall velocity because of the high probability of further particle movement following initial contact with the bed. The pronounced tail on the deposition density function is interpreted as evidence of some particle movement. It is also noted that a probability of deposit of 0.5 was used in predicting the concentration profiles from the numerical solution for flow condition A. A probability of deposit of 0.8 was first tried and from the results it appeared that a probability of 0.5 would be a better estimate for fitting the measured concentration profiles.

The fall velocities for the coarse sediment as computed from the concentration profiles indicated that the combined action of the injection system and turbulence was to increase the fall velocity of the particles by six, three and four percent respectively for flows A, B and C. Flow condition A was the only condition for which the effects of the injection and turbulence could be completely separated. The special tracer study indicated that the combined effects of the injection system accounted for only about 1.5 percent of the increase. Thus 4.5 percent of the increase in particle fall velocity for flow A should have been due to turbulence alone. The deposition pattern of the sediment on the floor indicates a lower bound to the turbulent fall velocities in the flume. These data indicated that the turbulent fall velocity was about

equal to the standard fall velocity. Taking all the evidence together, the turbulence probably increased the fall velocity slightly.

C. Transfer Coefficients

1. Momentum

The momentum transfer coefficient as determined from the vertical mean velocity profiles tended to have values larger than would be expected in the upper half of the flow. It is believed that the unusually high values observed in that part of the flow field were due to the effect of the sidewalls and secondary currents on the velocity profile and therefore may not be very indicative of the actual vertical transfer of momentum. For example, the velocity profile for flow condition C, indicated an infinite value of the momentum transfer coefficient at a relative depth of 0.9. No doubt the velocity profiles in the off-center sampling region reflected the influence of horizontal as well as vertical momentum transfer. It is believed that in the upper half of the flow the momentum transfer coefficient as measured from the centerline velocity profiles would be more representative of the true flow conditions. Centerline velocity profiles were very nearly logarithmic and therefore the momentum transfer coefficient was distributed nearly parabolically as indicated in Equation 22.

2. Mass Transfer of Dye

One of the most basic questions to be discussed is the validity of the mathematical model used in this experiment, that is the validity of Equation 37 as a description of the transport process. There are three assumptions in the derivation of Equation 37 that require verification.

The ones in question are whether a transfer coefficient of the type formulated in Equation 3 actually exists, the neglect of the transverse and longitudinal diffusion terms and the neglect of secondary currents.

In discussing the existence of a turbulent transfer coefficient, one should differentiate between long and short diffusion times. Short diffusion times are times before which the Lagrangian correlation coefficient has decayed to zero. Recalling that Equation 3 is defined in terms of a time-averaged product of concentration and velocity fluctuations and a time-averaged concentration gradient, it is questionable whether time averages such as these have any real meaning at very short diffusion times. Another factor which may be of equal fundamental importance to the validity of Equation 3 is the sharpness of the concentration gradient. The importance of this can be appreciated from such phenomenological theories as the "mixing length" theories. The validity of these theories is dependent upon the concentration gradient being small enough so that the change in concentration over a distance of one "mixing length" can be represented as the product of the mixing length and the concentration gradient (Hinze, 1959, p. 277). It is quite probable that if the concentration gradient is so sharp that it exhibits appreciable curvature over a distance of one "mixing length" then Equation 3 and Equation 37 are invalid. For short diffusion times it has been shown by Taylor (1921) that if Equation 3 applies then the transfer coefficient is a function of diffusion time in addition to the characteristics of the flow field. The results of this experiment indicate that the mass transfer occurs at a slower rate in the first few normal depths than would be predicted by Equation 37 with the asymptotic transfer

coefficient. It is believed that the sharp concentration gradient caused the mass transfer coefficient to be less initially and that this is in some way due to the type of behavior predicted by Taylor for short diffusion times. Sharp concentration gradients may also cause trouble in numerical solutions of finite difference equations.

For long diffusion times, there have been many theories advanced in attempts to relate the turbulent transfer coefficient to the flow field or to turbulence (Hinze, 1959, p. 277). This experiment stands with others such as Pien (1941), Al-Saffar (1964), Holley and Schuster (1967) in further substantiating Equation 3 when applied to the transfer of marked fluid.

The dye was injected from the top in such a way that the local flux of the dispersant was always proportional to the local flux of water below by matching the dispersant flux with the transverse distribution of flow velocity. Since the injected flux was matched with the mean flow velocity in the vertical, small local transverse concentration gradients could develop because the transverse velocity distribution at a particular relative depth was not identical with the mean transverse velocity distribution. However, these gradients should have been small relative to the vertical concentration gradients. The bottom injector did not work very well for flow condition B, and fairly large transverse concentration gradients could have occurred there. This is believed to be the cause of the relatively poor measured recovery ratios (0.42 - 1.32) obtained for these runs. The possibility of large transverse concentration gradients was one reason why not too much faith was placed in the dye runs made with the bottom injector.

The measurements of the longitudinal concentration gradient adequately justified the neglect of the longitudinal turbulent diffusion term. Assuming that $\varepsilon_{dx} = \varepsilon_{dy}$ indicated that the longitudinal diffusion would be on the order of one percent of the vertical diffusion. If ε_{dx} was three hundred percent larger than ε_{dy} the longitudinal diffusion would still be only three percent of the vertical diffusion.

The final question arising relative to the validity of Equation 37 is that of secondary currents. Secondary currents certainly existed in these flows as they probably do in all real open channel flows. By judiciously locating the sample probes in regions where the secondary currents are primarily horizontal in direction (as described in detail under secondary currents) their effect was eliminated to a large extent. The integrating probe runs allowed some estimate to be made of the effects of secondary currents. Since the limitations of the equipment allowed the probes to integrate only over the center six feet of the flume, the probes should have sampled the updraft region in the middle of the flume as shown in Figure 3-b, but not the downdraft regions near the flume walls. When dye was injected at the surface, the integral runs indicated smaller concentrations than the fixed probe runs in the upper half of the flow for distances from the source of 19 to 24 normal depths. It is believed that this was caused by the upward transport of relatively clear water in the central updraft region. These effects can easily be seen on the profiles for run DT20. Likewise when the dye was injected at the floor, the concentrations measured by the integral probes showed greater concentrations in the top half of the flow than in the bottom half, for distances greater than twelve normal depths. In

this case the updraft currents were transporting relatively concentrated material to the surface. This effect can easily be seen on the concentration profiles for run DB20 with X = 15, 19 or 24. The results just discussed appeared to be more pronounced for flow condition C than for flow condition A. This suggests that secondary currents were relatively stronger for flow condition C than for flow condition A.

Several combinations of the Eulerian longitudinal turbulence intensities and scales were tried but no definite relationship could be found between these turbulence properties and the measured mass transfer coefficient.

The measured concentration profiles could be reduced to a single set of curves for all flow conditions by using the dimensionless parameters in Equation 37. This is strong proof that the transfer coefficient is proportional to the depth times the shear velocity. Since the secondary currents were apparently not directly proportional to the depth times the shear velocity, the success of the non-dimensionalizing techniques also tends to justify the procedure for eliminating the effects of secondary currents.

Some thought was given to the procedure used in normalizing the measured concentration profiles. The easiest procedure would have been to normalize all curves such that the area under the concentration curve would be a constant, say 1.0. Since the velocity distribution is not uniform, then this would give different physical fluxes of dispersants for different concentration distributions. Since the flux was actually constant at all sections, this procedure would have been invalid from physical considerations. The more complex procedure of normalizing the

the curves such that the flux past any section was constant, was used because it agreed with the physical principle of the conservation of mass. Areas under the normalized concentration profiles are therefore not constant, but are a function of both the concentration and velocity distributions.

Figures like those shown in Figures 31 and 32 effectively condense the data from all measured profiles on to one graph. The value of the transfer coefficient can be computed from the results of any profile by merely matching the curves at that station. However, by viewing the two curves simultaneously the region where the two curves most nearly coincide can be quickly seen. It was assumed that the regions where the curves coincide best represented regions where the measured flux and concentration gradient were most accurate and therefore the regions from which the transfer coefficient should be computed. One may initially think that the regions where the measured quantities are a maximum should be the regions where the most accurate determination of the transfer coefficient could be made. Close observation of Figures 31 and 32, however, show that this is not necessarily true. That is, the shape of the peak regions of the two curves do not agree very well at all. This merely indicates that things are changing too rapidly to be accurately measured at the peak values. The regions given the most weight in determining the transfer coefficient depended somewhat upon the judgment of the observer. However, as a general rule of thumb, the region of relatively high values of the measured quantities just downstream of the peak value is good for determining the transfer coefficient. Mathematical curve fitting procedures were not used for the

dye runs because it was felt that the intuition of the observer was more valuable, for example, in deciding which regions to ignore.

There is a certain amount of scatter in the values of the concentration gradients shown in Figure 31. The part of the curve in Figure 31 with a negative slope was generally considered to be the most accurate region for the determination of the transfer coefficient. The confidence limits shown in Figure 33 were obtained from the curve shown in Figure 32 and the scatter indicated in Figure 31.

Hinze (1959, p. 298) states that the transfer of mass and momentum appear to be approximately analogous. Comparison of the momentum and mass transfer coefficients (Figure 33) supports Hinze's conclusions. In fact, both curves are within the confidence limits set for the measurements of the mass transfer coefficient. Figure 33 indicates that the mass transfer coefficient may be slightly smaller than the momentum transfer coefficient in the upper portion of the flow and slightly larger in the lower portion of the flow. Figure 33 also indicates that the value of the transfer coefficient is significantly less than that of the momentum transfer coefficient at mid depth. This agrees in general with the distributions found by Al-Saffar (1964, p. 66). Al-Saffar obtained an average turbulent Schmidt number of 0.986 in his experiments. In this experiment the average value of the Schmidt number was determined to be 1.03. Thus it is reasonable to conclude that Reynolds analogy for the equivalence of momentum and mass transfer, if not exact, is at least a very good approximation.

One of the most important considerations in the numerical solution of a differential equation is the grid or mesh size. The absolute size of the mesh generally controls the rate of convergence of the numerical solution to the true solution. However, one sometimes reaches a point of diminishing returns as the improvement in accuracy caused by reducing the grid size is balanced by the reduction in accuracy caused by truncation errors. Figure 45 clearly indicates that at least for DY = 0.02 truncation errors are not yet a problem. Computer costs controlled the minimum practical absolute grid size in this investigation. Figure 45 indicates that the effect of increasing the absolute grid size on the numerical solution is not unlike the effect of increasing the diffusion coefficient. The relative size of the sides of the grid controls the stability of the solution. In general, any relative grid size is satisfactory provided it works. A rule of thumb, that was always found to work in these experiments, was to determine relative grid size such that the sum of the absolute values of the coefficients of the concentration difference terms would always be less than 1.0.

Solutions that were run but not presented here indicated that the predicted profiles were not very sensitive to small changes in either the velocity profiles or the initial conditions. Different initial conditions and velocity profiles tended to converge to a common solution with increasing X. This result is not surprising since solutions resulting from all initial concentration and velocity distributions must eventually converge to a common uniform concentration. Figure 47 indicates that a ten percent change in the mean value of the transfer coefficient also does not change the predicted concentration profiles

greatly. After comparing all predicted profiles shown in Figure 47 with the measured profiles, it was concluded that the measured mean value of the transfer coefficient was accurate to within at least ten percent of the true value. The confidence limits shown in Figure 33 indicate that the measured values of the transfer coefficient are accurate to within at least eight percent. The agreement between these two confidence limits illustrates the validity of the computer program in checking the accuracy of the parameters computed from the concentration profiles. Figure 48 shows that the difference between the measured distribution and a parabolic distribution of the transfer coefficient on the predicted profiles is slight and that again no conclusive arguments can be presented that the measured distribution shown in Figure 33 is more correct than a parabolic distribution. Figure 48 does show that a uniform distribution of the transfer coefficient generates unacceptable profiles. The numerical solution of Equation 37 further verifies the measured values of the mass transfer coefficient and also the method of computing it.

3. Mass Transfer of Sediment Particles

The transfer of sediment was found to be a much more complex phenomenon than the transfer of dye. The measurement of ε_{se} was considered more complex than the measurement of ε_d for three reasons. First, two variables in Equation 44 need to be evaluated. In addition, it seems probable that both of these variables (ε_{se} and V_{ST}) may be functions of concentration and therefore of space, at least to some extent. To eliminate the dependence of these variables on concentration the experiments must be conducted with very low concentrations. However, the

concentrations must be large enough to enable their values to be determined accurately. Secondly, the boundary conditions at the floor become indeterminate to the extent that the particles upon reaching the floor can be either reflected back into the flow or deposited with some unknown probability ($0 \leq A \leq 1$). In addition, the probability of deposit, A, can be a function of both space and time because it is probable that A varies to some extent with the quantity of sediment deposited on the floor and this quantity of sediment was shown to vary with both time and space in this experiment. Actually the probability of deposit does not completely describe the boundary condition in the unsteady case; the length of time which particles remain on the bed before being re-entrained is important also. However, in the steady state case the rest periods of the particles on the floor are of no concern. All that matters is the net rate of transfer to the bed which can be expressed as a probability of deposit since particles are continuously being interchanged between the bottom layer of flow and the deposited material. The third reason for the added difficulty in computing the parameters is that various fall velocities were used and that ε_{se} may not be proportional to $Y_N u_*$ which makes it impossible to combine the results of different flow conditions as was possible with the results of the dye transfer experiments.

Even though values for ε_{se} were determined, its meaning remains more complex because of the factors considered in Chapter II. The interpretation of differences between turbulent and quiescent fall velocities is also difficult because the causes for the differences could not be pinned down exactly. As discussed previously, there could

be at least four causes for this difference, the injection system, the mean concentration, the group fall velocity and the effects of turbulence. The added scatter in the determination of ε_{se} and V_{ST} from the sediment transfer experiment can then be attributed to one or more of the above factors.

H. E. Hurst and Hunter Rouse (Task Committee, 1963, p. 55) have shown the validity of Equations 3 and 37 for describing the equilibrium steady state suspension of sediment in a turbulence tank. Dobbins (1944) has verified these equations for describing the unsteady suspension of sediment in a turbulence tank. The degree to which the numerical solution reproduced the measured concentration profiles in this experiment extends the verification of these equations to the steady non-equilibrium suspension of sediment in a two-dimensional open channel flow. Most of the discrepancies between the measured and predicted profiles shown in Figures 34 through 39 will be shown to be due to causes other than the insufficiency of Equations 3 and 37. Although only long diffusion times are considered here, the sediment transfer coefficient, like the mass transfer coefficient for dye is probably a function of time for short diffusion times or for very sharp concentration gradients.

Vertical transfer of sediment is due to the combined effects of convection due to the fall velocity and diffusion due to turbulent transfer. Longitudinal and lateral transfer on the average should have about the same effect on the sediment profiles as on the dye profiles. It was assumed that the longitudinal and transverse diffusion terms were always insignificant.

Secondary currents should have had no more effect on the measured sediment concentration profiles in this experiment than they did on the measured dye profiles. Unfortunately, the effects of secondary currents on equilibrium concentration profiles cannot be quantitatively predicted at this point. However, as discussed in Chapter II, secondary currents increase the vertical mixing which leads to disproportionately large apparent values of the sediment transfer coefficient being computed from equilibrium concentration profiles. The writer feels that the effects of secondary currents helps to explain many of the surprisingly large values of the sediment transfer coefficients which have been determined from equilibrium transport measurements. It has been shown in Chapter II how the effects of secondary currents can be represented by an effective transfer "coefficient" in the general suspended sediment transport equation for equilibrium conditions.

The various factors which affect the particle fall velocity in the flume have been discussed previously. Of these factors, the grouping effect due to the injection system and turbulence appear to be the main factors needing further consideration. For the coarse sediment runs the grouping effects did not appear to be significant. Turbulence appeared to increase the averaged coarse particle fall velocity slightly. If turbulence affects the fall velocity, it appears reasonable that the effect should be more pronounced near the floor where the turbulence levels are greatest. The measurements in this study were not complete enough to detect this tendency, so the turbulent fall velocity was assumed constant throughout the depth of flow. For the fine sediment runs both grouping and turbulence effects appeared to be present.

Particle fall velocities near the surface tended to be larger than those near the floor; this was attributed to the grouping effect. However, in predicting the concentration profiles, the particle fall velocity was assumed not to vary with depth. In natural channels the particle fall velocity may be a function of depth due to vertical variations in mean concentration and turbulence levels. Since both the concentration and turbulence levels are a maximum near the bed these effects should tend to compensate each other.

The flow was uniform before each run was started, however, for low flow conditions the sediment tended to be deposited on the bed and fill the spaces between the roughness blocks. Flow condition A with the coarse sediment was the worst condition, however, even in this case the problem was not considered to be very significant.

Because the measured values of the total sediment transfer coefficient showed so much scatter, no systematic vertical distribution was immediately discernible. To obtain a vertical distribution of the transfer coefficient the total sediment transfer coefficient, ε_{se}, was assumed to be made up of two components as proposed in Chapter II. Because of the close agreement between the mass transfer coefficient for dye and the momentum transfer coefficient (Figure 33), and for the sake of convenience, it was assumed that the part of the sediment transfer coefficient due to tangential components of turbulent velocity fluctuations, ε_T, was also distributed parabolically. For the reasons discussed in Chapter IV, the component of the transfer coefficient due to the centrifugal fluid particle acceleration, ε_c, was assumed to have a

maximum value at $\eta = 0.1$ and to decrease in proportion to the cube of the distance from $\eta = 0.1$, going to zero at both boundaries.

Fitting these distributions to the measured data shows that the value of ε_T decreased with increasing particle size as predicted by Carstens (1952). The ratio of $\varepsilon_T/\varepsilon_m$ was determined to be 0.985 and 0.492 respectively for the fine and coarse sediments.

The value of ε_c increased with increasing particle size as measured by Singamsetti (1966). The maximum values of $\varepsilon_c / Y_N u_*$ were found to be 0.0376 and 0.102 respectively for the fine and coarse sediments. Since there is so much scatter in the measured data these assumed distributions for the two components of the transfer coefficient cannot be adequately justified from this data. Further justification must await more detailed measurements.

Since the value of ε_T is apparently proportional to ε_d or ε_m, its relationship to the turbulence properties has previously been discussed. The distribution of ε_c is only assumed, so not much can be said about its relationship to turbulence. It is pointed out that the assumed distribution of ε_c appears somewhat similar to the measured distribution of the Eulerian turbulence intensities shown in Figure 21. Also, the maximum value of ε_c was assumed to occur where $\overline{u'^2}$ was a maximum.

It has often been stated that the presence of sediment particles in the water damps the turbulence (Vanoni, 1946) and therefore affects the transfer mechanism. This experiment was designed with the intention that the concentration of sediment would be low enough so that its effect on the transfer mechanism would be insignificant. Because the mean concentrations were apparently low enough to have a small effect on the fall velocity, it was assumed that the concentrations of sediment

would also be low enough to have negligible effects on the transfer coefficient. However, no velocity profiles were measured while sediment was being injected into the water.

No consistent variation of $\varepsilon_{se}/Y_N u_*$ with $Y_N u_*$ can be detected from the fine sediment data in Figure 43. The predominant part of ε_{se} in Figure 43 appears to be ε_T, which like ε_m, is assumed to be proportional to the depth times the shear velocity. This assumption is consistent with previous assumptions of the applicability of Reynolds analogy to sediment particles (Vanoni, 1946), and to the theory proposed in Chapter II. Neither could a trend in $\varepsilon_{se}/Y_N u_*$ be detected from the coarse sediment data in Figure 44. The values of $\varepsilon_{se}/Y_N u_*$ here depend to a significant extent on ε_c. The scatter in Figure 44 is so large, however, that no definite conclusion can be drawn. The value of ε_c was assumed to be proportional to depth times the shear velocity primarily for convenience. Figure 44 neither substantiates nor repudiates this assumption.

Originally the values of the sediment transfer coefficients were computed using a procedure like that outlined for the computation of the dye mass transfer coefficient. The fall velocities were assumed to be equal to that obtained from the sediment deposition data for flow condition A. This procedure was considered inadequate because of the sensitivity of the computed transfer coefficient to the assumed fall velocity. It is believed that the curve fitting procedures discussed in Chapter IV, which solve for $\varepsilon_{se}/Y_N u_*$ and V_{ST}/u_* independently, could not have been significantly improved with the limited data available.

There are many curve fitting techniques and all have their own advantages and disadvantages. The main disadvantage of the least squares technique was considered to be its tendency to give disproportionately large weight to large values of the measured coefficients. Its advantage was that no arbitrary decisions had to be made in applying the technique. The advantage of the method of averages technique was that it tended to give all data equal weight. Its disadvantage was that it required the data points to be divided into two groups and that the results depended upon how this division was made.

All sediment concentration profiles were normalized so that they indicated a flux equal to the product of the depth times the mean velocity times the recovery ratio. The maximum variation between the recovery ratio and its measured value was fairly large. Sayre and Chang (1968, p. 44) also experienced difficulty in obtaining consistent recovery ratios from measured sediment concentrations. An insufficient number of profiles were measured to completely determine the recovery ratio but it is believed that the estimated recovery ratios are accurate to within at least five percent.

The boundary conditions at the floor were indeterminate to the extent that the probability of a sediment particle being deposited once it hit the floor was not known. By integrating Equation 37 from some arbitrary depth to the surface this problem was partially eliminated when computing the values of $\varepsilon_{se}/Y_N u_*$ and V_{ST}/u_* from the measured profiles. However, it was not entirely eliminated because the probability of deposit affected the recovery ratio which was used in normalizing the concentration curves.

The probability of deposit was an elusive factor because its magnitude probably varied with time and space. Its value might have been computed from the slope of the recovery ratio curve, the concentration at the floor and the particle fall velocity at the floor. Because of the difficulty of obtaining these values, however, it was concluded that it would be just as valid to assume a value of the probability of deposit from intuition alone. It is pointed out that the probability of deposit seemed to be a function of particle size and not, as one might suspect, solely a function of the Rouse number. Note that the probability of deposit was about 0.2 for flow condition C with the coarse sediment which had a Rouse number of about 1.1, but about 0.5 for flow condition A with the fine sediment which had a Rouse number of about 0.6.

Figures 26, 28, 43 and 44 indicate to some extent the confidence limits of the parameters measured from the concentration profiles. After looking at the concentration profiles, it is not surprising that the coarse sediment profiles seem to give fairly good indications of fall velocities but poor indications of transfer coefficients, and that the fine sediment runs give relatively good indications of the transfer coefficients but poor indications of the fall velocities. This is because the major portion of the vertical transfer is due to convection by the fall velocity for the coarse sediment and due to turbulent diffusion for the fine sediment.

Before comparing the predicted and measured concentration profiles shown in Figures 34 through 39, it is helpful to have some feel for the variation of the predicted profiles with the various parameters. These effects are demonstrated for flow condition C with the coarse sediment

except for the fall velocity effect which is demonstrated for flow condition B with the fine sediment.

Figure 49 demonstrates the variations in the predicted profiles for various distributions of the transfer coefficient. Except for a slight difference in the predicted concentration between the relative depths of 0.1 and 0.5, Equation 51 and the parabolic distribution of $\varepsilon_{se}/Y_N u_*$ predict nearly identical profiles. A uniform distribution of $\varepsilon_{se}/Y_N u_*$, on the other hand, predicts higher concentrations for relative depths greater than 0.9 and less than 0.5 than the other two distributions, particularly at greater distances from the source. All distributions shown in Figure 49 have the same mean value of the transfer coefficient.

Figure 50 shows the effects of varying the mean value of the transfer coefficient while keeping its distribution constant. It can be seen that the peak values of the concentration profiles vary most with changes in the mean value of the transfer coefficient, at least near the source. For greater distances from the source the concentration in the upper half of the flow is most affected by variations in the magnitude of transfer coefficients.

Figure 51 shows the effect of varying the probability of deposit on the resulting concentration distributions. This factor has virtually no effect in the upper part of the flow. Unfortunately, in the lower half of the flow it has an effect very similar to that of increasing the transfer coefficient in that part of the flow.

Figure 52 shows the effect of decreasing the turbulent fall velocity on the resulting profiles. Near the source about the only effect of changing the value of fall velocity is to change the rate of fall of

the peak value of the concentration profile. Far from the source and in the lower half of the flow, decreasing the fall velocity has an effect similar to that of either decreasing the probability of deposit or locally increasing the sediment transfer coefficient. Far from the source and in the upper half of the flow, decreasing the fall velocity has an effect similar to that caused by locally increasing the value of the transfer coefficient.

If one considers that the fall velocity may be a function of depth and that the probability of deposit may be a function of X, then it can be seen that pinpointing causes of divergence between the measured and predicted profiles will be difficult. Considering the relatively large changes in parameters used in predicting the profiles in Figures 49 through 52, it can be seen that the gross shape of the profiles is not very sensitive to small changes in the magnitude or distribution of either the fall velocity or the sediment transfer coefficient.

Profiles predicted from the numerical solution using the measured parameters serve mainly as a check on the accuracy of the computations of the parameters from the measured concentration profiles. The numerical solutions are restricted somewhat by the assumption that the fall velocity and the probability of deposit were constant for all space coordinates whereas physical observations suggest that these parameters did not necessarily remain constant in space. The accuracy of the numerical solution also decreases at large values of the Rouse number. Figures 45 and 46 show approximately how this accuracy deteoriates with increasing Rouse number. It can be seen from Figure 45 that for all of

the coarse sediment runs the numerical solution will indicate somewhat greater diffusion than will the exact solution of Equation 37.

Figure 34 shows that for flow condition A with fine sediment the predicted profiles indicate that in the upper region of the flow, either the assumed distribution of the sediment transfer coefficient was too large or the assumed fall velocity was too small. Considering the measured distribution of the turbulent fall velocity (Figure 26) it is probable that the actual fall velocity was larger than the fall velocity assumed in the numerical solution at least in the uppermost part of the flow. Likewise in the bottom half of the flow the fall velocity used in the numerical solution was probably too large. It is quite probable that putting a fall velocity into the numerical solution that decreased from the top to the bottom would improve the agreement between the predicted and measured profiles shown in Figure 34. This variation in fall velocity is entirely consistent with the measured distribution of fall velocity shown in Figure 26.

The results of flow condition B for the fine sediment shown in Figure 35 show even more definitely that the value of the fall velocity used in the numerical solution was too small in the upper layers of the flow and too large in the bottom layers of flow. This is again consistent with the measured variation of the fall velocity with depth as shown in Figure 26. It is possible that a smaller value of the probability of deposit is also indicated at X = 15 in Figure 35.

The computed and measured profiles agree very well for flow condition C with the fine sediment (Figure 36) except at the very top. It is encouraging that the measured variation of the fall velocity was also

pretty uniform for flow condition C with fine sediment except in the upper twenty percent of the flow depth.

The results of flow condition A for the coarse sediment are shown in Figure 37. These results indicate that the turbulent fall velocity used in the numerical solution was quite appropriate. This is consistent with the relatively constant value of the fall velocity shown in Figure 28. The numerical solution shown in Figure 37 indicates more rapid diffusion throughout than does the measured profile. This can be partially attributed to error due to a finite grid size used in predicting the profiles (see Figure 45). Actually, Figure 45 is not as critical a test of the numerical solution as is Figure 37 because for $\eta \to 1$ and small values of X, $\varepsilon_{se}/Y_N u_*$ is constant in Figure 45 whereas it goes to zero in Figure 37 at $\eta = 1$ and at $\eta = 0$.

The results for flow condition B with the coarse sediment are shown in Figure 38. These results indicate that the assumed fall velocity in the upper region is smaller than the actual value in that part of the flow field. This appears to be consistent with Figure 28. The bottom layers of the predicted profiles do not agree well with the measured values either, however, this could be due to any of three causes or a combination thereof; first the actual value of the transfer coefficient being larger than the assumed value (Figure 50), second the actual value of the fall velocity being less than the assumed value of the fall velocity (Figure 52), or finally the actual value of the probability of deposit being less than the assumed value (Figure 51). If the actual value of the transfer coefficient is larger in the bottom portions of the flow than the assumed values of the transfer coefficient,

then the value of ε_c is more pronounced for the coarse sediment in this flow than is indicated by Equation 53.

About the same comments apply to flow condition C with the coarse sediment shown in Figure 39 as were made for flow condition B with the coarse sediment.

Three general conclusions can be made after comparing the measured concentration profiles with the predicted concentration profiles shown in Figures 34 through 39. Except for flow condition A with the coarse sediment, the fall velocity is a function of depth as indicated in Figures 26 and 28. This further verifies that the grouping effect did influence the fall velocity. The second conclusion is that ε_c may be even larger in the bottom layers for flow condition B and C with the coarse sediment than is indicated by Equation 53. Finally, the assumed distribution of the transfer coefficient for the fine sediment appears to be reasonably accurate.

Chapter VI

SUMMARY AND CONCLUSIONS

A. Summary

Briefly stated the goals of this investigation were to investigate some of the turbulent and convective transfer processes in an open channel shear flow. More specifically the goals were to:

a. Experimentally determine the mass transfer coefficient for both sediment and a dispersant which had the same fluid properties as water and to compare these transfer coefficients to the momemtum transfer coefficient.

b. Experimentally determine particle fall velocities in a turbulent open channel flow and compare it with those obtained in a quiescent fluid.

c. Use the measured values of the transfer coefficients and fall velocities in conjunction with a numerical solution of the conservation equation in order to check the mathematical model of the mixing process and to illustrate the effect of various parameters on the predicted profiles.

In order to make these measurements, a continuous line source of dispersant was injected across the surface of an open channel. Vertical concentration profiles were measured at several cross sections downstream of the source. An integrated form of the conservation of mass equation was used to compute transfer coefficients and fall velocities from measured distributions of velocity and concentration. The dispersants used were fluorescent dye, fine sand and medium sand.

Because secondary currents probably affect the flow in all open channels, a review of the patterns and intensities of these currents was given. A procedure was devised which largely eliminated the effects of secondary currents on the measured concentrations.

The particle fall velocity in the flume was determined from the pattern of sediment deposition as well as from the rate of change of the concentration profiles. Measurements from the concentration profiles allowed the vertical distribution of the fall velocity to be determined.

An hypothesis was presented which helps to explain the apparent divergence of previously measured sediment transfer coefficients. The measured values of the sediment transfer coefficients obtained in this experiment were also used to check the validity of the hypothesis.

Numerical solutions were obtained to the conservation of mass equation and the measured values of the transfer coefficient and fall velocity were used in conjunction with these solutions to predict the concentration profiles. The predicted profiles were compared with the measured concentration profiles.

From the experimental measurements and theoretical analysis the following conclusions are drawn.

B. Conclusions

1. Secondary Currents

a. Secondary currents have an important effect on the vertical transfer process. Failure to adequately account for the effects of secondary currents causes values of the sediment transfer coefficient determined from equilibrium concentration profiles to be distorted.

b. The secondary currents for the flows in this investigation consisted of two primary spirals as shown in Figure 3-b.

2. Particle Fall Velocity

a. The fall velocity of the sediment particles in the turbulent flume flow, when corrected to 24° C, was always greater than the standard fall velocity of the particles.

b. Four main factors could have affected the fall velocity of the sediment particles in this flume. These factors were the dry injection with non-zero initial velocity, the mean concentrations, the grouping effects, and turbulence. Tests in quiescent fall columns indicated that the first of these effects was insignificant.

c. Previous investigations indicate that the effect of the mean concentration should decrease the particle fall velocity but that for the range of concentrations used in this experiment the decrease should have been insignificant.

d. The grouping effects due to the injection system should increase the particle fall velocity. This effect appeared to be insignificant for the coarse sediment except possibly for flow conditions B and C and then only in the upper twenty percent of the flow. However, it appeared to be the main cause of the increase in fall velocity in the flume for the fine sediment.

e. Only for the coarse sediment dispersing in flow condition A could the effects of turbulence be completely isolated. For this case turbulence appeared to increase the fall velocity slightly.

f. Although complete isolation of the effects of turbulence could not be obtained with the fine sediment, data seemed to indicate that

the turbulence significantly increased the effective particle fall velocity.

g. The visual accumulation tube is inadequate for the determination of the standard fall velocity of very uniformly sized materials in the sand size range.

3. Diffusion of Marked Fluid Particles

a. Secondary currents cause additional mixing in open channels and must be accounted for in determining mass transfer coefficients.

b. The existence of the turbulent mass transfer coefficient is further verified. However, results suggest that the value of the transfer coefficient is not constant for very short diffusion times. This has been predicted by Taylor (1921) and demonstrated by Pien (1941).

c. As predicted by Hinze (1959, p. 298), the transfer of mass and momentum are shown to be similar at least as a first approximation, thus verifying Reynold's analogy for the equivalence of mass and momentum transfer in open channel turbulent shear flow.

d. The turbulent Schmidt number is shown to be approximately 1.03 for the vertical transfer coefficient in a rough open channel flow.

e. Eulerian point turbulence measurements of longitudinal velocity fluctuations are not sufficient to predict the value of the mass transfer coefficient.

f. Predicted concentrations are shown to be rather insensitive to either the magnitude or to minor variations in the distribution of the mass transfer coefficient.

4. Diffusion of Sediment Particles

a. Vertical mixing of suspended sediment in open channel flow occurs as a result of at least three semi-independent processes which are shown to be additive. These processes are:

1) Mixing due to secondary currents.

2) Diffusion due to tangential components of turbulent velocity fluctuations.

3) Diffusion due to the centrifugal acceleration of fluid particles.

b. After an initial period which is long compared to the time required for a secondary spiral to make one revolution, the effect of mixing due to secondary currents, when averaged over the entire width of the flow, can be represented as a diffusion process.

c. Diffusion due to tangential components of turbulent velocity fluctuations appears to be the predominant turbulent mixing process for fine sediment particles in general, and for all sediment particles in flows without strong vortex activity. That portion of the turbulent mass transfer coefficient for sediment particles which is directly attributable to tangential components of turbulent velocity fluctuations:

1) Is proportional to the product of the depth and shear velocity.

2) Is approximately proportional to the mass transfer coefficient for dye and the proportionality constant is always less than or equal to 1.0 as predicted by Carstens (1952).

3) Decreases with increasing particle size.

d. Diffusion due to centrifugal acceleration of the fluid particles appears to be predominant for coarse sediment in flows with significant

vortex activity. That portion of the transfer coefficient which is attributable to centrifugal acceleration:

1) Can logically be assumed to have a maximum value in the zone of most intense shear and to decrease rapidly in either direction going away from this zone.
2) Increases with particle size at least in the fine to medium sand range.
3) Is closely related to characteristics of the bed roughness, particularly those that give rise to flow separation.

e. The actual vertical distribution of sediment concentration is not very sensitive either to minor changes in the vertical distribution or to the magnitude of the transfer coefficient.

C. Suggestions for Future Research

During the course of this investigation, it became apparent that the following areas need further study.

1. Secondary Currents

a. More information is needed concerning the effect of non-homogeneous roughness on the strength and patterns of secondary currents. Leutheuser, Hoagland, Brudett, Gessner and Jones (Hinze, 1967, p. s122) have made a start in this direction, but their work needs to be extended.

b. The strength of secondary currents in straight open channels needs to be correlated with the conventional flow parameters such as velocity, roughness, slope, depth, etc.

c. The effects of secondary currents on sediment concentration profiles need further study. The work of Chiu and McSparran (1966) is an excellent start in this direction. The effects on equilibrium

profiles in particular requires attention. One objective of a study of this type might be to check the validity of Equations 13 and 14.

d. Extend the numerical solution to the three dimensional case with secondary circulation.

2. Particle Fall Velocity

a. The effects of hindered settling should be extended for particles above the Stokes range and for very small concentrations.

b. The effect of particle grouping on fall velocities as noted here and by Loyacano (1967) should be further investigated.

c. Much further work is required to evaluate the effect of turbulence on particle fall velocity. Measurements from both concentration profiles and deposition data show promise as methods for evaluating these effects for small particles in actual open channel flows.

d. A theoretical explanation for the effect of turbulence on fall velocity is needed.

3. Diffusion of Marked Fluid Particles

Equipment has now been advanced to the stage where direct measurements of the correlation $\overline{u_i'c'}$ appear to be possible. This should be done as a further check on the validity of Equation 3 and as a means to directly measure the transfer coefficient. Once this equipment has been perfected it should be possible to determine the dependence of the transfer coefficient on time and/or concentration gradients. Furthermore it should provide a means for indirectly measuring Lagrangian turbulence properties and relating them to the appropriate Eulerian properties.

4. Diffusion of Sediment Particles

a. More detailed experiments should be made to explore further the existence and interrelationship of transfer due to tangential components of velocity fluctuations and transfer due to the centrifugal acceleration of fluid particles.

b. The value of the transfer coefficient due to tangential components of velocity fluctuations should be more directly correlated with the work of Carstens (1952) and its relationship to the mass transfer of marked fluid should be further verified. The relationship of this coefficient to the Rouse number should be further explored.

c. The magnitude and distribution of the transfer coefficient due to the curvature of the fluid particle paths has received very little consideration. The variation of ε_c with flow parameters and intensity of vortex activity needs to be determined.

d. The nature of ε_c suggests that correlating sediment transport with the statistical properties of the bed forms may be quite fruitful. The statistical properties which are related to the angularity of the bed forms may be of most interest.

BIBLIOGRAPHY

BIBLIOGRAPHY

Al-Saffar, Adnan Mustafa, 1964, "Eddy diffusion and mass transfer in open channel flow," Ph. D. dissertation, Civil Engineering Department, University of California, Berkeley, California, 138 p.

Brush, Lucien M. Jr., 1962, "Exploratory study of sediment diffusion," Journal, Geophysical Research, Vol. 67, No. 4, pp. 1427-1435.

Camp, Thomas R., 1946, "Sedimentation and the design of settling tanks," Transactions, Am. Soc. of Civil Engr., Vol. 111, pp. 895-958.

Carstens, M. R., 1952, "Accelerated motion of a spherical particle," Transactions, American Geophysical Union, Vol. 33, No. 5, pp. 713-720.

Chiu, Chao-Lin, 1967, "Factors determining the strength of secondary flow," Am. Soc. of Civil Engr. Proc., Vol. 93, No. EM4, pp. 69-77.

Chiu, Chao-Lin, and McSparran, John E., 1966, "Effect of secondary flow on sediment transport," Am. Soc. of Civil Engr. Proc., Vol. 92, No. HY5, pp. 57-69.

Ciray, Cahit, 1967, "On secondary currents," Proceedings, Twelfth Congress of the International Association for Hydraulic Research, Vol. 1, Colorado State University, Fort Collins, Colorado, pp. 408-421.

Csanady, G. T., 1963, "Turbulent diffusion of heavy particles in the atmosphere," Journal of Atmospheric Science, Vol. 20, No. 3, pp. 201-208.

Delleur, J. W., and McManus, D. S., 1959, "Secondary flow in straight open channels," Proceedings of Sixth Annual Conference on Fluid Mechanics, University of Texas, Austin, Texas, pp. 81-97.

Dobbins, William E., 1944, "Effect of turbulence on sedimentation," Transactions, Am. Soc. of Civil Engr., Vol. 109, pp. 629-667.

Einstein, H. A., and Chien, Ning, 1954, "Second approximation to the solution of the suspended load theory," University of California Institute of Engineering Research, Berkeley, California, Missouri River Division Sediment Series, 29 p.

Einstein, H. A., and Li, Huon, 1958, "Secondary currents in straight channels," Transactions, American Geophysical Union, Vol. 39, No. 6, pp. 1085-1088.

Elder, J. W., 1959, "The dispersion of marked fluid in turbulent shear flow," Journal of Fluid Mechanics, Vol. 5, No. 4, pp. 544-560.

Frenkiel, F. N., 1953, "Turbulent diffusion: mean concentration distribution in a flow field of homogenous turbulence," Advances in Applied Mechanics, Acad. Press, Vol. III, Edited by Von Misis and Von Karman, pp. 61-107.

Friedlander, S. K., and Topper, Leonard, 1961, "Turbulence classic papers on statistical theory," Interscience Publishers, Inc., New York, 187 p.

Hino, Mikio, 1967, "Equilibrium-range spectra of sand-waves formed by flowing water," Department of Civil Engineering, Tokyo Institute of Technology, O'okayama, Meguro-ku, Tokyo, 12 p.

Hinze, J. O., 1959, "Turbulence," McGraw-Hill Book Company, Inc., New York, 586 p.

Hinze, J. O., 1967, "Secondary currents in wall turbulence," The Physics of Fluids Supplement, American Institute of Physics, New York, Vol. 10, Pt. II, No. 9, pp. 5122-5125.

Ho, Hau-Wong, 1964, "Fall velocity of a sphere in a field of oscillating fluid," Ph. D. dissertation, Department of Mechanics and Hydraulics, State University of Iowa, Iowa City, Iowa, 78 p.

Holley, Edward R., and Schuster, Jack C., 1967, "Radial diffusion in turbulent pipe flow," Proceedings, Twelfth Congress of the International Association for Hydraulic Research, Vol. 4, Colorado State University, Fort Collins, Colorado, pp. 124-137.

Hubbell, D. W., and Matejka, D. Q., 1959, "Investigations of sediment transportation Middle Loup River at Dunning, Nebraska," Geological Survey Water-Supply Paper 1476, U.S. Gov. Printing Office, Washington 25, D.C., 123 p.

Hunt, J. N., 1954, "The turbulent transport of suspended sediment in open channels," Proc. Royal Soc. of London, Vol. 224A, pp. 322-335.

Inter-Agency, 1941, "Methods of analyzing sediment samples," A study of methods used in measurement and analysis of sediment loads in streams, Report No. 4, St. Paul U.S. Engineer District Sub-Office Hydraulic Laboratory, State University of Iowa, Iowa City, Iowa, 203 p.

Inter-Agency, 1957, "The development and calibration of the visual-accumulation tube," A study of methods used in measurement and analysis of sediment loads in streams, Report No. 11, Subcommittee on Sedimentation, Inter-Agency Committee on Water Resources, @ St. Anthony Falls Hydraulic Laboratory, Minneapolis, Minnesota, 109 p.

Inter-Agency, 1957, "Some fundamentals of particle size analysis," A study of methods used in measurement and analysis of sediment loads in streams, Report No. 12, Subcommittee on Sedimentation, Inter-Agency Committee on Water Resources, @ St. Anthony Falls Hydraulic Laboratory, Minneapolis, Minnesota, 55 p.

Ismail, Hassan M., 1952, "Turbulent transfer mechanism and suspended sediment in closed channels," Transactions, Am. Soc. of Civil Engr., Vol. 117, pp. 409-446.

Kalinske, A. A., and Pien, C. L., 1943, "Experiments on eddy-diffusion and suspended-material transportation in open channels," Transactions, American Geophysical Union, Pt. II, pp. 530-536.

Kandala, Abdulahad S., 1966, "Fall velocity of spheres in open channel flow," Ph. D. dissertation, Civil Engineering Department, Colorado State University, Fort Collins, Colorado, 175 p.

Laufer, John, 1951, "Investigation of turbulent flow in a two-dimensional channel," National Advisory Committee for Aeronautics, Report No. 1053, U.S. Gov. Printing Office, Washington 25, D.C., 20 p.

Liggett, James A., Chiu, Chao-Lin and Miao, Ling S., 1965, "Secondary currents in a corner," Am. Soc. of Civil Engr. Proc., Vol. 91, No. HY6, pp. 99-117.

Loyacano, Joseph N., 1967, "Fall velocity of sand particles in turbulent flume flow," Master's thesis, Civil Engineering Department, Colorado State University, Fort Collins, Colorado, 76 p.

Majumdar, Hirendra, and Carstens, M. R., 1967, "Diffusion of particles by turbulence: effect of particle size," School of Civil Engineering, Georgia Institute of Technology, Atlanta, Georgia, 102 p.

Matthews, Robert J., and Liggett, James A., 1967, "Flow in a sharp corner," Am. Soc. of Civil Engr. Proc., Vol. 93, No. HY6, pp. 387-407.

Matyukhin, V. I., and Prokof'yev, O. N., 1966, "Experimental determination of the coefficient of vertical turbulent diffusion in water for settling particles," Soviet Hydrology: selected papers, No. 3, published by the American Geophysical Union, Washington, D.C., pp. 69-77.

McLaughlin, Ronald T., Jr., 1959, "The settling properties of suspensions," Am. Soc. of Civil Engr. Proc., Vol. 85, No. HY12, Pt. 1, pp. 9-41.

McNown, J. S., and Lin, Pin Nam, 1952, "Sediment concentration and fall velocity," Proceedings of the Second Midwestern Conference on Fluid Mechanics, Bulletin No. 149, College of Engineering, The Ohio State University, Columbus, Ohio, 403 p.

McQuivey, Raul S., 1967, "Turbulence in a hydrodynamically rough and smooth open channel flow," Ph. D. dissertation, Civil Engineering Department, Colorado State University, Fort Collins, Colorado, 105 p.

McQuivey, Raul S., and Richardson, E. V., 1968, "Measurements of turbulence in flow over a sand bed," Am. Soc. of Civil Engr., Hyd. Div. Conf. at M.I.T., Aug. 21-23.

Mickelsen, William R., 1960, "Measurements of the effect of molecular diffusivity----turbulent diffusion," Journal of Fluid Mechanics, Vol. 7, Pt. 3, pp. 397-400.

Nemenyi, Paul F., 1946, Discussion of "Transportation of suspended sediment by water," by Vito A. Vanoni, Transactions, Am. Soc. of Civil Engr., Vol. 111, pp. 116-125.

Neu, Hans A., 1967, "Transverse flow in a river due to earth's rotation," Am. Soc. of Civil Engr. Proc., Vol. 93, No. HY5, pp. 149-165.

Nordin, Carl F. Jr., 1968, "Statistical properties of dune profiles," Ph. D. dissertation, Civil Engineering Department, Colorado State University, Fort Collins, Colorado, 137 p.

Orlob, Gerald T., 1958, "Eddy diffusion in open channel flow," Sanitary Engineering Research Laboratory, University of California, Berkeley, California, Contribution No. 19, Water Resources Center.

Orlob, Gerald T., 1961, "Eddy diffusion in homogeneous turbulence," Transactions, Am. Soc. of Civil Engr., Vol. 126, Pt. 1, pp. 397-438.

Pai, Shih-I, 1957, "Viscous flow theory, II-turbulent flow," D. Van Nostrand Company, Inc., New York, 275 p.

Pien, Chung Ling, 1941, "Investigation of turbulence and suspended material transportation in open channels," Ph. D. dissertation, Department of Mechanics and Hydraulics, Graduate College of the State University of Iowa, Iowa City, Iowa, 114 p.

Powell, Ralph W., 1946, Discussion of "Transportation of suspended sediment by water," by Vito A. Vanoni, Transactions, Am. Soc. of Civil Engr., Vol. 111, pp. 103-106.

Prandtl, Ludwig, 1952, "Essentials of fluid dynamics," Hafner Publishing Company, New York, pp. 145-151.

Raichlen, Fredric, 1967, "Some turbulence measurements in water," Am. Soc. of Civil Engr. Proc., Vol. 93, No. EM2, pp. 73-97.

Rao, B. Vasudeva, and Seetharamiah, K., 1967, "Development and role of secondary currents in alluvial streams," Proceedings, Twelfth Congress of the International Association for Hydraulic Research, Vol. 1, Colorado State University, Fort Collins, Colorado, pp. 472-478.

Richtmyer, R. D., 1957, "Difference methods for initial-value problems," Interscience Publishers, Inc., New York, 237 p.

Robertson, James M., 1967, Discussion of "Some turbulence measurements in water," by Fredric Raichlen, Am. Soc. of Civil Engr. Proc., Vol. 93, No. EM6, pp. 278-293.

Rohsenow, Warren M., and Choi, Harry Y., 1961, "Heat, mass and momentum transfer," Prentice-Hall Inc., Englewood Cliffs, New Jersey, 186 p.

Sayre, W. W., and Albertson, M. L., 1963, "Roughness spacing in rigid open channels," Transactions, Am. Soc. of Civil Engr., Vol. 128, Pt. 1, pp. 343-427.

Sayre, W. W., 1968, "Dispersion of mass in open channel flow," Hydraulics papers, No. 3, Colorado State University, Fort Collins, Colorado, 73 p.

Sayre, W. W., and Chang, F. M., 1968, "A laboratory investigation of open-channel dispersion processes for dissolved, suspended and floating dispersants," U.S. Geological Survey Professional Paper 433-E, U.S. Gov. Printing Office, Washington 25, D.C., 71 p.

Singamsetti, Surya Rao, 1966, "Diffusion of sediment in a submerged jet," Am. Soc. of Civil Engr. Proc., Vol. 92, No. HY 2, pp. 153-168.

Stringham, Glen E., 1965, "Behavior of geometric particles falling in quiescent viscous fluids," Ph. D. dissertation, Civil Engineering Department, Colorado State University, Fort Collins, Colorado, 143 p.

Task Committee, 1962, "Sediment transportation mechanics; introduction and properties of sediment," Progress Report, Task Committee on Preparation of Sedimentation Manual, Committee on Sedimentation, Am. Soc. of Civil Engr. Proc., Vol. 88, No. HY4, pp. 77-107.

Task Committee, 1963, "Sediment transportation mechanics; suspension of sediment," Progress Report, Task Committee on Preparation of Sedimentation Manual, Committee on Sedimentation, Am. Soc. of Civil Engr. Proc., Vol. 89, Pt. 1, No. HY5, pp. 45-77.

Taylor, G. I., 1921, "Diffusion by continuous movements," Proc., London Math. Soc., A20, pp. 196-211.

Tracy, Hubert J., 1965, "Turbulent flow in a three-dimensional channel," Am. Soc. of Civil Engr. Proc., Vol. 91, Pt. 1, No. HY6, pp. 9-37.

Vanoni, Vito A., 1946, "Transportation of suspended sediment by water," Transactions, Am. Soc. of Civil Engr., Vol. 111, pp. 67-133.

Zimbelman, Darell D., 1966, "The fall velocity of spherical particles in a turbulent fluid," Master's thesis, Civil Engineering Department, Colorado State University, Fort Collins, Colorado, 71 p.

APPENDIX A

TABLES

TABLE 1 HYDRAULIC PARAMETERS

Run No.	Discharge	Depth	Slope	Temp.	Discharge / Area	u_*	$\frac{U}{u_*}$	Froude No.	Flow Reynolds No.	Probe Type	V_{sq}	FI	Average Conc.	Rouse No.	R_p
	$\frac{ft^3}{sec}$	ft		deg F	$\frac{ft}{sec}$	$\frac{ft}{sec}$					$\frac{cm}{sec}$	$\frac{lb}{ft\ sec}$			
			$x10^{-3}$						$x10^{+5}$			$x10^{-5}$			
Rhodamine WT															
DT1	9.96	1.312	0.610	72	0.950	0.161	5.90	0.146	1.20	fixed		0.115	14.8 ppb		
DT1A	9.96	1.312	.610	72	.950	.161	5.90	.146	1.20	fixed		.088	11.3		
DT2	10.27	1.328	.510	74	.968	.148	6.55	.148	1.27	integral		.080	10.0		
DT3	10.06	1.333	.506	74	.941	.146	6.42	.144	1.25	fixed		.144	18.4		
DT3A	10.06	1.333	.506	74	.941	.146	6.42	.144	1.25	fixed		.118	15.0		
DT11	20.07	1.331	1.94	70.5	1.89	.288	6.56	.289	2.38	fixed		.146	9.35		
DT11A	20.07	1.331	1.94	70.5	1.89	.288	6.56	.289	2.38	fixed		.160	10.2		
DT20	30.45	1.319	4.67	70	2.90	.446	6.50	.446	3.62	integral		.226	9.50		
DT21	30.45	1.315	4.70	74	2.90	.446	6.50	.446	3.80	fixed		.066	2.79		
DT21A	30.45	1.315	4.70	74	2.90	.446	6.50	.446	3.80	fixed		.183	7.71		
DB11	20.02	1.332	1.89	69.5	1.88	.285	6.59	.287	2.35	fixed		.113	7.22		
DB11A	20.02	1.332	1.89	69.5	1.88	.285	6.59	.287	2.35	fixed		.125	7.98		
DB20	30.49	1.316	4.63	71	2.90	.443	6.55	.446	3.65	integral		.690	29.0		
DB21	30.49	1.316	4.63	72	2.90	.443	6.55	.446	3.69	fixed		.227	9.58		
Glass Beads															
FS1	10.19	1.334	.505	72	.955	.147	6.48	.146	1.23	fixed	1.05	1060	133 ppm	0.604	1.34
FS1A	10.19	1.334	.505	72	.955	.147	6.48	.146	1.23	fixed	1.05	1050	133	.604	1.34
FS11	20.14	1.335	1.88	70	1.88	.284	6.64	.287	2.37	fixed	1.03	2360	146	.304	1.28
FS11A	20.14	1.335	1.88	70	1.88	.284	6.64	.287	2.37	fixed	1.03	2680	168	.304	1.28
FS21	30.60	1.317	4.60	71.5	2.91	.442	6.58	.448	3.68	fixed	1.04	3770	158	.195	1.32
FS21A	30.60	1.317	4.60	71.5	2.91	.442	6.58	.448	3.68	fixed	1.04	4720	198	.195	1.32
Uniform Sand															
CS1	10.44	1.349	.508	72	.970	.148	6.53	.147	1.26	fixed	6.20	1300	166 ppm	3.54	25.2
CS1A	10.44	1.349	.508	72	.970	.148	6.53	.147	1.26	fixed	6.20	1400	166	3.54	25.2
CS3	10.26	1.333	.480	73	.960	.144	6.69	.147	1.25	fixed	6.24	630	78.5	3.66	25.7
CS3A	10.26	1.333	.480	73	.960	.144	6.69	.147	1.25	fixed	6.24	630	78.5	3.66	25.7
CS11	20.08	1.334	1.90	71	1.88	.286	6.59	.287	2.40	fixed	6.17	2520	162	1.81	24.9
CS11A	20.08	1.334	1.90	71	1.88	.286	6.59	.287	2.40	fixed	6.17	2560	162	1.81	24.9
CS21	30.44	1.310	4.60	65	2.90	.441	6.58	.447	3.34	fixed	5.97	5070	213	1.12	22.0
CS21A	30.44	1.310	4.60	65	2.90	.441	6.58	.447	3.34	fixed	5.97	5060	213	1.12	22.0
CS23	30.48	1.309	4.68	68	2.91	.444	6.56	.449	3.49	fixed	6.08	1240	51	1.14	23.4
CS23A	30.48	1.309	4.68	68	2.91	.444	6.56	.449	3.49	fixed	6.08	1190	51	1.14	23.4
T1	10.81	1.338	.494	70	1.010	.146	6.93	.154	1.28		6.15		191 ppm	3.50	24.4

TABLE 2 RELATIVE CONCENTRATIONS

Run	X[1]	η	c	X	η	c	X	η	c	X	η	c	X	η	c	X	η	c
DT1	3.0	0.127		5.0	0.127		7.00	0.127	0.04	9.0	0.127	0.20	11.0	0.127	0.30	68.5	0.126	0.98
		.254			.254	0.05		.254	.11		.254	.32		.254	.39		.414	1.03
		.381	0.03		.381	.08		.381	.23		.381	.45		.381	.48		.890	.99
		.508	.05		.508	.27		.508	.50		.508	.70		.508	.71			
		.635	.31		.635	.72		.635	.97		.635	1.09		.635	1.04			
		.762	1.14		.762	1.64		.762	1.60		.762	1.54		.762	1.36			
		.889	3.10		.889	2.48		.889	2.12		.889	1.71		.889	1.72			
DT1A	3.0	.127		5.0	.127		7.00	.127	.05	9.0	.127	.27	11.0	.127	.25	68.5	.126	.97
		.254			.254			.254	.05		.254	.37		.254	.33		.414	1.02
		.381			.381	.06		.381	.21		.381	.54		.381	.50		.890	1.01
		.508	.02		.508	.25		.508	.49		.508	.85		.508	.75			
		.635	.20		.635	.70		.635	.94		.635	1.11		.635	1.10			
		.762	1.45		.762	1.55		.762	1.51		.762	1.45		.762	1.45			
		.889	3.05		.889	2.57		.889	2.20		.889	1.56		.889	1.67			
DT2	3.0	.157		5.0	.157		7.00	.157	.07	9.0	.157	.19	11.0	.157	.12	15.0	.157	.45
		.282			.282	.01		.282	.14		.282	.26		.282	.34		.282	.54
		.408	.03		.408	.05		.408	.27		.408	.36		.408	.38		.408	.71
		.533	.03		.533	.20		.533	.47		.533	.56		.533	.64		.533	.87
		.659	.18		.659	.52		.659	.84		.659	.82		.659	.91		.659	1.07
		.784	.83		.784	1.34		.784	1.52		.784	1.36		.784	1.59		.784	1.23
		.910	3.95		.910	3.27		.910	2.53		.910	2.40		.910	2.13		.910	1.59
DT2A	19.0	.157	.61	24.0	.157	.82	68.5	.109	1.00									
		.282	.66		.282	.86		.258	1.00									
		.408	.73		.408	.88		.548	1.00									
		.533	.87		.533	.91		.821	1.00									
		.659	1.01		.659	1.00												
		.784	1.20		.784	1.09												
		.910	1.47		.910	1.20												
DT3	3.0	.125		5.0	.125		7.0	.125	.02	9.0	.125	.11	11.0	.125	.18	68.5	.109	1.01
		.250			.250			.250	.04		.250	.18		.250	.25		.258	.99
		.375			.375	.06		.375	.12		.375	.30		.375	.38		.548	1.00
		.500	.02		.500	.21		.500	.31		.500	.55		.500	.64		.821	1.01
		.625	.10		.625	.53		.625	.61		.625	.89		.625	.94			
		.750	.55		.750	1.17		.750	1.29		.750	1.35		.750	1.28			
		.875	3.14		.875	2.62		.875	2.44		.875	2.02		.875	1.89			

1/ Distance in depths (x/Y_N)

TABLE 2 - Continued

Run	X[1]	η	c	X	η	c	X	η	c	X	η	c	X	η	c	X	η	c
DT3A	3.0	.125		5.0	.125		7.0	.125	.01	9.0	.125	.12	11.0	.125	.25	68.5	.109	1.00
		.250	.01		.250	.03		.250	.03		.250	.17		.250	.33		.258	1.00
		.375	.02		.375	.08		.375	.14		.375	.28		.375	.47		.548	1.01
		.500	.04		.500	.18		.500	.27		.500	.50		.500	.65		.821	.99
		.625	.06		.625	.51		.625	.58		.625	.82		.625	.96			
		.750	.55		.750	1.20		.750	1.29		.750	1.39		.750	1.29			
		.875	3.14		.875	2.61		.875	2.48		.875	2.07		.875	1.77			
DT11	5.0	.113		7.0	.117	.05	10.0	.110	.17	14.0	.125	.56	19.0	.121	.67	67.5	.125	1.01
		.239	.03		.243	.11		.235	.21		.250	.64		.247	.72		.270	1.02
		.364	.03		.368	.20		.360	.36		.376	.73		.372	.76		.563	.98
		.489	.12		.493	.45		.485	.59		.501	.85		.495	.86		.833	.99
		.614	.39		.618	.78		.610	.88		.626	1.02		.622	.99			
		.740	1.07		.743	1.30		.736	1.28		.751	1.14		.747	1.17			
		.865	2.54		.869	2.10		.861	1.81		.877	1.37		.873	1.29			
DT11A	5.0	.113		7.0	.117		10.0	.110	.13	14.0	.125	.55	19.0	.121	.76	67.5	.125	.98
		.239			.243	.05		.235	.18		.250	.59		.247	.81		.270	1.00
		.364	.02		.368	.16		.360	.33		.376	.72		.372	.83		.563	1.00
		.489	.09		.493	.35		.485	.57		.501	.80		.497	.89		.833	1.01
		.614	.35		.618	.82		.610	.88		.626	.98		.622	1.02			
		.740	1.14		.743	1.37		.736	1.34		.751	1.16		.747	1.08			
		.865	2.56		.869	2.16		.861	1.83		.877	1.43		.873	1.20			
DT20	5.0	.138	.01	7.0	.138	.04	10.0	.138	.14	14.0	.138	.59	19.0	.138	.81	24.0	.138	1.00
		.264	.01		.264	.08		.264	.22		.264	.74		.264	.87		.264	1.03
		.390	.06		.390	.30		.390	.42		.390	.87		.390	.94		.390	1.04
		.517	.20		.517	.55		.517	.79		.517	.98		.517	1.01		.517	1.00
		.643	.73		.643	1.06		.643	1.11		.643	1.06		.643	1.03		.643	.99
		.770	1.22		.770	1.67		.770	1.48		.770	1.17		.770	.99		.770	.95
		.896	2.95		.896	2.12		.896	1.87		.896	1.24		.896	1.10		.896	.92
DT21	3.0	.127		5.0	.127		7.0	.127	.02	10.0	.127	.18	14.0	.127	.40	68.5	.127	.98
		.253			.253			.253	.04		.253	.25		.253	.48		.274	1.00
		.380			.380	.40		.380	.11		.380	.39		.380	.58		.570	1.01
		.507			.507	.16		.507	.27		.507	.64		.507	.75		.845	1.01
		.634	.06		.634	.46		.634	.66		.634	.96		.634	1.03			
		.760	.52		.760	1.37		.760	1.49		.760	1.46		.760	1.35			
		.887	3.60		.887	2.89		.887	2.61		.887	1.95		.887	1.62			

TABLE 2 - Continued

Run	X[1]	η	c	X	η	c	X	η	c	X	η	c	X	η	c	X	η	c
DT21A	3.0	.127		5.0	.127		7.0	.127	.03	10.0	.127	.23	14.0	.127	.40	68.5	.127	.99
		.253			.253	.01		.253	.04		.253	.32		.253	.47		.274	1.01
		.380			.380	.40		.380	.15		.380	.50		.380	.61		.570	1.00
		.507			.507	.21		.507	.40		.507	.62		.507	.72			
		.634			.634	.56		.634	.76		.634	1.00		.634	1.04			
		.760	.48		.760	1.37		.760	1.43		.760	1.39		.760	1.37			
		.887	3.66		.887	2.81		.887	2.48		.887	1.87		.887	1.61			
DB11	5.0	.121	2.06	7.0	.125	1.95	9.0	.117	1.34	12.0	.121	1.27	15.0	.121	1.21	67.5	.125	1.00
		.246	1.74		.25	1.81		.242	1.29		.246	1.23		.246	1.09		.270	1.00
		.371	1.59		.375	1.57		.368	1.21		.371	1.20		.371	1.16		.561	1.01
		.497	1.25		.501	1.24		.493	1.12		.497	1.12		.497	1.06		.835	1.00
		.622	.85		.626	.87		.618	1.01		.622	1.06		.622	1.01			
		.747	.53		.751	.49		.743	.85		.747	.90		.747	.88			
		.872	.28		.876	.34		.868	.73		.872	.73		.872	.87			
DB11A	5.0	.121	2.26	7.0	.125	1.64	9.0	.117	1.14	12.0	.121	1.15	15.0	.121	1.15	67.5	.125	.99
		.246	2.26		.250	1.48		.242	1.19		.246	1.09		.246	1.14		.270	1.00
		.371	1.73		.375	1.34		.368	1.15		.371	1.08		.371	1.10		.561	1.00
		.497	1.13		.501	1.18		.493	1.10		.497	1.09		.497	1.03		.835	1.00
		.622	.74		.626	.85		.618	1.00		.622	1.05		.622	.96			
		.747	.39		.751	.73		.743	.92		.747	.95		.747	.95			
		.872	.18		.876	.47		.868	.81		.872	.87		.872	.90			
DB20	9.0	.166	1.34	12.0	.166	.97	15.0	.166	.80	19.0	.166	.73	24.0	.166	.74			
		.293	1.25		.293	.97		.293	.80		.293	.78		.293	.81			
		.420	1.12		.420	.97		.420	.85		.420	.84		.420	.88			
		.546	.93		.546	1.01		.546	.93		.546	.98		.546	1.00			
		.673	.80		.673	.98		.673	1.13		.673	1.16		.673	1.02			
		.799	.85		.799	1.00		.799	1.16		.799	1.22		.799	1.17			
		.926	.85		.926	1.09		.926	1.22		.926	1.18		.926	1.25			
DB21	5.0	.127	2.20	7.0	.119	2.25	9.0	.123	1.05	12.0	.119	1.13	15.0	.127	1.09	68.5	.118	.97
		.253	1.90		.245	2.05		.249	1.14		.245	1.23		.253	1.09		.300	.99
		.380	1.46		.372	1.83		.376	1.14		.372	1.13		.380	1.09		.561	.99
		.507	1.10		.499	1.20		.503	1.12		.499	1.07		.507	1.04		.835	1.05
		.633	.70		.625	.68		.629	.97		.625	1.01		.633	.96			
		.760	.47		.752	.38		.756	.92		.752	.92		.760	.93			
		.887	.27		.879			.883	.82		.879	.80		.887	.91			

TABLE 2 - Continued

Run	X[1]	η	c	X	η	c	X	η	c	X	η	c	X	η	c	X	η	c
FS1	6.0	.128	.16	8.0	.128	.93	12.0	.128	1.40	16.0	.128	1.40	22.0	.128	.84	67.0	.111	.14
		.255	.35		.255	.93		.255	1.36		.255	1.17		.255	.77		.263	.13
		.383	.67		.383	1.05		.383	1.25		.383	.97		.383	.65		.560	.11
		.510	1.19		.510	1.27		.510	1.10		.510	.81		.510	.51		.840	.07
		.638	1.66		.638	1.29		.638	.91		.638	.64		.638	.38			
		.766	1.74		.766	1.09		.766	.65		.766	.45		.766	.26			
		.893	1.10		.893	.73		.893	.37		.893	.28		.893	.15			
FS1A	6.0	.126	.14	8.0	.126	.69	12.0	.126	1.58	16.0	.126	1.50	22.0	.126	.88	67.0	.111	.16
		.252	.28		.252	.78		.252	1.45		.252	1.19		.252	.78		.263	.13
		.378	.63		.378	1.06		.378	1.28		.378	1.01		.378	.66		.560	.10
		.504	1.09		.504	1.32		.504	1.03		.504	.83		.504	.51		.840	.07
		.629	1.59		.629	1.44		.629	.86		.629	.65		.629	.39			
		.755	1.84		.755	1.17		.755	.63		.755	.45		.755	.26			
		.881	1.25		.881	.72		.881	.36		.881	.25		.881	.16			
FS11	5.0	.121	.01	7.0	.125	.17	9.0	.117	.58	12.0	.125	1.11	15.0	.129	1.47	67.5	.125	1.17
		.246	.06		.250	.25		.242	.59		.250	.95		.254	1.20		.270	.95
		.371	.19		.375	.45		.367	.70		.375	.95		.378	1.10		.560	.80
		.496	.49		.499	.83		.492	.94		.499	1.01		.503	1.02		.830	.56
		.620	.97		.624	1.26		.616	1.15		.624	1.06		.628	.98			
		.745	1.67		.749	1.55		.741	1.35		.749	1.07		.753	.88			
		.870	2.08		.874	1.56		.866	1.29		.874	.97		.878	.74			
FS11A	5.0	.121		7.0	.125	.22	9.0	.117	.65	12.0	.125	1.13	15.0	.129	1.50	67.5	.125	1.26
		.246	.03		.250	.25		.242	.65		.250	.97		.254	1.27		.270	.88
		.371	.13		.375	.48		.367	.69		.375	1.02		.378	1.13		.560	.81
		.496	.48		.499	.83		.492	.87		.499	1.07		.503	1.03		.830	.59
		.620	1.01		.624	1.23		.616	1.15		.624	1.09		.628	.97			
		.745	1.76		.749	1.56		.741	1.39		.749	1.06		.753	.89			
		.870	2.01		.874	1.56		.866	1.34		.874	.91		.878	.73			
FS21	5.0	.127		7.0	.119	.10	9.0	.123	.32	12.0	.119	.79	15.0	.127	1.06	67.0	.119	1.14
		.253	.01		.245	.16		.249	.38		.245	.83		.253	.97		.277	1.06
		.380	.05		.372	.37		.376	.58		.372	.91		.380	.95		.561	.90
		.506	.26		.498	.67		.502	.93		.498	1.00		.506	.98		.840	.73
		.633	.76		.625	1.20		.629	1.24		.625	1.14		.633	1.02			
		.759	1.84		.751	1.66		.755	1.42		.751	1.17		.759	1.07			
		.886	2.53		.878	1.77		.882	1.46		.878	1.09		.886	.99			

TABLE 2 - Continued

Run	X[1]	η	c	X	η	c	X	η	c	X	η	c	X	η	c	X	η	c
FS21A	5.0	.127	.01	7.0	.119	.11	9.0	.123	.48	12.00	.119	.80	15.0	.127	1.04	67.0	.119	1.21
		.253	.04		.245	.24		.249	.52		.245	.82		.253	.99		.277	1.08
		.380	.18		.372	.40		.376	.66		.372	.91		.380	.98		.561	.90
		.506	.35		.498	.74		.502	.90		.498	1.07		.506	1.02		.840	.72
		.633	.83		.625	1.25		.629	1.11		.625	1.15		.633	1.09			
		.759	1.82		.751	1.63		.755	1.32		.751	1.11		.759	1.07			
		.886	2.42		.878	1.70		.882	1.42		.878	1.04		.886	.94			
CS1	2.0	.125		2.75	.125	.02	3.50	.125	.75	4.25	.125	1.22	5.0	.125	1.48	67.5	.125	
		.250	.01		.250	.19		.250	1.51		.250	1.69		.250	1.23		.268	
		.374	.03		.374	1.28		.374	1.92		.374	1.34		.374	.68		.454	
		.499	.61		.499	3.06		.499	1.75		.499	.78		.499	.29		.740	
		.624	3.50		.624	1.79		.624	.67		.624	.31		.624	.09			
		.749	2.36		.749	.36		.749	.15		.749	.08		.749	.01			
		.873	.09		.873	.04		.843	.01		.873	.01		.873				
CS1A	2.0	.123		2.75	.123	.04	3.50	.123	.87	4.25	.123	1.31	5.0	.123	1.76	67.5	.125	
		.245			.245	.21		.245	1.61		.245	1.54		.245	1.18		.268	
		.368	.04		.368	1.37		.368	2.07		.368	1.44		.368	.62		.454	
		.490	.78		.490	2.89		.490	1.68		.490	.85		.490	.25		.740	
		.613	3.62		.613	2.03		.613	.74		.613	.31		.613				
		.735	2.07		.735	.40		.735	.18		.735	.07		.735	.03			
		.858	.15		.858	.02		.858	.03		.858	.01		.858				
CS3	2.0	.125		2.75	.125	.01	3.50	.125	.85	4.25	.125	1.70	5.0	.125	1.38	67.5	.125	
		.250	.01		.250	.16		.250	1.75		.250	1.69		.250	1.10		.268	
		.374	.20		.374	.87		.374	2.33		.374	1.31		.374	.71		.454	
		.499	1.03		.499	2.85		.499	1.45		.499	.68		.499	.34		.740	
		.624	3.26		.624	2.20		.624	.50		.624	.21		.624	.15			
		.749	1.93		.749	.46		.749	.10		.749	.05		.749	.03			
		.873	.25		.873	.03		.873	.01		.873			.873				
CS3A	2.0	.126		2.75	.126	.03	3.50	.126	1.19	4.25	.126	1.84	5.0	.126	1.40	67.5	.125	
		.251	.01		.251	.28		.251	1.64		.251	1.77		.251	1.07		.268	
		.377	.09		.377	1.22		.377	2.04		.377	1.19		.377	.71		.454	
		.503	.90		.503	2.82		.503	1.42		.503	.63		.503	.34		.740	
		.628	3.71		.628	2.06		.628	.60		.628	.21		.628	.12			
		.754	2.11		.754	.51		.754	.12		.754	.05		.754	.02			
		.880	.13		.880	.07		.880			.880			.880				

TABLE 2 - Continued

Run	X[1]	η	c	X	η	c	X	η	c	X	η	c	X	η	c	X	η	c
CS11	3.0	.133	.01	4.50	.133	.36	6.0	.113	1.63	7.50	.113	1.92	9.0	.129	1.80	67.5	.125	.02
		.258	.03		.258	.74		.238	1.43		.238	1.38		.254	1.34		.270	
		.383	.26		.383	1.33		.363	1.55		.363	1.20		.379	0.92		.560	
		.508	1.05		.508	1.73		.488	1.41		.488	0.91		.504	0.65		.830	
		.632	2.46		.632	1.71		.613	1.06		.613	0.59		.629	0.37			
		.757	2.14		.757	1.01		.738	0.58		.738	0.30		.753	0.20			
		.882	.61		.882	.34		.863	0.25		.863	0.12		.878	0.07			
CS11A	3.0	.133		4.50	.133	.43	6.0	.113	2.79	7.50	.113	1.94	9.0	.129	1.93	67.5	.125	
		.258	.01		.258	.76		.238	1.44		.238	1.39		.254	1.28		.270	
		.383	.11		.383	1.42		.363	1.54		.363	1.09		.379	0.90		.560	
		.508	.68		.508	1.90		.488	1.42		.488	0.88		.504	0.63		.830	
		.632	2.24		.632	1.65		.613	1.16		.613	0.62		.629	0.37			
		.757	2.76		.757	.90		.738	0.58		.738	0.34		.753	0.16			
		.882	.73		.882	.25		.863	0.21		.863	0.15		.878	0.06			
CS21	4.0	.127	.02	5.0	.107	.16	7.0	.107	1.91	9.0	.107	2.07	12.0	.123	3.49			
		.254	.12		.235	.39		.235	1.36		.235	1.62		.251	1.78			
		.382	.39		.362	.85		.362	1.31		.362	1.48		.378	1.12			
		.509	1.20		.489	1.47		.489	1.29		.489	1.23		.505	0.72			
		.636	2.13		.616	2.15		.616	1.14		.616	0.92		.632	0.49			
		.763	2.18		.744	1.82		.744	0.83		.744	0.58		.759	0.28			
		.891	.73		.871	.82		.871	0.55		.871	0.28		.887	0.12			
CS21A	4.0	.127	.02	5.0	.107	.22	7.0	.107	1.84	9.0	.107	2.34	12.0	.123	3.34			
		.254	.15		.235	.37		.235	1.26		.235	1.62		.251	1.81			
		.382	.52		.362	.78		.362	1.30		.362	1.38		.378	1.18			
		.509	1.28		.489	1.48		.489	1.32		.489	1.20		.505	0.78			
		.636	2.38		.616	1.84		.616	1.13		.616	0.91		.632	0.52			
		.763	2.13		.744	1.56		.744	0.80		.744	0.61		.759	0.29			
		.891	.80		.871	.63		.871	0.39		.871	0.28		.887	0.12			
CS23	5.0	.127	.26	7.0	.119	1.23	12.0	.127	3.72	15.0	.127	3.02	68.5	.100	.30			
		.255	.50		.247	1.38		.255	1.72		.255	1.57		.247	.21			
		.382	.97		.374	1.57		.382	1.16		.382	1.02		.545	.12			
		.509	1.59		.501	1.52		.509	0.68		.509	0.64		.828	.03			
		.637	1.85		.629	1.16		.637	0.47		.637	0.41						
		.764	1.28		.756	0.64		.764	0.30		.764	0.21						
		.891	.45		.883	0.23		.891	0.10		.891	0.10						
CE23A	7.0	.119	1.30	9.0	.123	2.71	12.0	.127	2.98	15.0	.127	3.31	68.5	.100	.55			
		.247	1.15		.251	1.56		.255	1.72		.255	1.56		.247	.34			
		.374	1.43		.378	1.25		.382	1.13		.382	0.90		.545	.12			
		.501	1.46		.505	1.00		.509	0.86		.509	0.55		.828	.04			
		.629	1.24		.633	0.82		.637	0.58		.637	0.34						
		.756	0.73		.760	0.50		.764	0.35		.764	0.19						
		.883	0.32		.887	0.26		.891	0.11		.891	0.08						

TABLE 3 RECOVERY RATIOS AND PROBE LOCATIONS

Run	X	Dist. off C_L inches [1]	RRM	RR	Run	X	Dist. off C_L inches	RRM	RR	Run	X	Dist. off C_L inches	RRM	RR	Run	X	Dist. off C_L inches	RRM	RR
BT1	3.0	18L	1.06	1.00	DT1A	3.0	18L	1.17	1.00	DT2	3.0	var.	0.72	1.00	DT2	19.0	var.	1.14	1.00
	5.0	20R	.98	1.00		5.0	20R	1.03	1.00		5.0	var.	.86	1.00		24.0	var.	1.04	1.00
	7.0	12L	1.16	1.00		7.0	12L	1.04	1.00		7.0	var.	.91	1.00					
	9.0	18R	.81	1.00		9.0	18R	.81	1.00		9.0	var.	.95	1.00					
	11.0	18L	1.11	1.00		11.0	18L	1.16	1.00		11.0	var.	.93	1.00					
	68.5	16L	.85	1.00		68.5	16L	.79	1.00		15.0	var.	1.07	1.00					
DT3	3.0	18L	.62	1.00	DT3A	3.0	18L	.74	1.00	DT11	5.0	20L	.90	1.00	DT11A	5.0	20L	.81	1.00
	5.0	20R	1.02	1.00		5.0	20R	.94	1.00		7.0	20R	1.04	1.00		7.0	20R	1.19	1.00
	7.0	12L	.91	1.00		7.0	12L	.98	1.00		10.0	12L	.91	1.00		10.0	12L	1.03	1.00
	9.0	18R	1.12	1.00		9.0	18R	.90	1.00		14.0	18R	1.01	1.00		14.0	18R	1.12	1.00
	11.0	18L	1.30	1.00		11.0	18L	1.40	1.00		19.0	18L	1.14	1.00		19.0	18L	1.11	1.00
	68.5	16L	1.05	1.00		68.5	16L	.95	1.00		67.5	16L	.95	1.00		67.5	16L	.93	1.00
DT20	5.0	var.	.99	1.00	DT21	3.0	17L	.74	1.00	DT21A	3.0	17L	.66	1.00	DB11	5.0	18L	.73	1.00
	7.0	var.	.99	1.00		5.0	20R	1.25	1.00		5.0	20R	1.34	1.00		7.0	20R	1.11	1.00
	10.0	var.	.96	1.00		7.0	10L	.85	1.00		7.0	10L	.88	1.00		9.0	12L	1.21	1.00
	14.0	var.	1.04	1.00		10.0	13R	1.04	1.00		10.0	13R	1.15	1.00		12.0	18R	1.20	1.00
	19.0	var.	1.00	1.00		14.0	19L	1.22	1.00		14.0	19L	1.24	1.00		15.0	18L	.88	1.00
	24.0	var.	1.01	1.00		68.5	16L	1.00	1.00		68.5	16L	1.04	1.00		67.5	16L	.95	1.00
DB11A	5.0	18L	.71	1.00	DB20	9.0	var.	.80	1.00	DB21	5.0	20L	.63	1.00	FS1	6.0	10L	.95	1.00
	7.0	20R	1.19	1.00		12.0	var.	.86	1.00		7.0	20R	.42	1.00		8.0	12R	.90	.99
	9.0	12L	1.32	1.00		15.0	var.	1.04	1.00		9.0	11L	1.14	1.00		12.0	17L	.93	.90
	12.0	18R	1.24	1.00		19.0	var.	1.07	1.00		12.0	12R	.70	1.00		16.0	20R	.70	.72
	15.0	18L	.92	1.00		24.0	var.	.93	1.00		15.0	18L	.78	1.00		22.0	21L	.45	.44
	67.5	16L	1.04	1.00							68.5	16L	.75	1.00		67.0	12L	.10	.10
FS1A	6.0	10L	.91	1.00	FS11	5.0	20L	1.14	1.00	FS11A	5.0	20L	1.26	1.00	FS21	5.0	20L	1.39	1.00
	8.0	12R	1.03	.99		7.0	20R	1.07	1.00		7.0	20R	1.02	1.00		7.0	20R	1.51	1.00
	12.0	17L	.89	.90		9.0	12L	.80	.99		9.0	12L	.80	.99		9.0	11L	1.09	1.00
	16.0	20R	.74	.72		12.0	13R	.85	.99		12.0	13R	.96	.99		12.0	12R	1.21	1.00
	22.0	21L	.44	.44		15.0	18L	1.11	.98		15.0	18L	1.12	.98		15.0	18L	1.26	.99
	66.5	12L	.09	.10		67.5	16L	.67	.73		67.5	16L	.78	.73		67.0	16L	.88	.88
FS21A	5.0	20L	1.62	1.00	CS1	2.0	18L	1.01	1.00	CS1A	2.0	18L	.69	1.00	CS3	2.0	18L	1.07	1.00
	7.0	20R	1.62	1.00		2.75	20R	.83	.97		2.75	20R	.96	.97		2.75	20R	.98	.97
	9.0	11L	.88	1.00		3.5	10L	.92	.86		3.50	10L	.85	.86		3.50	10L	1.06	.86
	12.0	12R	1.21	1.00		4.25	11R	.63	.63		4.25	11R	.73	.63		4.25	11R	.69	.63
	15.0	18L	1.30	.99		5.0	19L	.38	.40		5.00	19L	.28	.40		5.00	19L	.45	.40
	67.0	16R	.87	.88		67.5	16L				67.5	16L				67.5	16L		
CS3A	2.0	18L	.99	1.00	CS11	3.0	20L	1.15	1.00	CS11A	3.0	20L	1.13	1.00	CS21	4.0	20L	1.22	1.00
	2.75	20R	.92	.97		4.5	20R	.96	1.00		4.5	20R	1.10	1.00		5.0	20R	1.01	1.00
	3.50	10L	.95	.86		6.0	12L	.91	.95		6.0	12L	1.00	.95		7.0	11L	.92	1.00
	4.25	11R	.66	.63		7.5	12R	.75	.72		7.5	12R	.69	.72		9.0	12R	1.00	.98
	5.06	19L	.43	.40		9.0	20L	.56	.61		9.0	20L	.67	.61		12.0	17L	.97	.92
	67.5	16L				67.5	12L				67.5	12L							
CS21A	4.0	20L	1.08	1.00	CS23	5.0	20L	1.33	1.00	CS23A	7.0	20R	1.00	1.00					
	5.0	20R	1.25	1.00		7.0	20R	1.05	1.00		9.0	11L	1.08	.98					
	7.0	11L	.98	1.00		12.0	12R	.82	.92		12.0	12R	.68	.92					
	9.0	12R	.95	.98		15.0	17L	.77	.80		15.0	17L	1.15	.80					
	12.0	17L	.89	.92		68.5	18L	.10			68.5	18L	.18						

[1] C_L is centerline, R and L are right and left.

APPENDIX B

COMPUTER PROGRAM

COMPUTER PROGRAM

```
*LIMIT,T=2,PR=20
*FORTRAN
      PROGRAM CONPRE
C     CONCENTRATION PREDICTION VARIABLE BARRIORS
C  THIS PROGRAM ALSO HAS THE PLOTTING ROUTINE
      DIMENSIONC(2,200),E(200),UI(200),UD(200),ED(200)
      DIMENSIONC1(50),P(150,54)
      READ(5,301)DE,AS,PL,B,Z,D1,E1,P1,T,M
      READ(5,301)A1,A2,A3,A4,A5,A6,A7,A8,A9
C     VS IS FALL VELOCITY/SHEAR VELOCITY
C     A IS THE PROBABILITY OF DEPOSIT
C     XO IS THE DISTANCE (IN DEPTHS) OF THE INITIAL CONDITION
      READ(5,200) VS,A,XO
      READ(5,203)M,N
      AN=N
      AM=M
      DY=1.0/AN
      DX=1.0/AM
C     E(I) IS TRANSFER COEFFICIENT/(YN*SHEAR VE-OCITY)
C     E/YN*US IS UNIFORM WITH SAME MEAN AS THE MEASURED DISTRIBUTION
C     FLOW C COARSE
      READ(5,204)(E(I),I=1,N)
C     UD IS VELOCITY/SHEAR VELOCITY
      READ(5,204)(UD(I),I=1,N)
      DO7J=1,N
      AJ=J
    7 UI(J)=1.0/UD(J)
C     C(I,J) IS CONCENTRATION
      READ(5,204)(C(1,J),J=1,N)
      FLUX=0.0
      VB=0.0
      EM=0.0
      AN=N
      DO8J=1,N
      VB=VB+UD(J)/AN
      EM=EM+E(J)/AN
    8 FLUX=FLUX+C(1,J)*UD(J)/AN
      DO9J=1,N
    9 C(1,J)=C(1,J)*VB  /FLUX
      WRITE(6,212)XO
  212 FORMAT(3H X=,F6.2,20H RECOVERY RATIO= 1.0D
      WRITE(6,207  )
  207 FORMAT(15H CONCENTRATIONS)
      WRITE(6,205)(C(1,J),J=1,N)
      WRITE(6,208)VS,A,VB,EM
  208 FORMAT(18H0FALL VELOCITY/US=,F6.3,20H          PROB. DEP.=,F6.2,13H
     1 AVE. VEL/US=,F6.3,14H AVE. E/YN*US=,F6.3D
      WRITE(6,206)DX,DY
  206 FORMAT(4H0DX=,F6.4,10H        DY=,F6.3)
      WRITE(6,209)
  209 FORMAT(27H0VELOCITY/FRICTION VELOCITY)
      WRITE(6,205)(UD(J),J=1,N)
      WRITE(6,211)
  211 FORMAT(10H0E/(YN*US))
      WRITE(6,205)(E(J),J=1,N)
```

```
      D=DX/(DY*DY)
      DS=DX*VS/DY
C     M2 IS NUMBER OF STEPS BETWEEN PRINTOUTS
      M2=1200
      AM2=M2
      AM=M
      AX=AM2/AM
      X=XO
C     DO AS MANY TIMES AS PRINTOUTS
      DO21K=1,8
      X=X+AX
      DO4I=1,M2
      C(2,1)=C(1,1)+D*E(2)*UI(1)*(C(1,2)-C(1,1)D
      C(2,1)=C(2,1)+DS *UI(1)*(C(1,2)-C(1,1)*A)
      C(2,N)=C(1,N)+D*E(N)*UI(N)*(C(1,N-1)-C(1,N))
      C(2,N)=C(2,N)-DS *UI(N)*C(1,N)
      KA=N-1
      DO5J=2,KA
      C(2,J)=D*UI(J)*(E(J+1)*(C(1,J+1)-C(1,J))-E(J)*(C(1,J)-C(1,J-1)))
    5 C(2,J)=C(2,J)+C(1,J)+DS*UI(J)*(C(1,J+1)-CU1,J))
      FLUX=0.0
      DO4J=1,N
      FLUX=FLUX+C(1,J)*UD(J)/AN
    4 C(1,J)=C(2,J)
      FLUX=FLUX/VB
      WRITE(6,202)
      WRITE(6,207)
    3 WRITE(6,205)(C(1,J),J=1,N)
      DO20J=1,50
   20 C1(J)=C(1,J)
C     MAKE ALL SPACES BLANK
      DO11J=1,54
      DO11I=1,127
   11 P(I,J)=B
C     DEFINE LEFT MARGIN
      DO13J=4,54
   13 P(7,J)=DE
      DO12J=14,54,10
      P(4,J)=Z
   12 P(5,J)=DE
      P(2,27)=D1
      P(2,26)=E1
      P(2,25)=P1
      P(2,24)=T
      P(2,23)=H
      P(6,14)=A2
      P(6,24)=A4
      P(6,34)=A6
      P(6,44)=A8
      P(4,54)=A1
      P(5,54)=DE
      P(6,54)=Z
C     DEFINE BOTTOM MARGIN
      DO14I=7,127
   14 P(I,4)=DE
      DO15I=37,127,30
   15 P(I,4)=AS
      P(37,3)=A1
```

```
      P(67,3)=A2
      P(97,3)=A3
      P(127,3)=A4
C     DEFINE THE POINTS
      DO16J=4,53
      C1=C1(J-3)*300.0
      IC=C1/10.0
      ICB=C1
      IF(ICB-10*IC-5)17,18,18
   17 L=IC
      GO TO 16
   18 L=IC+1
   16 P(L+7,J)=PL
      DO19J=1,54
      KB=55-J
   19 WRITE(6,316)(P(I,KB),I=1,127)
   21 WRITE(6,210)X,FLUX
  210 FORMAT(75H0
     1 CONCENTRATION   X=,F6.2,20H     RECOVERY RATIO=,F6.3)
  200 FORMAT(5E12.5)
  201 FORMAT(1H ,10E12.5)
  202 FORMAT(1H1)
  203 FORMAT(2I6)
  204 FORMAT(10F6.2)
  205 FORMAT(1H ,20F6.3)
  301 FORMAT(10A1)
  316 FORMAT(3X,127A1)
      CALL EXIT
      END
*RUN
*END
```